Master's thesis

NTNU
Norwegian University of Science and Technology
Faculty of Medicine and Health Sciences
Kavli Institute for Systems Neuroscience

Inger Kristine Fjeldskaar Aukrust

Defensive Behaviors in Juvenile Zebrafish, and the Impact of Serotonergic Manipulation on Their Behavioral Phenotype

Master's thesis in Neuroscience
Supervisor: Prof. Dr. Emre Yaksi
Co-supervisor: Bram Serneels
September 2023

NTNU
Norwegian University of
Science and Technology

Inger Kristine Fjeldskaar Aukrust

Defensive Behaviors in Juvenile Zebrafish, and the Impact of Serotonergic Manipulation on Their Behavioral Phenotype

Master's thesis in Neuroscience
Supervisor: Prof. Dr. Emre Yaksi
Co-supervisor: Bram Serneels
September 2023

Norwegian University of Science and Technology
Faculty of Medicine and Health Sciences
Kavli Institute for Systems Neuroscience

NTNU
Norwegian University of
Science and Technology

Abstract

The overarching aim of this thesis is to explore defensive behaviors in juvenile zebrafish, with a special interest in how manipulation of the serotonergic system influences the expression of these behavioral responses. The behavioral patterns engaged during fear and anxiety make up the repertoire of responses available for assessing, preventing and handling stress and perceived danger. Different situations call for different responses, and the interplay between several brain regions is required for computing the scope of a threat and then execute the appropriate behavioral response. Serotonin has been identified as a key neuromodulator in this circuit. The main site of synthesis and subsequent release of serotonin is the dorsal raphe nucleus, which has innervation to forebrain and midbrain regions modulating these threat responses.

The work in my project can be subcategorized into three parts. The first part consisted of a series of optimization steps for the analysis of defensive behaviors in freely behaving juvenile zebrafish. Zebrafish are capable of expressing a broad range of behaviors, and their brain anatomy shares many traits with mammals due to the conservation of fundamental architecture across vertebrate species. The second part was to make use of the refined experimental protocol to shed more light on the relationship between the serotonergic system and defensive behaviors. For this purpose, I investigated how chemo-genetic ablation of the dorsal raphe affected the animals' behavioral phenotype. For the last part of the project, I examined the forebrain activity in these ablated zebrafish. I performed post-hoc immunostaining of the phosphorylated- versus total ERK ratio to measure the neuronal activity related to the observed behavior.

Refinement of the behavioral experiment protocol revealed that unique stimuli showed different abilities to elicit defensive reactions in the juvenile zebrafish. Stimuli of longer duration and higher frequency seemed particularly well suited for promoting strong stereotypical defensive responses. Furthermore, my results indicated that ablation of the DR is associated with stronger defensive phenotypes. While I found this to be less conclusive for the novel-tank test, the stimulus delivery test showed prominent differences in the defensive behavior. Here I observed that ablated animals had a reduced capability to attenuate their defensive response after repeated stimuli exposure. This reinforces the concept that the DR and its serotonergic influence has a significant role in modulating defensive behaviors in the aversive brain system, i.e., for the habituation of the adaptive fear response. The ERK immunostaining analysis revealed a difference in brain activity between ablated and control animals that was consistent with previous work in the lab in several areas, but also differed in others. Here, my findings suggested that DR ablation causes decreased neuronal activity in the forebrain except for the anterior and posterior region of the telencephalon. Overall, the project enlightens the use of juvenile zebrafish as a solid approach to observe and study defensive behaviors. Discoveries made with this approach and model organism may be evolutionary conserved in vertebrate species. This would allow us to broaden our understanding of the serotonergic system in mammals, and ultimately perhaps improve our clinical understanding of disorders associated with this neural circuit.

Sammendrag

Det overordnede målet med denne avhandlingen er å utforske forsvarsadferd hos juvenile sebrafisker, med særlig interesse for hvordan manipulering av det serotonergiske systemet påvirker uttrykket av disse adferdsresponsene. Adferdsmønstrene som settes i gang ved frykt og angst utgjør repertoaret av responsmuligheter som er tilgjengelige for å vurdere, forhindre og håndtere stress og oppfattet fare. Ulike situasjoner krever forskjellige responser, og samspillet mellom flere hjerneregioner er nødvendig for å beregne omfanget av en trussel og deretter igangsette den riktige adferdsresponsen. Serotonin er identifisert som en viktig neuromodulator i denne hjernekretsen. Den dorsale rafekjernen er hovedområdet for syntesen og den påfølgende frigjøringen av serotonin, og har innervasjoner til områder i forhjernen og midthjernen som modulerer disse trusselresponsene.

Arbeidet i prosjektet mitt kan inndeles i tre deler. Den første delen besto av en serie optimaliseringstrinn for analysen av defensive adferder hos fritt agerende juvenile sebrafisker. Sebrafisker er i stand til å uttrykke et bredt spekter av adferder, og hjerneanatomien deres har mange fellestrekk med pattedyr grunnet konservering av grunnleggende arkitektur på tvers av virveldyrarter. I den andre delen brukte jeg den forbedrede eksperimentelle protokollen for å kaste mer lys over forholdet mellom det serotonergiske systemet og defensive adferder. For dette formålet undersøkte jeg hvordan kjemogenetisk ablasjon av den dorsale rafekjernen påvirket dyrenes adferdsfenotype. I den siste delen av prosjektet undersøkte jeg forhjerneaktiviteten hos disse ablaterte sebrafiskene. Jeg utførte post-hoc immunfarging av fosforylert versus total ERK-forhold for å måle den nevrale aktiviteten knyttet til den observerte adferden.

Forbedringen av protokollen for adferdseksperimentet avslørte at unike stimuli viste forskjellige evner til å fremkalle defensive reaksjoner hos juvenile sebrafisker. Stimuli med lengre varighet og høyere frekvens virket spesielt godt egnet til å fremkalle sterke stereotypiske defensive responser. Resultatene mine indikerte videre at ablasjon av DR er assosiert med sterkere defensive fenotyper. Mens jeg fant dette mindre konkluderende for novel tank-testen, viste stimulus-testen tydelige forskjeller i den defensive adferden. Her observerte jeg at ablaterte dyr hadde mindre evne til å redusere sin defensive respons etter gjentatt eksponering for stimulusen. Dette forsterker konseptet om at DR og dets serotonergiske innflytelse har en betydelig rolle i å modulere defensive adferder i det aversive hjernesystemet, med andre ord habituering av den adaptive fryktresponsen. ERK-immunfargingsanalysen avslørte en forskjell i hjerneaktivitet mellom ablaterte dyr og kontrolldyr som samsvarte med tidligere laboratoriearbeid på flere områder, men var også forskjellige på andre områder. Her antydet funnene mine at DR-ablasjon førte til redusert nevral aktivitet i forhjernen, bortsett fra den fremre og bakre delen av forhjernen. Samlet sett belyser prosjektet bruken av juvenile sebrafisker som en god tilnærming for å observere og studere defensive adferder. Funn ved bruk av denne tilnærmingen og modellorganismen kan være evolusjonært konservert i virveldyrarter. Dette kan bidra til å utvide forståelsen vår av det serotonergiske systemet hos pattedyr, og muligens til slutt øke den kliniske forståelsen av lidelser knyttet til denne nevrale kretsen.

Preface and Acknowledgements

This master project is affiliated with the Norwegian University of Science and Technology (NTNU) and was made possible thanks to the amazing members of the Yaksi group at the Kavli Institute for Systems Neuroscience (KISN). Alongside the Jurisch-Yaksi group, this environment forms an inspiring scientific community that I have been very lucky to be a part of for the past year.

I would like to extend my thankfulness to Prof. Dr. Emre Yaksi, for the invaluable guidance and mentorship throughout these two semesters. Your support has made my thesis work a truly enjoyable learning experience while providing me with the freedom to explore and grow within the research field. As my supervisor, your counseling, insight, and readiness to discuss either data or difficulties have been vital in shaping the process and honing the result.

I express my deepest gratitude to Bram Serneels, who always makes time to teach me experimental procedures and share practical knowledge; none of the data in this project would have been generated without your patient guidance. Furthermore, I would like to extend sincere thanks to Kadir Aytac Mutlu for the valuable insights when discussing my results and advice with data analysis. Your generosity in sharing your time to assist me is greatly appreciated. I also want to thank Anna Maria Ostenrath for the technical support, I am truly grateful for your aid with the data analysis codes. Credit also goes to previous lab members whose ideas and findings make up the groundwork that the thesis is built on, especially Oda Bjørnevik Håheim and Ricarda Bardenhewer and their work with defensive behaviors.

Lastly, I want to thank my parents Inger Reidun and Audun for the boundless encouragement throughout this project. Your constructive feedback and advice helped me overcome challenges and turn them into accomplishments, and motivated me when I needed it. This project would not have been the same without you, and I am so grateful for your moral support.

Table of Contents

List of Abbreviations (or Symbols)

5-HT	5-hydroxytryptamine (serotonin)
5-HTP	5-hydroxytryptophan
AADC	Aromatic amino acid decarboxylase
AFW	Artificial fish water
AP-1	Activating protein-1
AR	Auto-reference
BH4	Tetrahydrobiopterin
BL	Baseline
cAMP	Cyclic adenosine monophosphate
CAS	Conspecific alarm substance
CB1954	Tretazicar
Da	Anterior zone of the dorsal pallium
DAG	Diacylglycerol
DAPI	4’,6-diamidino-2-phenylindole, blue fluorescent dye
Dc	Central zone of the dorsal pallium
Dl	Lateral zone of the dorsal pallium
Dm	Medial zone of the dorsal pallium
DMSO	Dimethyl sulfoxide
Dp	Posterior zone of the dorsal pallium
dpf	Days post fertilization
DR	Dorsal raphe nucleus
ERK	Extracellular signal-regulated kinases
fps	Frames per second
GAM	Goat anti mouse antibody
GAR	Goat anti rabbit antibody
GC	Griseum centrale
GCamp6s	Green fluorescent protein, calcium-binding protein calmodulin (CaM), M13
Hb	Habenula
IP_3	Inositol triphosphate
IPN	Interpeduncular nucleus
ISI	Inter-stimulus interval
ITI	Inter-trial interval
MAO-A	Monoaminergic oxidase A
MAPK	Mitogen activated protein kinase
mCherry	Red fluorescent protein variant derived from DsRed
MTZ	Metronidazole
NMDA-receptor	N-methyl-D-aspartate receptor
NT-test	Novel tank-test
PAG	Periaqueductal gray
PBS	Dissolved phosphate buffer saline
PBTx	Dissolved phosphate buffer saline + TritonX
pERK	Phosphorylated extracellular signal-regulated kinases
SERT, 5-HTT	Serotonin transporter
tERK	Total extracellular signal-regulated kinases
Tg	Transgenic

TPH	Tryptophan hydroxylase
Tph2	Tryptophan hydroxylase 2
UAS	Upstream activation sequence
VB-test	Vibration-test
VIB(1-6)	Vibration stimulus (1-6)
VP(1-3)	Vibration Protocol (1-3)
WT	Wildtype

1 Introduction

1.1 Defensive behaviors

1.1.1 Computation of defensive behaviors: fear and anxiety

Defensive behaviors are a range of action- and response patterns that are often associated with perceived danger or stressors. Being able to detect a threat and avoid it is an important defense mechanism against harm, which in turn enhances the organism's survival chances. Fundamental behavioral programs such as the fight-or-flight response are highly conserved across vertebrate species. For example, when escaping from a dangerous situation, fish flee the threat with a transient burst in swim velocity, whereas rodents seek hiding places [1]. The base requirements underlying these behaviors are that the organism must take in the sensory information from the environment, decipher these inputs, process the danger of the situation, compute the appropriate response, and execute the planned actions. This is why threat assessment is a crucial prerequisite for the expression of defensive behaviors.

The aversive brain system enables organisms to not only react to an acute threat in the present moment, but also to adapt their actions based on their evaluation of potential dangers in the future. In this way, the defensive system contributes to a dynamic and proactive approach to survival and self-preservation. Although these internal states are tightly connected and may sometimes overlap in certain situations, this thesis will use the terms "fear" and "anxiety" to distinguish the two nuances of defensive behaviors. The initial fear behaviors in response to an immediate danger will be referred to as "fear-like" defensive behaviors. On the other hand, behaviors that are more passive and suggestive of foreboding or apprehension in anticipation of an incoming danger (often after a threat has ceased), will be referred to as "anxiety-like" defensive behaviors. The reason for this distinction is the knowledge that the computation of responses associated with defensive behaviors are represented differently in the brain: fear and anxiety are modulated by different functional brain regions, through different neural circuits and cellular components, and affected by distinct pharmaceuticals and stimulations [2-8].

1.2 The serotonergic system

1.2.1 Serotonin

Serotonin is a versatile chemical compound that can function as a hormone, mitogen, or neurotransmitter, exerting influence in the central nervous in addition to a range of peripheral processes [9]. Within the brain, the serotonergic system does not only contribute to physiological homeostasis like cardiovascular regulation, respiration, and thermoregulation, but it also plays a role in a wide spectrum of behavioral functions. Indeed, the system has been found to modulate mood, circadian rhythm, feeding,

arousal, pain sensitivity, and learning [9, 10]. Abnormal regulation of the system is linked to various psychiatric conditions and affective disorders, including depression, anxiety disorders, obsessive-compulsive disorder, eating disorders, and substance abuse [10]. Thus, studying the neurobiology of this circuit may improve our understanding of emotional behavior and elucidate the mechanisms behind related human affective disorders.

This multifaceted neural circuit influences target brain regions mainly through the modulation by serotonin. Serotonin is a monoaminergic neurotransmitter derived from the amino acid tryptophan. The neuromodulator is synthesized through two successive chemical reactions: first, tryptophan is converted into 5-hydroxytryptophan (5-HTP) by the enzyme tryptophan hydroxylase (TPH) and its cofactor tetrahydrobiopterin (BH4); subsequently, this intermediate compound is decarboxylated by the enzyme aromatic amino acid decarboxylase (AADC) to form 5-hydroxytryptamine, also known as serotonin (5-HT) [8, 11-13]. An overview of these reactions is illustrated in Figure 1.

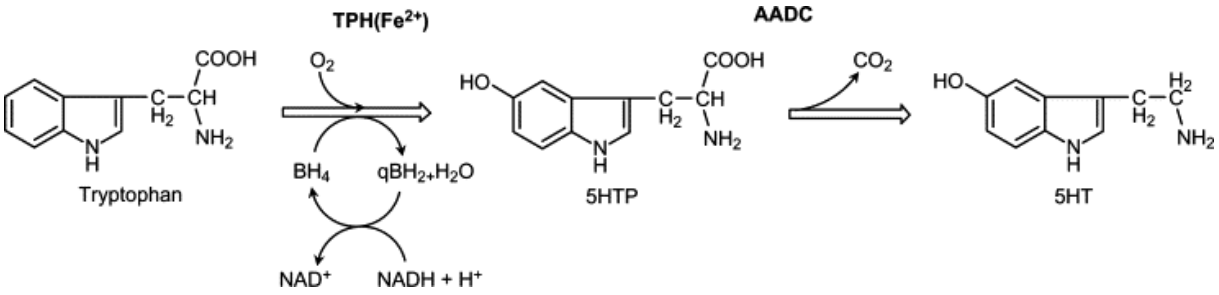

Figure 1: The two-step reaction converting the amino acid tryptophan to the neurotransmitter serotonin. *A hydroxyl group (-OH) is added to tryptophan by the enzyme TPH and the cofactor BH4. The carboxyl group (-COOH) on the resulting 5-HTP intermediate is then removed by the enzyme (AADC), yielding serotonin (5-HT). Adapted from Maximino, 2012 [8].*

Neurotransmitter delivery of serotonin is achieved through chemical transmission between a presynaptic and a postsynaptic cell, which is shown in Figure 2. Serotonin stored in synaptic vesicles is released from the axon terminal into the synaptic cleft, and can bind to serotonin receptors on the postsynaptic cell membrane [9]. It can also bind to serotonin autoreceptors in the presynaptic neuron, which acts as a feedback mechanism to inhibit further serotonin release [14, 15]. Lastly, serotonin transporters (5-HTT, SERTs) mediate neurotransmitter removal from the synaptic cleft and back into the presynaptic membrane. Once inside the presynaptic cell, the enzyme monoamine oxidase-A (MAO-A) breaks down the serotonin.

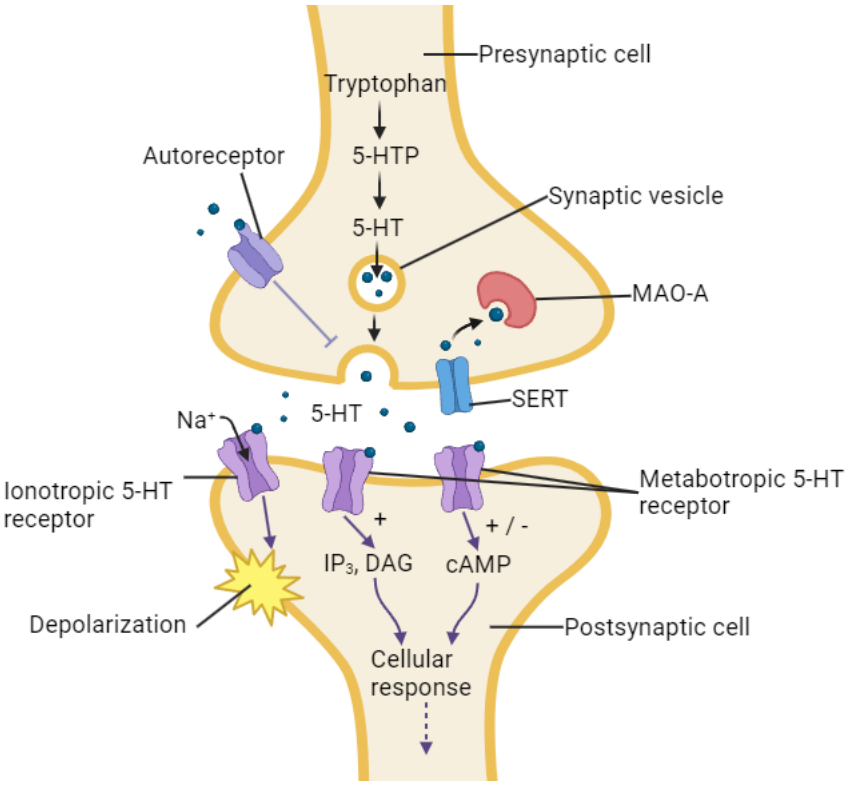

Figure 2: Illustration of synaptic transmission of serotonin. *The figure shows synthesis of serotonin and storage in synaptic vesicles in the presynaptic cell, and its release into the synaptic cleft. Serotonin can bind to ionotropic 5-HT receptors and cause depolarization of the postsynaptic cell membrane. Or it can bind to postsynaptic metabotropic receptors to modulate cellular responses through the increase or decrease of second messenger levels (IP_3, DAG or cAMP). Binding to presynaptic autoreceptors causes feedback inhibition of further serotonin exocytosis. Presynaptic SERTs remove serotonin from the synaptic cleft, where it is broken down by MAO-A. Illustration made with BioRender.com.*

In the serotonergic system, synthesis of serotonin is facilitated by serotonergic neurons found in the raphe nuclei of the brainstem. These neurons express the gene for tryptophan hydroxylase 2, *tph2*, and communicate with their target areas by synaptic transmission via serotonergic innervations. The raphe nuclei and their roles in defensive behavior will be discussed in more detail in the following section.

1.2.2 The dorsal raphe

The raphe nuclei are clusters of cells, many among them being serotonergic neurons, that are located in the brainstem (Figure 3) [16, 17]. These nuclei can be categorized into two groups along their rostro-caudal expansion and have ascending projections to the forebrain and descending projections to the brainstem and spinal cord [15]. The caudal group is located in the caudal pons and medulla, and comprises three nuclei: the raphe magnus nucleus, the raphe obscurus nucleus and the raphe pallidus nucleus, which predominantly innervate the brain stem and spinal cord [18-20]. Efferent processes from the caudal group are involved in nociception and motor tone [9].

Conversely, the rostral group is located in the midbrain and rostral pons, and encompasses the caudal linear nucleus, dorsal raphe nucleus (DR), medial raphe nucleus,

and the raphe pontis nucelus [18-21]. These nuclei have extensive projections to forebrain regions, including the prefrontal cortex and primary somatosensory cortices (mainly terminating in layer IV), and subcortical areas such as the hypothalamus, hippocampus and amygdala. Serotonergic input from this group contributes to stress response, emotion, and the modulation of appetite, sleep/wake cycles and arousal.

The rostral group contains approximately 85% of the brain's serotonergic neurons, and within these, the DR constitutes the largest portion, accounting for approximately one third of the entire serotonergic system [18]. The DR has been found to be a key player in mood regulation, anxiety, pain sensitivity, food intake and arousal. In the context of defensive behaviors, serotonergic innervations to the amygdala and the periaqueductal gray (PAG) have been shown to regulate threat responses. However, the effect on the target sites is not uniform, but rather dependent on several factors, one which is the type of serotonin receptor that is expressed on the postsynaptic cell.

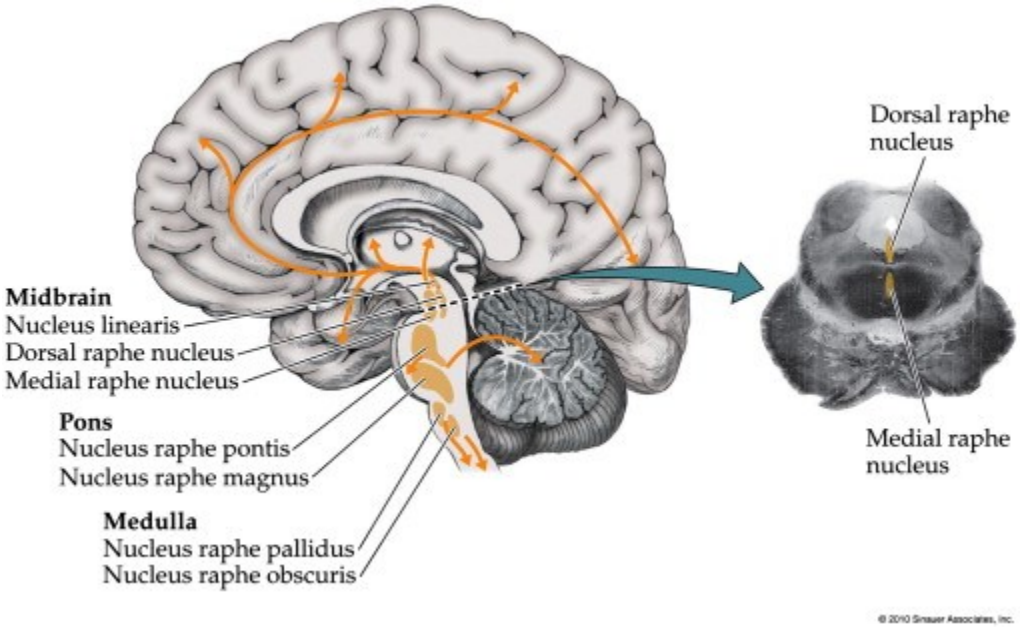

Figure 3: Figure of the raphe nuclei in the human brainstem and their projections. *Sagittal view of the human brain illustrating the location of raphe nuclei in the brainstem. Efferent connections for the nuclei are visualized by the orange arrows. A cross-section view of the brainstem at the level of the pons is provided on the right for a closer look at the dorsal and medial raphe. Figure from Blumenfeld, 2002 [21].*

There are seven different subclasses of serotonin receptors, 5-HT_1 – 5-HT_7 [22, 23]. Six of these are metabotropic, involving intracellular signal transduction through G-protein-coupled receptors and second messengers, whereas type 3 receptors are ionotropic with Na^+/K^+-channels. Ligand binding of serotonin to 5-HT_3 receptors on the postsynaptic membrane causes depolarization of the cell. The metabotropic receptors give either excitatory or inhibitory responses upon ligand binding, achieved through the upregulation or downregulation of second messenger levels, respectively. Activation of receptors 5-HT_4, 5-HT_6 and 5-HT_7 leads to increased levels of the second messenger cAMP, which enhances the intracellular signaling cascade; conversely, activation of 5-HT_1 and 5-HT_5 receptors is associated with lower cAMP levels and weakening of the signal transduction. Finally, activation of the 5-HT_2 receptor type leads to increased levels of the second

messengers IP_3 and DAG, which enhances the cellular responses. With the extent of serotonergic projections from the raphe nuclei, as well as the variety of serotonin receptors, it becomes evident that mapping the full extent of this circuit is a challenge.

To add to the complexity of the serotonergic system, serotonin release from the DR has been found to exact opposing behavioral effects, eliciting both anxiolytic as well as anxiogenic responses [24-28]. Sanford Kiser and colleagues demonstrated that serotonin roused anxiolytic responses in rats: the fear-like escape behavior induced by PAG-stimulation became suppressed upon stimulation of serotonergic DR-neurons (Sanford Kiser et al., 1980). On the other hand, a positive correlation between serotonin and defensive behaviors in rats was observed by Wise et al. and later by Hodges et al., as they observed that pharmacological inhibition of serotonin levels with benzodiazepines lead to the decrease of anxiety-like behavior [27, 28].

These discoveries lead Deakin and Graeff to propose their "dual role" hypothesis in 1991, suggesting that serotonin acts as a key modulator on separate target structures in the aversive brain system, thus enabling the organism to express a range of defensive behaviors in response to different situations [29, 30]. They postulated that serotonin released from the dorsal raphe activates metabotropic 5-HT_2 receptors and ionotropic 5-HT_3 receptors found in the amygdala, which promotes the anxiety-like defensive behaviors modulated by this region. Conversely, they suggested that serotonergic input to the periaqueductal gray (PAG) activates metabotropic 5-HT_{1A} and 5-HT_2 receptors, which causes inhibition of the fear-like defensive behaviors mediated by this brain area. Hence, the result of serotonin release can lead to an anticipatory-like state of anxiety, that lets the organism avoid an approaching danger without triggering panic-associated fight-or-flight responses. A schematic view of these two roles of serotonin is illustrated in Figure 4.

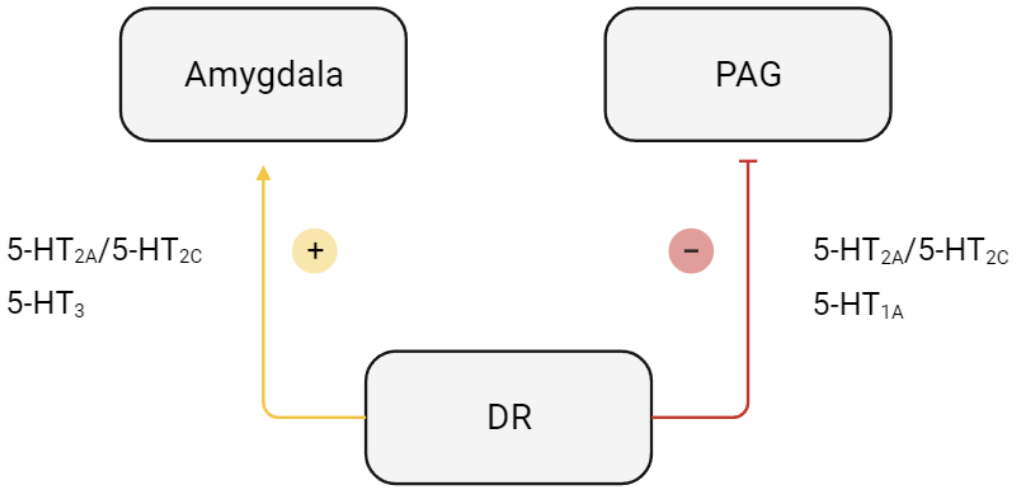

Figure 4: Illustration of Deakin and Graeff's "dual role" hypothesis of serotonin in the aversive brain system. *In the amygdala, serotonin from the DR increases anxiety-like defensive responses through the activation of 5-HT_{2a}, 5-HT_{2c} and 5-HT_3 receptors. In the PAG, serotonin from the DR decreases fear-like defensive responses by the activation of 5-HT_{2A}, 5-HT_{2C} receptors and the inhibitory 5-HT_{1A} receptor. Adapted from Maximino, 2012 [8]. Illustration made with BioRender.com.*

Later research corroborates elements of the Deakin and Graeff hypothesis [31-33]. In rats, chemical stimulation of the ventrolateral DR, which projects to the ventrolateral PAG, was found to inhibit panic-like escape behavior [34]. And injection of 5-HT_{1A} receptor agonists directly to the dorsal PAG has been shown to impair escape behavior, while receptor antagonists could restore escape in DR stimulated animals [35, 36]. Anxiogenic properties linked to DR serotonergic innervations to the amygdala have also been demonstrated. Rats exposed to a mildly anxiogenic open-field arena were shown to have increased neuronal activity in serotonergic neurons in the DR as well as projections to the basolateral nucleus of the amygdala by c-Fos protein expression measurements [37]. Moreover, these regions were also activated by anxiogenic drugs in rats that were not exposed to a novel environment nor any aversive stimuli, and this caused the animals to display increased defensive behaviors [38, 39].

Lastly, yet another determining factor of serotonin effect is the environmental conditions the organism is exposed to, for instance the level of control the animal has over the aversive stimulation. Studies in rats have shown that the extent of serotonin release was higher when the animals were exposed to a series of inescapable electric shocks as opposed to escapable ones [7, 40]. Furthermore, it has been observed that inhibitory 5-HT_{1A} autoreceptors in the DR were weakened in response to uncontrollable tail shocks in rats, thereby causing increased serotonin release [41]. Taken together, such findings could indicate that the mechanism of feedback inhibition of DR serotonin release might become desensitized in response to uncontrollable and unavoidable aversive conditions, thereby enhancing the defensive behavior in response to stimulation.

1.3 Zebrafish as a model organism

1.3.1 Functional similarities between zebrafish and mammalian brains

The zebrafish nervous system bears many anatomic and physiologic similarities to other vertebrate species due to evolutionary conservation across the Vertebrata subphylum. In terms of the forebrain architecture, the dorsal portion of the telencephalon is called the pallium in teleost species. By utilizing molecular markers and various labeling techniques, several subregions within this structure have been revealed to share features such as connectivity, topography, and functional roles with mammalian brain regions [42-45]. The zebrafish's medial (Dm), central (Dc) lateral (Dl), and posterior (Dp) dorsal pallial areas have been demonstrated to be regions homologous to mammals, namely the pallial amygdala, isocortex/neopallium, hippocampus, and piriform cortex respectively [43, 46-49]. Figure 5 shows the subregions of the zebrafish pallium as well as their mammalian homologs. The Dm has limbic-like functions in fear conditioning, avoidance behavior, motivated behavior, and emotional learning and memory [48, 50-53]. The Dc matches topographically with the dorsal pallium division found in other vertebrate species, and the neocortex in mammals [43]. The Dl is reminiscent of the mammalian hippocampus with implication in for example spatial and temporal memory [48, 51]. Meanwhile, the Dp is involved in processing of olfactory sensory information [54].

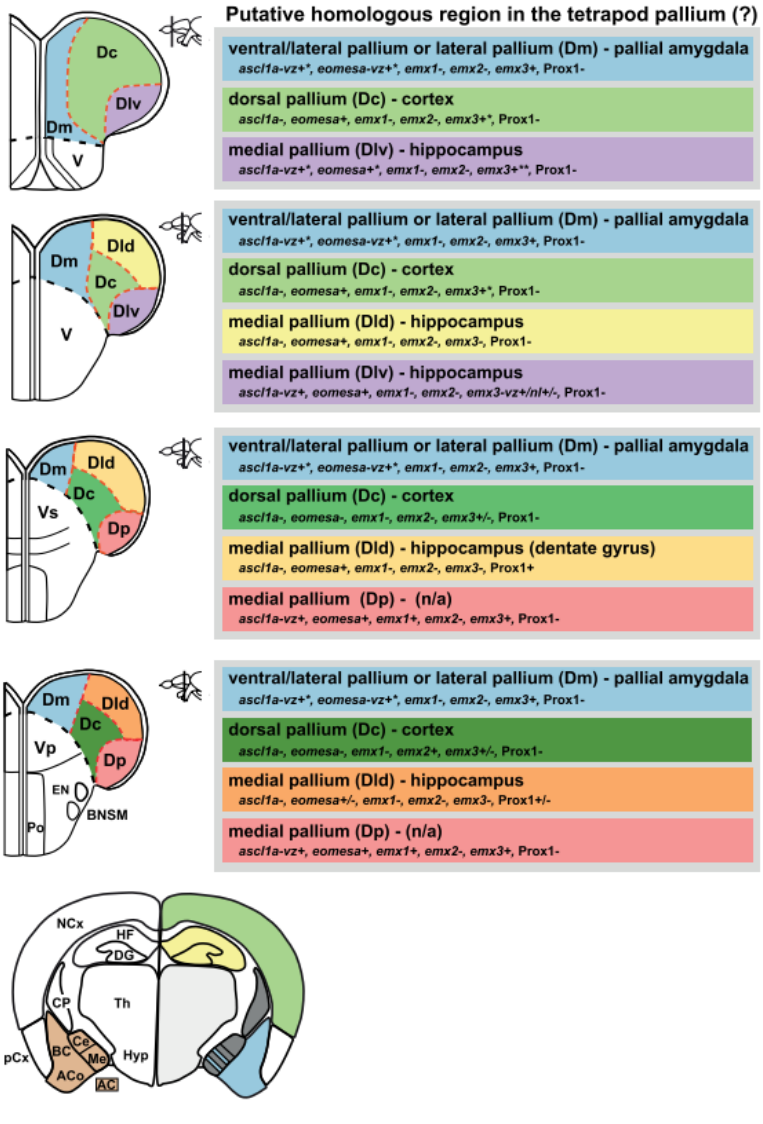

Figure 5: The distinct zones of the pallium (dorsal telencephalon) in adult zebrafish. *Left figure: coronal sections of the of the adult zebrafish brain illustrating regions speculated to be homologous to mammalian brain areas. The top panels show the anterior part of the brain, and the below panels show more posterior parts of the brain. Figure adapted from Ganz et al., 2014 [42]. Right figure: Z-projected image of the dorsal telencephalon in juvenile zebrafish depicting different brain areas in the horizontal plane. Abbreviations of zebrafish dorsal pallium zones: anterior (Da), lateral (Dl, and its posterior region Dl_p), central (Dc), medial (Dm, and its posterior part Dm_p) and dorsal (Dd). The medial and lateral habenula (Hb) in the diencephalon are terms relative to the image, and do not refer to the mammalian Hb subregions, nor their homolog structures in zebrafish (dorsal Hb and ventral Hb, respectively). The raw image was obtained by Zeiss LSM confocal imaging, which was processed in Fiji (ImageJ) and delineated in MATLAB by Bram Serneels (unpublished work [55]). The area of focus is described by the image at the top, and was obtained from Z Brain [56].*

Serotonin in zebrafish is produced in the raphe nuclei, but also in two other neuron populations, namely the hypothalamic region and the pretectal area (Figure 6) [57]. Here, serotonin is involved in sleep as an intermediate compound for melatonin synthesis in the pineal glands, and in the integration and processing of visual sensory input within the optic tectum [57, 58]. Regarding defensive behaviors, the aversive brain system is functionally conserved in teleost species [59]. As mentioned, the Dm is homologous to

the mammalian amygdala in terms of function and connectivity. This forebrain region is innervated by the zebrafish DR. And as with the mammalian system (Figure 4), serotonergic input via this circuit is associated with anxiogenic behaviors that increase anxiety-like responses [60]. Furthermore, the key mammalian structure facilitating fear-like defensive behaviors, the PAG, also has a functional homolog in zebrafish, which is the griseum centrale (GC) [61]. This structure is found in the interpeduncular nucleus (IPN) of the mesencephalon [62]. Moreover, a circuit involving the habenula, IPN and GC is thought to mediate freezing response in zebrafish [63]. As a target region of the serotonergic circuit, the GC serves an analogous function to the PAG in the aversive brain system: DR serotonergic input to the GC exacts anxiolytic effects on the zebrafish defensive phenotype by decreasing panic-like responses [60].

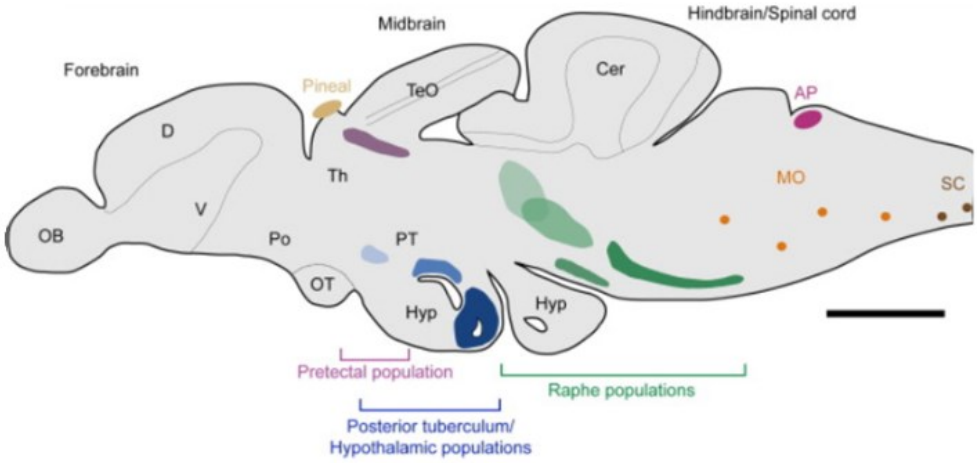

Figure 6: ***Schematic illustration of the serotonergic neuron populations in the adult zebrafish brain.*** *The figure shows a sagittal view of the zebrafish brain where the main three brain regions that express* tph2 *and thus synthesize serotonin are indicated by colored brackets. From anterior (left) to posterior (right): the pretectal area (pink), the hypothalamic region (blue) and the raphe nuclei (green), and the clusters belonging to each of these three populations are labelled in matching colors. The scale bar in the bottom right corner is 500 µm. Abbreviations in the figure are olfactory bulb (OB), dorsal telencephalic area (D), ventral telencephalic area (V), preoptic region (Po), optic tract (OT), thalamus (Th), optic tectum (TeO), posterior tuberculum (PT), hypothalamus (Hyp), cerebellum (Cer), area postrema (AP), medulla oblongata (MO), spinal cord (SC). Figure from from Lillesaar, 2011 [57].*

In fact, recent work of Lima-Maximino et al. elaborated further on Deakin and Graeff's "dual role" of serotonin in zebrafish by viewing its modulation as a switch-like function in the aversive brain system [29, 60]. An illustration of this system can be seen in Figure 7. Their theory suggested that a shift in serotonin release pattern from phasic to tonic enables the organism to transition from an active coping mechanism into a passive coping mechanism. When a threat arises, phasic serotonin promotes initial panic-like responses. But once the threat ceases, the aversive brain system switches to tonic serotonin release. This leads to inhibition of the previously promoted acute fear-like behaviors, and instead the activation of anxiety-like behaviors to assess if the danger really has passed. Through their zebrafish studies, they discovered that following the initial fear-like reaction to conspecific alarm substance (CAS), the fish exhibited reduced

mobility in the form of freezing and cautious swimming near the tank's bottom, which are typical anxiety-like behaviors for the species.

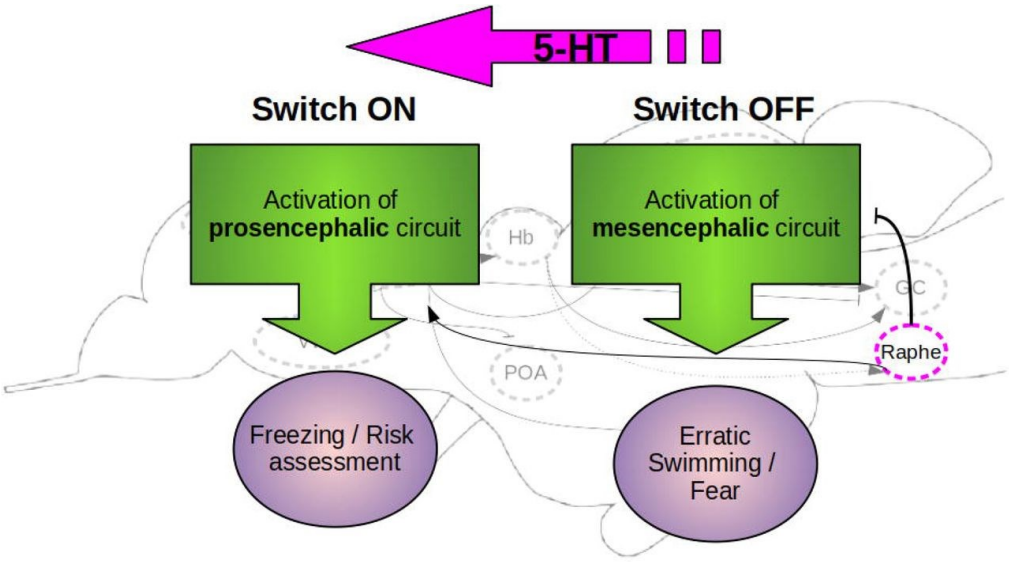

Figure 7: Illustration of the "switch"-like modulatory role of DR serotonin in zebrafish defensive behaviors during and after threat exposure proposed by Lima-Maximino et al. *The fish swims erratically in a fear-like manner upon aversive stimulation, but this decreases as the danger recedes. After stimulus exposure, the fish displays anxiety-like freezing behavior. Transition from phasic to tonic release of serotonin in the DR engages the switch from OFF to ON, leading to inhibition of initial fear responses in the mesencephalon and enhanced anxiety-like risk-assessment in the prosencephalon. Abbreviations: habenula (Hb); preoptic area (POA); griseum centrale (GC). Figure from Lima-Maximino et al., 2020 [60].*

1.3.2 Advantages of zebrafish as a model organism

Zebrafish (*Danio rerio*) has proven to be an excellent model organism for studying medical conditions and clinical disorders [64-68]. Some advantages of this animal's application in research lie in the species' small size, ease of reproduction, cheap maintenance, genetic similarities to mammalian models and ethical concerns. Firstly, the zebrafish is a teleost fish, and therefore a vertebrate species. The adult organism reaches 3-5 cm approximately four months after hatching, at which point they can produce offspring. Once sexually mature, they are fertile throughout the whole year for almost their entire adult lifespan. The female can spawn every week, yielding a clutch size of several hundred eggs per breed. Furthermore, the pace of embryonic development is quick, as organs are formed already 1 day post fertilization (dpf), and the eggs hatch by the third day [69]. Zebrafish husbandry is therefore cost-effective and promotes sustainable research practices: their small size and short development time significantly reduce the resources and space required to house them compared to larger animals. Furthermore, the organism is transparent during development, enabling non-invasive observation of embryo development including the expression of fluorescent genes, as well as at the larval and juvenile stage [70]. The small size and transparency during these stages enable in vivo imaging of the entire brain at single-cell resolution. This is a

huge advantage over larger mammalian models, where imaging is often limited to only a subset of neurons or a certain brain area.

The zebrafish also boasts a large egg size at the one-cell stage, which is convenient for experimental manipulations directly in the fertilized egg. The availability of animals on demand due to the rapid reproductive cycle and big clutch size, in combination with easy microinjection, makes zebrafish exceptionally amenable for genetic engineering [71, 72]. The whole zebrafish genome is sequenced and has been found to contain many genes encoding functionally active proteins that coincide with mammalian genes. In fact, the work of Howe and colleagues shows that zebrafish have ortholog genes of 71% of human genes and 82% of human disease-related genes [73]. Consequently, a vast selection of transgenic fish lines has been established, many of which model human conditions due to topologic and physiologic conservation among vertebrate species [74].

Lastly, the zebrafish is an approved model organism under EU Directive 2010/63/EU for scientific research. Being vertebrates with a less complex nervous system than higher vertebrate species such as mammals, they may perceive reduced pain and suffering during experiments. Additionally, their small size allows for less invasive techniques, which also decreases the study severity. Zebrafish as a model organism may therefore be a more ethical option than selecting higher vertebrate species.

1.3.3 Experimental approaches for zebrafish defensive behavioral studies

There are several ways to study defensive behaviors, one of which is to introduce the organism to novelty. The animal typically expresses anxiety-like defensive behaviors in confrontation with sources of unknown potential threats [8]. For rodents, a commonly used approach is the open field test, where the animals are placed in a large unfamiliar arena [75, 76]. Locomotion, defecation and behavioral traits can be measured as indications of anxiety-like behaviors, for example freezing and staying near the walls of the arena (thigmotaxis) [76, 77]. The novel tank test (NT-test) is a similar novelty experimental paradigm developed for zebrafish [78]. From an evolutionary perspective, staying out in the open and near the water surface makes the fish vulnerable to predators, so keeping to the bottom and along edges is a defensive measure against danger. In juvenile and adult animals, the NT-test typically promotes responses associated with anxiety-like defensive behaviors such as bottom-diving, freezing and bottom-dwelling during the first 5-10 minutes of the assay, followed by cautious exploration upon habituation to the tank [79-82].

Another way to study zebrafish defensive behavior is to expose them to aversive stimuli such as etiologically relevant alarm substances, electric shocks or mechanic vibrations [78]. For juvenile and adult animals, a mechano-acoustic vibration elicits fear-like startle responses, followed by anxiety-like risk assessment behavior: upon stimulation, the fish will typically escape with a burst in swim speed as they dive down in the tank, and then proceed to bottom-dwell and reduce their locomotion (freeze) in the wake of the stimulus [60, 81, 83, 84]. In the lab, we aim to promote defensive behaviors in a standardized way with our experimental paradigm for freely behaving juvenile zebrafish. Recent master theses in the lab studied the effect of chemo-genetic DR ablation as well as anxiogenic and anxiolytic pharmaceutics on defensive behaviors in juvenile zebrafish with the NT-test as well as a mechano-acoustic vibration test (VB-test) with a previous lab

setup [85, 86]. The aversive VB-test in these works applied a stimulus with a duration of 0.5 s and a strength of 6 V. Other unpublished lab work on defensive behaviors utilized the same two behavioral assays, but with the current lab setup (Zantiks LT) to investigate zebrafish behaviors in a defensive context [55]. Here, three different stimulus types categorized as "mild", "medium" and "strong" were used, where the "strong" stimulus had a duration of 0.84 s and a frequency of 238 Hz and elicited the strongest defensive responses.

1.3.4 Experimental approaches for zebrafish brain activity measurement

To map the neuronal activity of the fish without disturbing their behavior, one possibility is to perform a post-hoc immunohistochemical analysis [56]. This is accomplished by addition of an antibody to the sample with a high affinity for the element of interest (antigen). Subsequently, a second type of antibody expressing a fluorescent tag is added. This secondary antibody specifically binds to the primary antibody, thereby labelling the element it is bound to [87]. Finally, visualization of the labelled target is attained by confocal microscopy, which gives a volumetric snapshot of the fluorescence signal in the entire zebrafish brain at the time of fixation. This method can stain three additional elements by selecting other sets of antibodies that specifically bind to their respective target and have distinct fluorescent markers whose signal wavelengths do not overlap.

Furthermore, traces of intracellular signal transduction can act as a footprint of the transpired neuronal activity. Following synaptic transmission and activation of the NMDA-receptor, one such signaling pathway is the mitogen-activated protein kinase (MAPK) cascade. Here, phosphorylation of the extracellular signal-regulated kinase (ERK) is one of the final steps. Once active, it can phosphorylate transcription factors such as activating protein-1 (AP-1), which in turn leads to gene expression of for example *c-Fos* [88-90]. Immunostaining of ERK and pERK and the resulting fluorescence intensity ratio between pERK and total ERK (tERK) amount can therefore be a measure of neuronal activity [56, 87, 91]. Since ERK and pERK remain intracellular, this approach yields a single-cell imaging resolution. However, the temporal specificity is poor due to the delay between the synaptic transmission and the signaling cascade activation. The signal peaks at about 5-15 minutes after the activity occurred [56, 92]. mRNA of the immediate early gene *c-Fos* or even c-Fos protein are other commonly used staining targets, but have even lower temporal specificities due to their downstream position in the signal pathway relative to ERK phosphorylation [91, 93, 94].

Another approach to acquire information about neuronal activity is by calcium imaging. This method measures the signal from transgenic induced calcium indicators through a multiphoton microscope *in vivo [*95*]*. Advantages of this method over post-hoc analysis is its high temporal sensitivity, as data from calcium imaging is sampled during the experiment in awake behaving animals and as a whole recording rather than one frame in time. But unlike the volumetric imaging of the zebrafish brain, this method is limited to only one horizontal plane of focus. Additionally, the head of the animal must be fixed for imaging and thus they cannot express behaviors freely.

1.4 Aim of the thesis

This project aimed to improve the experimental design for studying defensive behaviors in freely behaving juvenile zebrafish. Subsequently, I aimed to employ this methodology to investigate the behavioral effects of serotonergic manipulation on the behavior as well as the neuronal activity. To achieve this, I sought to optimize the mechano-acoustic stimulus used in the vibration assay of the behavior experimental protocol. Afterward, I would perform behavioral experiments on juvenile zebrafish with ablated serotonergic DR-neurons to investigate the effect of serotonergic manipulation on the defensive behavior. Lastly, I sought to analyze the neuronal activity in these ablated fish by immunostaining of the pERK/tERK ratio.

1.4.1 Optimization of the mechano-acoustic stimulus in the vibration test

For the vibration test of my behavioral studies, I used the Zantiks LT setup to deliver different mechano-acoustic stimulus types to the juvenile zebrafish. The system enables the expression of a large range of behaviors in zebrafish, which full extent had not been investigated within the lab. Experimental paradigms utilizing the most optimal setup conditions, among them the stimulus properties, would prompt stronger and more robust stereotypical responses in our research animals. The first experiment in this project therefore aimed to assess the potency of a selection of such vibration stimuli in juvenile zebrafish. Implementing the ideal stimulus in future experimental protocols would improve data quality and provide a reliable fundament for assessing our research questions. An optimized protocol would not only validate the construct of my next experiments, but it could also benefit future behavioral studies with this setup. Previous work in the lab with the Zantiks setup utilized three vibration stimuli characterized as "mild", "medium", and "strong" based on their duration and frequency, and were found to elicit unequal defensive behaviors, where the "strong" stimulus evoked the most pronounced responses [55]. I therefore hypothesized that the various stimulus types would elicit different degrees of defensive behaviors, and furthermore that long duration and high frequency stimulus types would elicit the most prominent responses.

1.4.2 The effect of DR-ablation on the defensive behavior

The DR constitutes the primary site for serotonin synthesis in the brain and plays a key modulatory role in defensive behaviors through their serotonergic innervations [3]. The DR in zebrafish has anxiogenic and anxiolytic effects through their projections the amygdala homologue Dm and the PAG-homologue GC, respectively [29, 31, 37]. A dynamic interaction between these structures has also been proposed as a mechanism for a highly flexible defensive system that enables the organism to trigger a fear-like response in confrontation with immediate danger, but initiate an anxiety-like state of risk-assessment once the threat subsides [60]. Previous research has also shown that prolonged exposure of aversive stimulation serves to desensitize the animals' immediate fear reaction [83, 96]. Based on this, I expected the DR-animals to have a stronger initial defensive response to aversive stimulation than controls. I also hypothesized that control

animals would habituate their fear-like response to the repeated stimulus delivery. Finally, I hypothesized that the DR-ablated fish would express less anxiety-like behavior in the NT-test and in the wake of each individual stimulus in the VB-test. This would cause them to display a quicker tank habituation in the NT-test and intra-stimulus habituation in the VB-test compared to the control animals.

1.4.3 Effect of DR-ablation on the neuronal activity

For the neuronal activity analysis, I expected my results to align with previous lab work with vibration stimulation of DR-ablated animals, which was obtained through pERK immunostaining and 2-photon calcium imaging. These findings demonstrated that the forebrain generally exhibited decreased neuronal activity in DR-ablated animals compared to control animals in response to aversive mechano-acoustic stimulation [85, 86, 97]. Therefore, I hypothesized that animals lacking serotonergic modulation from the DR would have less neuronal activity in their dorsal telencephalon (pallium) as well as the habenulas of the diencephalon. Moreover, since serotonergic input to the medial zone of the dorsal pallium (Dm) produces anxiogenic responses in healthy fish, I especially expected this telencephalic region to harbor less neural activity in DR-ablated animals compared to the controls [37, 38].

2 Methods

2.1 Research animals

2.1.1 Compliance with ethical legislation and animal handling qualifications

The zebrafish is an approved model organism according to the EU legislation. For research involving animals, teleost species are considered lower vertebrates compared to that of other popular mammalian models such as rodents. Thus, regarding animal welfare, the use of *Danio rerio* for scientific purposes contributes to the replacement ideal of the "Three R's" (refine, reduce, replace): while research animals are not excluded from the project, it is favorable to use lower ranking vertebrate models to achieve the same quality data.

The experiments performed as part of the project comply with the national legislation for animal research provided Norwegian Food Safety Authorities (NFSA). Approval from the relevant authorities was granted from NFSA through their digital FOTS-application system, and from the veterinarian at Kavli Institute for Systems Neuroscience.

To handle and perform research with zebrafish, I have undergone theoretical education and practical training equivalent to the FELASA C course. The theoretical qualifications were attained through the course "NEVR8014 – Laboratory Animal Science for Researchers / Course in Animal Research in Norway (CareIn)" taught at NTNU. Practical requirements were fulfilled by training and assessment from a lab instructor, with the approval of the institute veterinarian. With these qualifications, I was responsible for the breeding, raising and general maintenance of the fishlines involved in the thesis, in addition to performing the actual experiments and sacrificing the animals thereafter.

2.1.2 Zebrafish breeding, husbandry and handling

The zebrafish are raised and kept in the lab's fish facility, which is approved by the NFSA. The animals are housed in separate 3.5 L plastic water tanks that are connected by a Tecniplast ZebTec Multilinking System that controls the water quality to ensure optimal conditions close to the animals' natural environment. In accordance with existing guidelines for zebrafish husbandry [98], tropical water is simulated by keeping the water alkalinity at pH=7, oxygen concentration at 6.0 ppm O_2, conductivity at 300-1200 µS, and temperature at 28 °C. The facility simulates the zebrafish's native habitat in terms of light intensity and the light-to-dark hour ratio (14:10 h). The feeding schedule alternates between dry flake food or live *Artemia nauplii* to provide a balanced diet and enrichment in the form of predation behavior.

The animals in my project were born 3 weeks in advance of the behavioral experiments. Parent fish were transferred to special breeding tanks, with a sloped tank filter for the

eggs. The filter mimics shallow shores, which constitute the natural spawning sites of the species and promotes natural breeding behavior. The eggs are typically laid in the morning, simulated by the onset of light in the facility. The parent fish were returned to the system tanks the next day, and the eggs were collected with a strain and washed with AFW. The eggs were raised in an incubator on petri dishes containing special egg water (0.1% methylene blue in AFW). The medium was exchanged every day, and substituted with regular AFW on the third day, when the eggs hatched into larvae. After 5 dpf, the larvae were transferred to the main facility with a special nursery filter in the regular tank. Animals were split over several tanks to prevent issues from crowding and keep consistent growth rates.

The data collected in this thesis are derived from zebrafish aged 21-28 dpf. A sample number of 30-36 was considered satisfactory to yield statistically significant results. At 3-4 weeks old, the fish are in the transition between the larval and juvenile developmental stages. Animals of middle to large size, approximately 9-10 mm long, were therefore picked for use in experiments in favor of their smaller siblings. Selection based on size rather than age was supported by the fact that individuals, even if born of the same cross and raised in the same tank, show great differences in development rate. Ensuring consistency of the animals within a sample was important because size differences impact the zebrafish's mobility and thus behavior, as well as the brain size and morphology for further immunostaining steps. Additionally, refinement of the experimental group complied with the ideals of animal welfare and was a measure to improve the quality of the data.

2.1.3 Transgenic zebrafish lines with the Gal4;UAS gene manipulation system

In addition to ordinary wildtype fish, the genetically modified fishlines used in my project were as follows: *Tg(tph2:Gal4;UAS:ntr-mCherry)* and *Tg(tph2:Gal4;UAS:GCamp6s)*. The genetic backgrounds of these animals were already well established within the lab and had several generations available for breeding. Common for both was that they were developed with the binary Gal4;UAS transgenic system. Organisms developed through this method have targeted gene expression in a subset of their tissues depending on their engineered genetic background.

The Gal4 protein is derived from yeast and contains a DNA-binding domain and a transcription activation domain [72]. This allows it to bind to a UAS (upstream activation sequence) enhancer to drive expression of genes located downstream. Subjecting the *Gal4* gene to the regulation of tissue-specific promoters will restrict its expression to a specific location in the organism. On the other hand, the effector gene can be introduced to the UAS-fishline under transcriptional control of the UAS, which is ubiquitously present in the organism's tissues but remains latent and inactive in the absence of Gal4. Therefore, by crossing a tissue-specific Gal4-fishline with a UAS-fishline, one can obtain doubly transgenic offspring whose UAS activation, and the subsequent expression of the effector gene, only occurs in a controlled subset of cells within the organism. A reporter gene, for instance a fluorescent dye, is usually introduced along with the effector gene to enable screening and measurement of the effector gene expression rate. When using this system, a possible degenerative side effect in the transgenic fish called "squelching" can

occur by the expression of a strong transcription activator, which can cause toxicity [72, 99]. Nonetheless, the Gal4;UAS system makes for a convenient and easy transgenic tool with high spatial fidelity and efficiency, and an illustration of this process can be seen in Figure 8.

For the zebrafish in my project, the *Tg(tph2:Gal4;UAS:ntr-mCherry)* and *Tg(tph2:Gal4;UAS:GCamp6s)* animals have tissue-specific Gal4 protein in cells expressing *tph2*, a tryptophan hydroxylase gene found in serotonergic neurons. Additionally, these lines have been engineered to express *Gal4* mainly in the DR and not in other serotonergic cells, except for some expression in the spinal cord [100]. For the *Tg(tph2:Gal4;UAS:ntr-mCherry)* fishline, the Gal4 protein activates transcription of the *ntr-mCherry* effector-reporter fusion gene explicitly in these cells, and thus production of the fusion protein of nitroreductase enzyme and the red/orange fluorescent dye mCherry in the DR (and some of the spinal cord). For the *Tg(tph2:Gal4;UAS:GCamp6S)* fish, Gal4 activates transcription of *GCamp6,* which leads to production of the green fluorescent protein GCamp6S only, because the fishline has no effector gene under the UAS element.

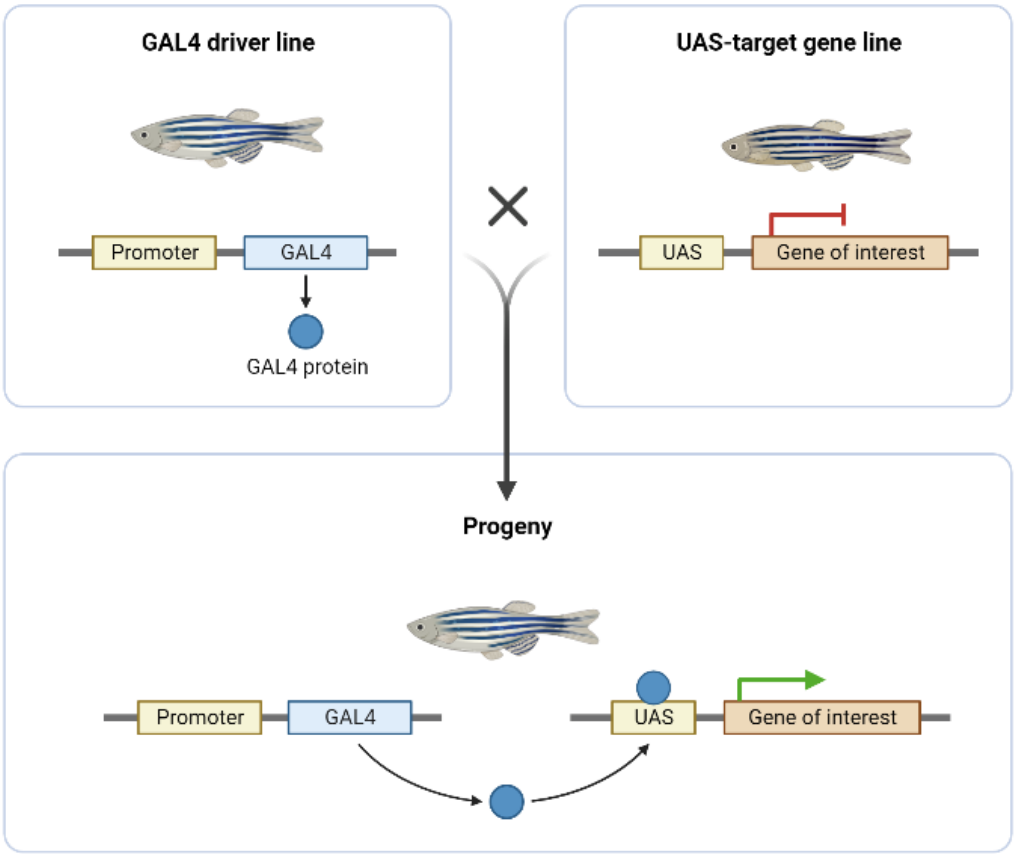

Figure 8: Illustration of the Gal4;UAS transgenic system in zebrafish. *Crossing a parent from a tissue-specific Gal4 line with a parent from a UAS reporter line gives rise to doubly transgenic offspring that express the effector gene in the targeted subset of cells. Adapted from [101] by BioRender.com.*

2.2 Chemo-genetic ablation

Specific ablation of serotonergic neurons expressing the *tph2* gene, which are primarily found in the DR in my transgenic fishlines, was achieved by a combinational approach of chemical drug administration and genetic engineering. The underlying mechanism in this technique is to deliver an inactive prodrug that requires catalyzation by an enzyme counterpart to activate its latent cytotoxic effect. Assuming the organism does not express this enzyme endogenously, ablation can be limited to a specific tissue by transgenic introduction of the enzyme gene to the targeted cells.

The enzyme nitroreductase was used for the purpose of this project, and was incorporated into the genome in tph2-expressing DR-neurons (and some cells in the spinal cord) through the Gal4;UAS transgenic approach described in the methods section 2.1.3. The genetic background for the animals undergoing ablation was *Tg(tph2:Gal4;UAS:ntr-mCherry)*. Thus, administration of prodrug ablated the serotonergic DR neurons and left the rest of the tissues intact (ablation in this fishline does not affect the animals' locomotion ability [100]).

In this project, MTZ (Sigma-Aldrich) was the prodrug substrate utilized for the ablation procedure. The active site of nitroreductase shows selectivity for several substrates, among them metronidazole (MTZ) and tretazicar (CB1954), and the metabolization products cause crosslinking within the DNA, which in turn facilitates apoptosis in the serotonergic neurons. However, an important difference between MTZ and CB1954 is the latter's ability to exact the bystander effect on neighboring cells where the CB1954-catalyzation product migrates and causes cell death in nearby cells, which is not desired for spatially specific cell destruction [102, 103]. On the other hand, MTZ prodrug catalyzation is restricted to the tph2-expressing neurons. However, high drug concentration and long treatment time may be detrimental to the animals, possibly causing unintentional cell death in the brain and even death of zebrafish larvae [103, 104].

Experimental approach is used was based on previous work in the lab [105] utilizing chemo-genetic ablation. This was a protocol adapted from Agetsuma and colleagues [63]. Drug concentration, exposure- and washout periods were decided based on optimization studies carried out by previous lab member Christoph Wiest. The fish were transferred to the lab area in AFW filled falcon tubes and then pipetted onto empty petri dishes. Drug solution containing MTZ and DMSO (Sigma-Aldrich) was added for the animals of the ablation group and MTZ-treatment control group. Placebo solution containing DMSO was added for the placebo group. Preparing ablation solution for one petri plate was done by adding 250 µL DMSO and 0.85 mg MTZ to a falcon tube and filling it up with AFW to the 50 mL mark (total concentration of 10 mM MTZ and 0.5% DMSO in AFW). DMSO is not essential for the prodrug's activation but acts as a solvent for the MTZ crystals, for a more effective delivery to the animals [103].

For the sham solution, only 250 µL DMSO was added to a falcon tube and filled with AFW up to 50 mL total volume. MTZ degrades in reaction to light, but all petri plates were protected from exposure regardless of content to keep the administration procedure consistent. The plates were wrapped in aluminum foil and stored at 28 °C overnight for a minimum of 24 h. The fish underwent an equal period of drug washout the following day: the petri dishes were discarded and exchanged with new ones filled solely with AFW. This

step did not require light protection, but a bit of flake food was added to the plates before placing them in the incubator overnight again. The fish were ready for experiments the next day and were taken directly from the petri dishes.

Screening with a fluorescent microscope was done when the fish were 3 dpf (days post-fertilization). Animals were selected for raising to be included in the experiment if they expressed their background's fluorescent marker at the expected target site in the DR. Larvae without clear expression patterns were sacrificed. Post-ablation screening was not performed before the behavioral experiments, as previous iterations of the protocol in the lab have verified the effectiveness of the ablation procedure. However, upon confocal imaging, all samples were checked for fluorescence patterns consistent with their genetic background and congruent with the received treatment (see methods section 2.4 and limitations section 4.5.2 for more information).

2.3 Novel-tank test and mechano-acoustic vibration assay with the Zantiks behavioral setup

2.3.1 The Zantiks experimental setup

Within the lab, the Zantiks experimental setup is currently the preferred method for studying zebrafish while they express their behavior freely, and this setup can accommodate zebrafish at the adult, juvenile and larvae life stage. The adult and juvenile Zantiks LT setup can study 6 fish per experimental trial in individual tanks. Images of this setup are presented in Figure 9. These had plastic containers have an interior XYZ-dimension of 10 cm x 11.5 cm x 3 cm. The front and back walls are transparent, to allow video tracking of the inside, but are black on their sides. To prevent mis-tracking of ripples at the water surface, the experimental arenas are covered with opaque tape on the top 2 cm. If the fish swim higher than the taped area, their movements will not be tracked by the system or incorporated in the dataset. The arenas are filled up to just above the border of the tape before each experiment to reduce the amount of untracked data.

The six tanks are slotted into the system's interior rack, three tanks in the upper row, and three tanks in the lower row. This configuration improves tank stabilization and proper alignment relative to the video camera, which is integrated into the setup behind the tank rack. The rotating motor that generates the mechano-acoustic vibrations is also fastened to the base of the rack. The light source inside the setup is an LED screen (LG) on the adjacent wall facing the tank rack, and external light is prevented by placing black Styrofoam plates over the configuration opening. The setup is installed on a special surface (Thorlabs Optical Table) to improve stability of the setup in response to stimulation delivery and disturbances from the surroundings.

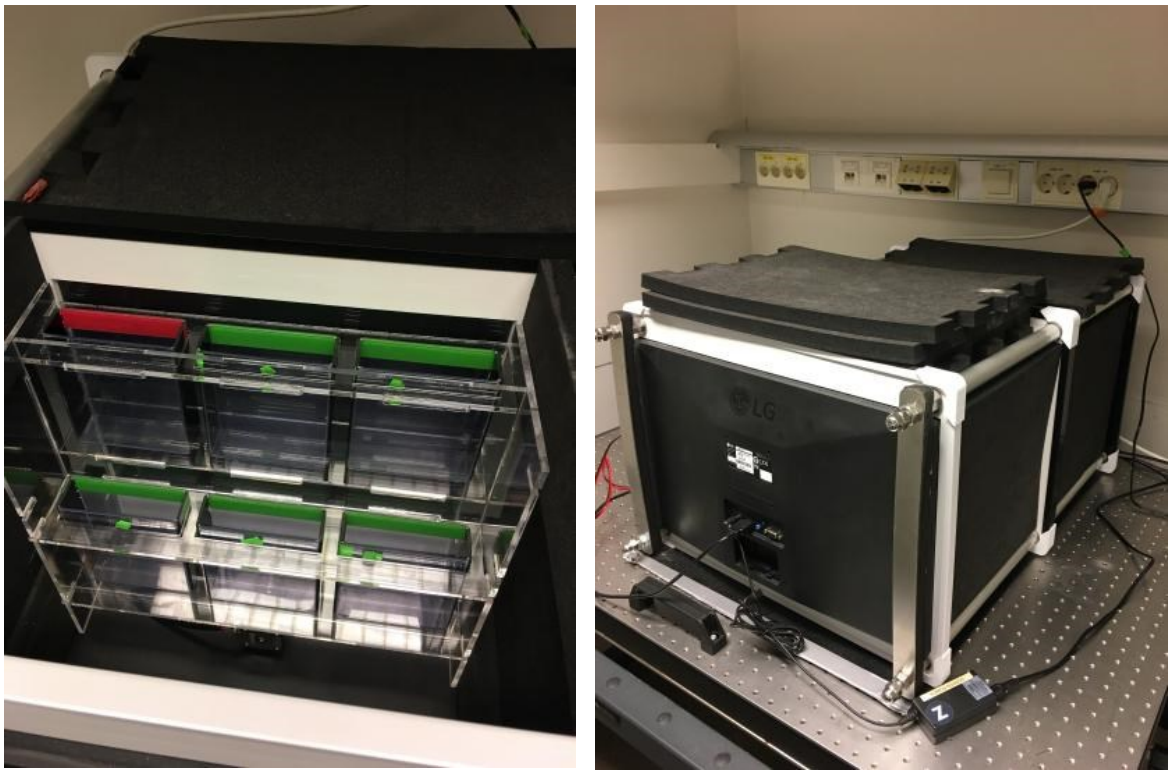

Figure 9: Images of the Zantiks LT behavioral setup. *The setup is used for the study of adult and juvenile zebrafish in the lab. Left image shows the interior of the setup, including the tank rack, the six experimental tanks and the rotating motor fastened to the bottom of the rack. The camera is integrated to the back wall of the setup (not shown). The right image shows the ulterior of the setup with the Styrofoam plates in place over the setup opening, as well as the back of the LED screen that projects toward the tanks.*

Once the experiment is started, the animals are dropped into their respective tanks filled with room tempered AFW from small, connected Eppendorf tubes: first, the three animals of the lower row are put in simultaneously, and subsequently, the three animals of the upper row are also put in simultaneously. Water temperature is not a factor that can be controlled with fidelity as there is no way to control or measure the water temperature within the system this is discussed in limitations section 4.5.1. From that point onward, they are free to swim around inside their individual tanks. Their movement during the experimental procedure is tracked on a video with a 15-fps resolution.

An experimental procedure combining a novel-tank test (NT-test) and a mechano-acoustic vibration test (VB-test) was employed for the behavioral experiments using the Zantiks LT setup. The former test is proficient at evoking anxiety-like responses, whereas the latter excels at eliciting acute fear-like responses and followed by anxiety-like behaviors during the recovery phase between stimulations [60, 78, 79, 84]. Dropping the animals into the experimental tanks marks the start of the NT-test. The animals' tank depth position and swim velocity are parameters used to measure their defensive behaviors for both assays.

It is worth mentioning that even though the fish can swim in all three dimensions, the video only tracked their position in the XY-plane for the corresponding time points. Data of the tank position (horizontal and vertical position) for each timepoint of the video is stored in a separate Excel file. These files are the foundation for the data analysis as interpretation of my results is based on this raw data. Post-processing, as well as

statistical calculations and plot visualization were performed with the programming tool MATLAB, which reads the Excel file and extracts the collected data. Removal of outliers in the dataset was performed manually by evaluating the stability of the video tracking in each experimental tank: here I excluded noisy data where the camera failed to track the animals' movements (mis-tracking). Due to the camera auto-referencing between the NT-test and the VB-test, the transition between the two assays improved mis-tracking in some cases, but introduced noise in other cases. The evaluation of outliers was therefore done for each behavioral assay separately, meaning one animal could be included in the dataset for the NT-test analysis, but be excluded for the VB-test analysis, and vice versa.

The NT-test is a very straightforward procedure, where the fish are dropped into empty water tanks and their movement and tank position are tracked on video. The recording starts before the fish are dropped in, so mis-tracking from water movement in the arenas and the handling of the equipment for the first few seconds are tracked in the video. Data analysis on the raw data therefore excludes the first 10-20 seconds of each recording due to this issue. Typical behavior to the novel tank test is to initially dive down rapidly in the tank (bottom-diving), keep close to the bottom (bottom-dwelling) and reduce their velocity (freezing) to assess the new environment for potential danger, all which are indicative of anxiety-like defensive behaviors [79-81]. This behavior eases with time (5-10 min) as the fish evaluate the arena to be non-threatening and void of immediate danger [82]. From there they will eventually start to get more explorative of their environment, choosing to inhabit more of the tank's space. Their swim velocity typically also increases as the initial wariness recedes; these are both signs of habituation to the novel environment.

On the other hand, the VB-test delivers mechano-acoustic stimulations to the tanks of the fish, and test parameters like the number of stimuli, the timing between each stimulus and each vibration's intensity and duration can be customized to make comprehensive behavioral experiment protocols. Typical behavior to the mechano-acoustic vibration stimuli is a strong transient increase in swim speed (burst swim) and diving to the tank bottom (bottom-diving) as an acute reaction, which are suggestive of acute fear-like defensive behaviors [81, 83, 84]. This is typically followed by a continued period of low swim depth (bottom-dwelling) and a decrease in swim speed (freezing), which are indicative of anxiety-like defensive behaviors [60]. Similar to the NT-test, these anxiety-like behaviors decrease over time after the threat has passed: their tank position and swim speed recover as they habituate after the stimulus delivery.

For the behavioral experiments in the thesis, the NT-test was the same: it consisted of 20 minutes of video recording where the fish were first added to their respective tanks, and their behavior was tracked with a camera. For the VB-tests in my experiments, I devised and adapted different code scripts that directed the setup's application of vibration stimuli, called Vibration Protocol 1 (VP1), Vibration Protocol 2 (VP2) and Vibration Protocol 3 (VP3). These protocols had variations in length, number of mechano-acoustic vibration stimuli given, intervals between the stimuli (inter-stimulus interval (ISI) and inter-trial interval (ITI)), and the duration and frequency of the vibration. The exact VB-test used in a particular experiment is discussed in more detail in the sections below.

2.3.2 First optimization experiment: NT-test and VB-test with Vibration Protocol 1

For the very first step of my behavioral experiments, I wanted to get familiar with how the Zantiks setup operated, and investigate the stereotypical defensive behaviors the system could prompt in freely behaving juvenile zebrafish compared to previous research. The NT-test was as described in the previous section. The protocol script devised for the VB-test was Vibration Protocol 1 (VP1), and a schematic overview can be seen in Figure 10. The total duration for the experimental procedure was 3 h 24 min 30 s.

This approach has been successfully used previously in the lab, with consistent results for the NT-test, though previous findings with the currently used setup suggest that the nature of the delivered stimulus may have an impact on the expressed behavioral phenotype (unpublished work of Bram Serneels [55]). My secondary goal was therefore to investigate these differences in elicited defensive responses to a range of different mechano-acoustic vibration stimuli. For the VB-assay, animals were exposed to six stimulus trials consisting of ten repetitions of one of six different mechano-acoustic stimuli VIB1 up to VIB6. A detailed overview of these stimulus types' frequency and duration can be seen in Table 1; based on the combination of these two factors, the stimuli were considered to progress in intensity from VIB1 being the "weakest" type, to VIB6 being the "strongest". Only one experimental group was included in this set of experiments: WT animals aged 21-28 dpf, which were considered juvenile in size and shape. The reason I chose WT animals for this procedure was to limit interference of any transgenic condition on the expressed behavior.

Stimulus name	***M (number of steps)***	***U (size of each step)***	***D (delay between steps)***	***D (ms)***	***Frequency (Hz)***	***Stimulus duration (ms)***
VIB1	2	0	100000	420	2	840
VIB2	20	0	10000	42	24	840
VIB3	100	0	10000	42	24	4200
VIB4	40	0	5000	21	48	840
VIB5	200	0	1000	4.2	238	840
VIB6	1000	0	1000	4.2	238	4200

Table 1: Overview of the six vibration stimulus types VIB1-VIB6. *The rows contain information about each of the vibration types; the stimulus name is indicated by the first column ("VIB1" to "VIB6"). The parameters given to the experimental setup are M (number of steps), U (size of each step) and D (delay between steps), and the input values for the individual stimuli are shaded in gray. M is the number of motor rotation steps, U is how much it rotates per step, and D is the temporal interval between the steps. For a given vibration type, the last three columns show the corresponding step delay in ms, stimulus frequency (Hz) and total stimulus duration (ms), which have been calculated from the shaded inputs for that particular stimulus.*

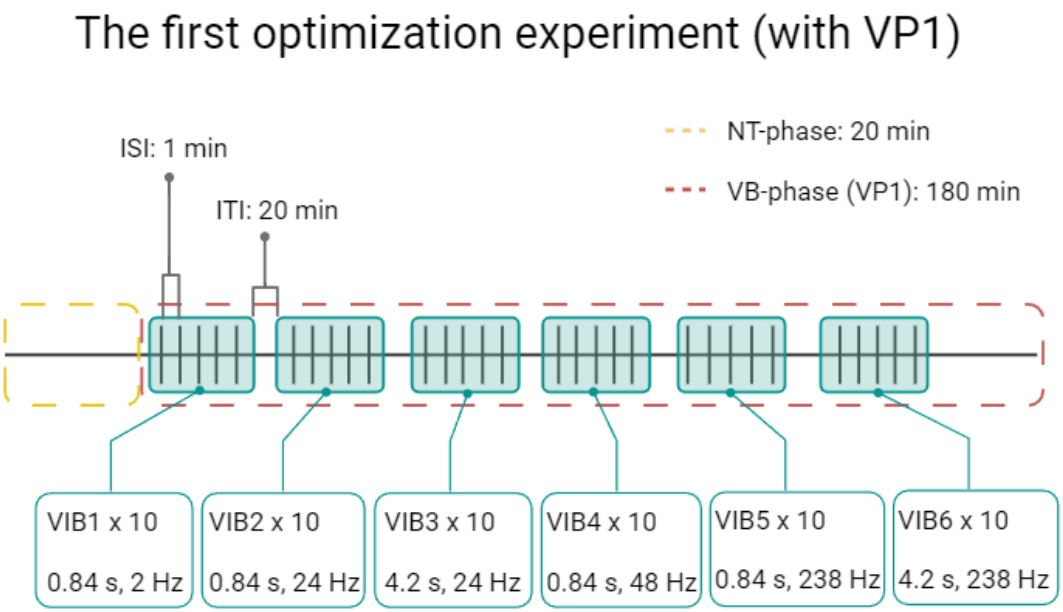

Figure 10: Schematic view of the NT-test and VB-test (VP1) of the first optimization experiment. *The protocol duration is 3 h 24 min 30 s (204.5 min) and is illustrated by the black horizontal line. Elements of the protocol are labelled in chronological order from left to right, however position and size are not scaled to the actual experiment time. Dashed rectangles indicate the duration of the NT-test (yellow, 20 min) and mechano-acoustic VB-test (red, 160 min). Between the NT-phase and the VB-phase, is a baseline period of 4.5 min (not shown in the figure). The end resting period after the last stimulus is 20 min. Within the VB-test, the turquoise shaded boxes with vertical lines represent the six stimuli trials in VP1: each trial contains 10 repetitions of one of the vibration types VIB1 up to VIB6. Duration (s) and frequency (Hz) for the stimulus type given in the particular trial is shown in the connected box. ISI is the inter-stimulus interval between the repetitions within the trials (1 min). ITI is the inter-trial interval between the six trials (20 min). Created with BioRender.com.*

2.3.3 Second optimization experiment: VB-test with Vibration Protocol 2

The second stage of the optimization process was to refine the behavioral essay to further investigate any candidate stimulus types picked from the previous experiment. From the first optimization experiment, I chose to examine juvenile WT animals' responses to VIB3 (24 Hz, 4.2 s) and VIB6 (238 Hz, 4.2 s) stimulus types. A schematic view of the experimental procedure is shown in Figure 11.

The experimental protocol script for this investigation included a 20 min tank habituation period followed by a short auto-reference update (30 s), then an 80 min VB-test. This protocol script, named Vibration Protocol 2 (VP2), was run twice, back-to-back, and the same animals remained in the system for both iterations of the protocol without interference. In other words, the fish were dropped into their respective arenas for the first run of the protocol, were still in the system when the second iteration started, and were not taken out before the end of the second protocol was finished.

In the first iteration, the VB-test delivered 30 VIB3 vibrations with a 2 min ISI. Meanwhile, the second run of the script was started manually immediately after the end resting period of the first iteration. The VB-test of the second iteration delivered 30 VIB6 stimuli (ISI = 2 min). The same animals were therefore exposed to 20 min habituation (NT-test), 30 VIB3 stimuli repeats, 20+20 min timeout (ITI), and then 30 VIB6 stimuli repeats, which was followed by a 20 min end resting period. The total duration for the experimental procedure was 3h 21min (1h, 40 min and 30 s per protocol iteration).

I chose to manually restart the experimental protocol instead of creating a single continuous script that incorporated both vibration stimuli to prevent camera mis-tracking noise from potentially excluding extensive portions of the dataset. By dividing the experiment in this way, I sought to contain the risk of unstable recordings due to only a subset of the whole experiment.

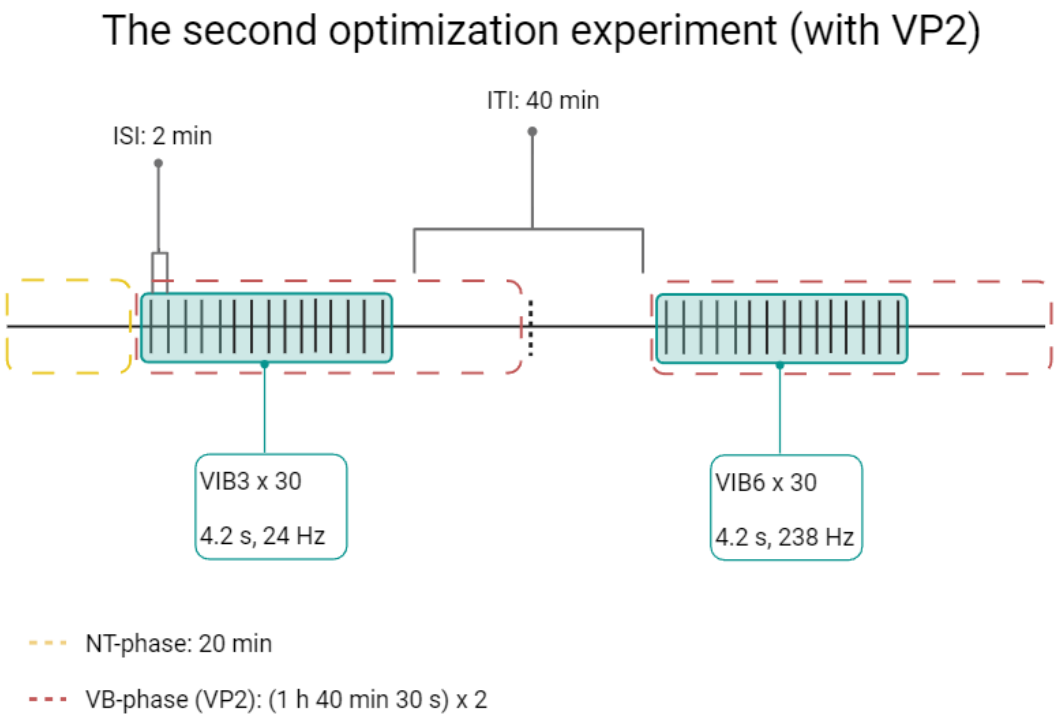

Figure 11: A schematic representation of the second optimization experiment utilizing VP2. *The experiment duration is represented by the long horizontal line, which was 3 h 21 min in total. The red dashed rectangles indicate the VB-period for each protocol iteration: 30 VIB3 stimuli for the first, then 30 VIB6 stimuli for the second. Turquoise shaded boxes with vertical lines symbolize the vibration trials, and details about the stimulus delivered are shown in the connected box. The black dashed line in the middle of the figure indicates the divide between the two protocol iterations. The intertrial interval (ITI) is the total amount of time between the last VIB3-delivery to the first VIB6-delivery: this encompasses the end resting period of the first iteration (20 min), and the habituation period of the second iteration (20 min) plus the auto-reference period from the second iteration (30 s, not shown in the figure). ISI is the same for the whole experiment and was 2 min, contrary to 1 min in VP1 in first optimization experiment's VB-test.*

2.3.4 DR-ablation effect on the defensive behavior

The mechano-acoustic vibration stimulus that was found to be most optimal among the tested candidates was used to create Vibration Protocol 3 (VP3) for the VB-test of the serotonergic manipulation experiment. A schematic view of the protocol can be seen in Figure 12. The purpose of this experiment was to study the effect on the defensive behavior in juvenile zebrafish with a manipulated serotonergic system. Thus, I aimed to shed more light on the relationship between this circuitry's involvement in defensive behaviors. The experimental protocol lasted 1 h and 27 min in total (5220 s). The NT-phase was the same as in my earlier experiments, and lasted 20 min. After a 4.5 min period with baseline and camera auto-reference timeout, the vibration phase started. The VB-test exposed the fish to 30 repetitions of the VIB6 stimulus type (4.2 s and 238 Hz), with an ISI of 2 min.

Since I wanted to study the neuronal activity in these animals by post-hoc immunostaining of the pERK/tERK ratio, and this protein's peak expression remains for about 10-15 min, I shortened the end resting period after the last stimulus to 4.5 min [56, 92]. The animals were fixed in PFA directly after the end of the behavioral experiment in an average time of 4.5 min. It therefore took around 9 min from the last stimulus onset to the fish were fixed. Thus, I aimed to capture the brain activity of the defensive behavior in response to the last few vibration stimuli.

Fish from the manipulated group were of *Tg(tph2:Gal4;UAS:ntr-mCherry)* origin. These nitroreductase-expressing fish were given MTZ for chemo-genetic ablation of the serotonergic neurons found mainly in the DR (see methods section 2.2 for details about this approach). Animals of the placebo group were siblings to the fish in the ablated group, but they were instead given the sham solution containing just DMSO and AFW. The animals in the third group were of the *Tg(tph2:Gal4;UAS:GCamp6s)* genetic background that did not synthesize the nitroreductase enzyme required for prodrug metabolization, thus rendering MTZ in its harmless state. I expected these MTZ-treated control fish to behave more similar to the placebo animals than DR-ablated animals due to the shared non-ablated condition of the two controls.

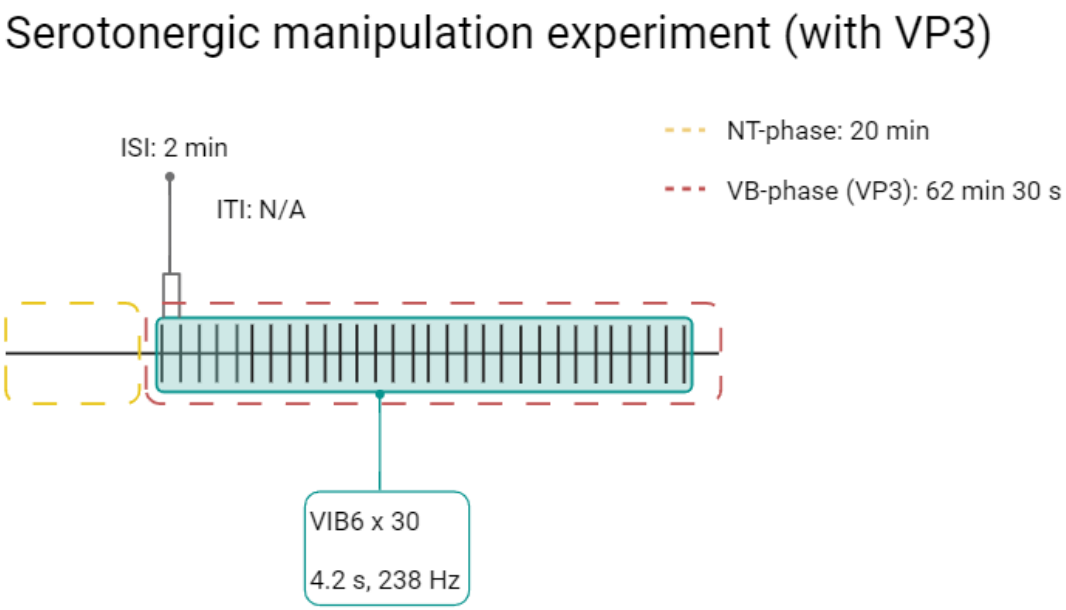

Figure 12: A schematic view of the serotonergic manipulation experiment. *The illustration's composition is the same as for the previous vibration protocols: the whole experiment duration is represented by the black horizontal line (1 h and 27 min). Dashed boxes indicate the periods for the two behavioral assays, NT-test (yellow) and mechano-acoustic VB-test (red). The turquoise shaded box with vertical lines symbolizes the vibration trial, and details about the stimulus are shown in the connected box. The auto reference and baseline period between the NT-phase and the vibration phase is not shown in the schematic, but amount to 4.5 min combined. The protocol had only one vibration trial, so the inter-trial interval (ITI) was not applicable for this particular experiment. The trial consisted of 30 stimulations of the VIB6 stimulus type. ISI between each repetition was 2 min. End resting period after the last delivered stimulus was 2.5 min.*

2.4 Post-hoc immunostaining and confocal imaging of brain activity

The staining procedure prepared the juvenile zebrafish from the serotonergic manipulation behavioral experiment for imaging with the confocal microscope. 15 animals per group were selected for a total of 45 animals, which were all prepared and stained in one single batch. Sample selection was based on the latest performed experiments, which coincides with the oldest animals since all were born the same day. This decision was made because the fluorescence tends to fade the longer the samples are kept, so the most recent samples would have the best starting point for further confocal imaging. Moreover, larger sized samples were easier to handle in terms of dissection, pipetting and overall visualization during the protocol, thus making them more practical to operate with compared to smaller samples. This therefore increased the efficiency of each protocol step, as well as reduced the number of wasted samples due to damaged samples.

The animals were kept in PFA overnight in a cooling room (4°C) immediately after the behavioral experiment. The staining process started the next day. The staining protocol used in this project was adapted from Bram Serneels, and originally included antibodies for pERK and tERK as well as DAPI [55]. The detailed protocol description is provided in

Appendix 2. Only four distinct channels can be used for confocal imaging to prevent overlap of the fluorescent signals, and is limited to the spectrum of visual light. The experimental groups already had two different fluorescent backgrounds: orange/red mCherry for the ablated and placebo, and green GCamp6s for the MTZ-treatment control, which would occupy two of these channels. Since DAPI is a fluorescent dye that labels the cell nucleus and is convenient for anatomical reference, but not necessary for the neuronal activity measurement, it was omitted from the protocol. More details about the selection of antibodies can be found later in this section.

The whole process from until the brain is ready to be imaged takes 4 days, with several optional "storage points" throughout the protocol. To retain as much fluorescence as possible from the staining steps, all steps were performed consecutively without storing the samples unnecessarily. The full protocol can be viewed in detail in Appendix 2, and was followed with some exceptions, which were approved by the senior lab technician Bram Serneels: PBT was used instead of PBTx during the PFA washout on the first protocol day, as the two can be used interchangeably at this step with no detrimental effects on the confocal visualization; DAPI was not added to the samples; the concentration of the secondary antibodies GAM 405+ and GAR 647+ was doubled from 1:1000 to 1:500; the brain samples were mounted in 4% gelatin and 65% glycerol in PBS.

For the dissection, each animal was transferred to a petri dish in a droplet of PBT. The main technique to remove tissue was to use finer forceps to gently pinch and/or pull away material while positioning the rest of the body with rougher forceps. The lower jaw and jawbone were removed along with the heart, swim bladder, spine and tail to stabilize the sample during mounting. The skin on top of the head as well as the dura mater were also removed to expose the brain tissue for the staining protocol and clear away debris from the image focal point. The eyes were preferably kept intact and attached, which had several advantages for the samples. For example, the black eyes provide a visual cue that is easy to recognize, which made pipetting steps more efficient and prevented samples from getting lost and damaged as the brains are very small and otherwise semi-translucent. It also helped stabilize the samples during mounting and improved consistency of the imaging angle. The eyes also assisted as anatomical reference for orientation of the sample under the confocal microscope.

For the secondary antibodies, I used goat anti mouse for labelling the tERK (GAM 405+), and goat anti rabbit for the pERK (GAR 647+). The dye for tERK emitted blue light, whereas the dye for the pERK emitted far-red light. The choice of antibodies was because the two transgenic backgrounds included in the study expressed green (GCamp6s) or red (mCherry) endogenously. Selecting antibodies with wavelengths between 500 nm (blue/green) and 600 nm (yellow/orange) would mix with the fishlines' tissue-specific expression and obscure the actual ERK results. Since DAPI emits blue light, it was removed from the protocol to prevent interference with the tERK antibody (GAM 405+).

The brains were imaged with the 20x air objective of the Zeiss LSM 880 confocal microscope. Operation of the microscope was done through the ZEN LSM program. The imaging's focus was aligned to capture the forebrain, namely the telencephalon and the habenulas located in the anterior part of the diencephalon. Imaging with the confocal microscope yielded several images with constant XY-orientation (horizontal plane), but varying location along the dorsoventral axis. The result was a Z-stack of images that together gave a composite representation of the sample, which could be used to measure the neuronal activity of the dorsal part of the forebrain. Each sample was imaged with

the four channels mentioned channels. Imaging settings were adjusted to the respective excitation ranges for the two secondary ERK antibodies and the two fishlines' fluorescent markers for, one for each channel. The imaging settings were tailored to a representative initial sample, and were kept constant for all the images generated thereafter for comparative results. The image tool FIJI (ImageJ) was used to process the raw data, whereas the coding program MATLAB was used for the statistical analysis and visualization of the results.

Right before each image was taken, I screened the sample's fluorescence signal from the DR region with the confocal microscope to confirm consistency between the sample's group origin and the result of the ablation procedure. The images in Figure 13 show a representative example of the screening result for each of the three groups. The ablated and placebo fish were consistent relative to their group origin and their received treatment. However, no strong fluorescent signal was seen in the DR-area for the MTZ-treatment control fish. These animals were supposed to express GCamp6s in the DR region due to a non-ablated condition (the fishline lacks nitroreductase to activate the MTZ prodrug). Though there was an absence of signal post-staining (and therefore also post-treatment), all animals had been screened with a fluorescent microscope and were confirmed for experiments at 3 dpf. One possibility was the MTZ-treatment control animals retained their serotonergic neurons, but the fluorescent signal from GCamp6s had weakened during the MTZ-treatment or the staining process. The second possibility was the MTZ-treatment control animals did in fact not have serotonergic DR neurons, thus making them another ablation group. Based on this observation, I chose to not comment nor interpret the behavioral and neuronal activity comparison between the ablated and MTZ-treatment groups further in the thesis (discussion sections 4.3 and 4.4, conclusion section 5). This is, however addressed in more detail in the limitations section 4.5.2.

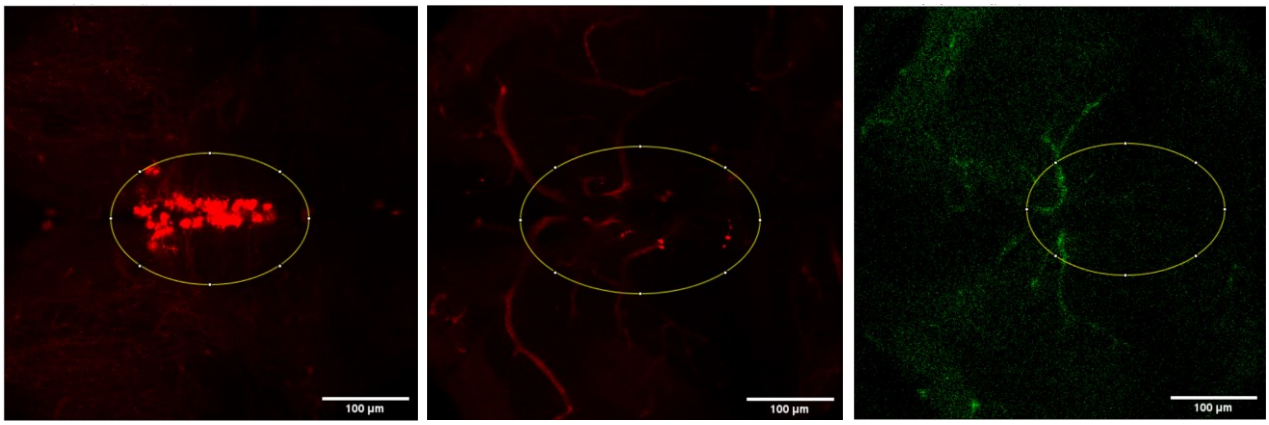

Figure 13: Example of post-staining screening of samples from each experimental group with the ZEISS LSM confocal microscope. *The images show representative examples of the fluorescent signals from the genetic marker proteins in each of the experimental groups: mCherry for the placebo (left, n=15) and ablated (middle, n=15), and GCamp6s for the MTZ-treated control (right, n=15). The images show the deep part of the juvenile zebrafish hindbrain (dorsal view) where the DR nuclei are found. The animals are oriented anterior (left) to posterior (right). Left panel: serotonergic neurons of the DR are intact in the placebo group, indicated by the abundant mCherry expression. Middle panel: successful removal of the serotonergic cells in the ablated group, indicated by absence of mCherry expression. Right panel: all samples in the MTZ-treatment control group had very weak GCamp6s signals, and would show mostly noise or blood vessels if*

anything at all. The example in the figure has a contrast of 0/1, whereas the other images have a contrast of 0/200 (placebo) and 0/50 (ablated). This was contrary to expectation, which was that these samples would have strong GCamp6s expression in the DR.

2.5 Statistical tests

I chose to make use of non-parametric hypothesis testing to perform statistical analyses on the data in my thesis, as this approach is less stringent in its assumptions: for example, the requirement of a normally distributed data, which my dataset deviated from in some cases (Supplementary Figure 1). All the inter-group comparisons of the Y-position and velocity parameters were computed with the Wilcoxon rank sum test for equal medians with the built-in MATLAB function: [P,H] = RANKSUM(...,'tail',TAIL). This performed three hypothesis tests between dataset X and Y:

Left-tailed test alternative hypothesis: "The median of X is less than median of Y" or

"$\tilde{x} < \tilde{y}$".

Two-tailed test alternative hypothesis: "Medians of X and Y are not equal" or "$\tilde{x} \neq \tilde{y}$".

Right-tailed test alternative hypothesis: "The median of X is larger than the median of Y" or "$\tilde{x} > \tilde{y}$".

Differences with p-values below 0.05 were deemed statistically significant (denoted as *, symbolized as ** for p-values below 0.001). Since the primary focus for testing the hypothesis was either of the one-tailed tests, special attention to the formulation of the statement is therefore given to indicate the directionality of the significance. Terms like for example "significantly lower" are presented with a corresponding left-tailed p-value to support this claim. On the other hand, terms like "significantly higher" are supplied with the right-tailed p-value. Intra-group comparisons between individuals of the same group at different time points were calculated with the Wilcoxon signed-rank test.

3 Results

3.1 Defensive behaviors in juvenile WT zebrafish in the first optimization step

The first step of the optimization process was a set of Zantiks behavioral experiments that included a NT-test and VB-test. VP1 was the protocol used for the VB-test. The experimental group consisted of a total of n=42 WT juvenile (21-28 dpf) zebrafish, but the data analysis sample sizes for the NT-test and VB-test are both adapted to remove noisy subjects in the respective tests, as mentioned in methods section 2.3.1.

The goals were to 1) verify my approach to studying zebrafish defensive behavior by generating behavioral data aligning with prior research, and 2) evaluate the different mechano-acoustic stimuli in VP1 and assess their ability to prompt defensive behavioral responses. An overview of these mechano-acoustic vibrations is shown in Table 2, and a chart of the entire experimental procedure can be seen in Figure 14 (as represented in the methods section 2.3.2).

Stimulus name	***M (number of steps)***	***U (size of each step)***	***D (delay between steps)***	***D (ms)***	***Frequency (Hz)***	***Stimulus duration (ms)***
VIB1	2	0	100000	420	2	840
VIB2	20	0	10000	42	24	840
VIB3	100	0	10000	42	24	4200
VIB4	40	0	5000	21	48	840
VIB5	200	0	1000	4.2	238	840
VIB6	1000	0	1000	4.2	238	4200

Table 2: Overview of the six vibration stimulus types VIB1-VIB6, as presented in the methods section. *The rows contain information about each of the vibration types; the stimulus name is indicated by the first column ("VIB1" to "VIB6"). The parameters given to the experimental setup are M (number of steps), U (size of each step) and D (delay between steps), and the input values for the individual stimuli are shaded in gray. M is the number of motor rotation steps, U is how much it rotates per step, and D is the temporal interval between the steps. For a given vibration type, the last three columns show the corresponding step delay in ms, stimulus frequency (Hz) and total stimulus duration (ms), which have been calculated from the shaded inputs for that particular stimulus.*

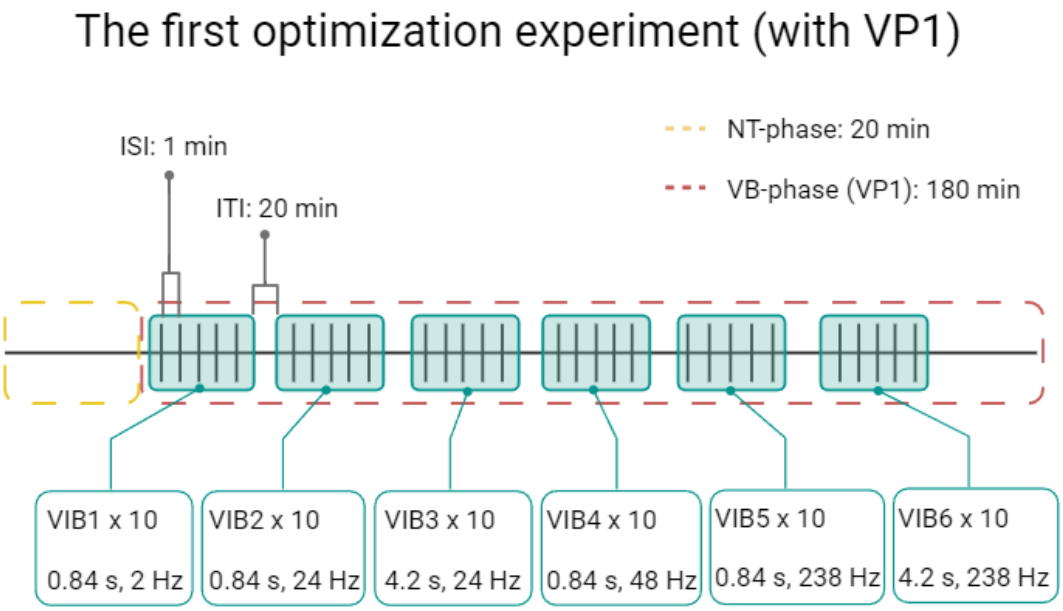

Figure 14: Overview of the NT-test and VB-test (VP1) of the first optimization step, as presented in the methods section. *The protocol duration is 3 h 24 min 30 s (204.5 min) and is illustrated by the black horizontal line. Elements of the protocol are labelled in chronological order from left to right, however position and size are not scaled to the actual experiment time. Dashed rectangles indicate the duration of the NT-test (yellow, 20 min) and mechano-acoustic VB-test (red, 160 min). Between the NT-phase and the VB-phase, is a baseline period of 4.5 min (not shown in the figure). The end resting period after the last stimulus is 20 min. Within the VB-test, the turquoise shaded boxes with vertical lines represent the six stimuli trials in VP1: each trial contains 10 repetitions of one of the vibration types VIB1 up to VIB6. Duration (s) and frequency (Hz) for the stimulus type given in the particular trial is shown in the connected box. ISI is the inter-stimulus interval between the repetitions within the trials (1 min). ITI is the inter-trial interval between the six trials (20 min). Created with BioRender.com.*

As mentioned in the methods section, swim depth and velocity were the parameters measured to investigate the defensive behaviors. For the behavioral experiments in the first optimization step, the positional- and velocity results averaged over the n=32 WT juveniles in the NT-phase can be seen in Figure 15, and were representative of typical responses to the NT-test.

Figure 15A shows the fish's tank depth (Y-position) as the average vertical distance from the top of the tank during the 20 min of the NT-phase. As noted in the methods section 2.3.1, there are no tracked Y-positions from the top 2 cm due to the taped region on the tank, and data from the first 10 seconds of the experiment have been cropped out to exclude mis-tracking from handling of the drop-in equipment.

The fish expressed stereotypical bottom-diving behavior upon introduction to the novel tank, as seen from the sharp decline in Y-position at the start of the NT-test (Figure 15A). Afterward, their continued low Y-position for the first couple of minutes into the test was an indication of anxiety-like bottom-dwelling behavior. The following rise in average Y-position until around 5 minutes into the experiment (300 s) was suggestive of cautious exploratory behavior. This levelled out to a stable plateau for the remainder of the NT-test, indicating that the fish had habituated to the tank.

In Figure 15C, the two cumulative heatmaps of tank position probability averaged over the animals support these observations in the Y-position data in Figure 15A. The left panel of Figure 15C shows the tank distribution during the "early" phase of the NT-test (first 3 min): the distribution of warmer colored pixels near the bottom of the tank arena indicated a higher probability of the fish to inhabit the lower portion of the tank at the start of the test. Similarly, the right panel of Figure 15C depicts the average tank position during the "late" phase of the NT-test (last 3 min): the vertical distribution of warm colored pixels was more homogenous compared to the early phase heatmap, which corroborates the observation of increased exploration tendency and habituation in the late part of the NT-test.

The corresponding velocity data during the NT-test averaged over the fish was also consistent with stereotypical NT-behavior (first few seconds excluded due to mis-tracking) (Figure 15B). The speed values were calculated from a sample bin size of 1 s. The reduced velocity observed during the first 10 min (600 s) of the test was indicative of a defensive decrease in locomotion (anxiety-like freezing behavior). The following increase in exploratory behaviors and gradual habituation to the tank was indicated by the observed increase in swim speed in the later parts of the NT-test.

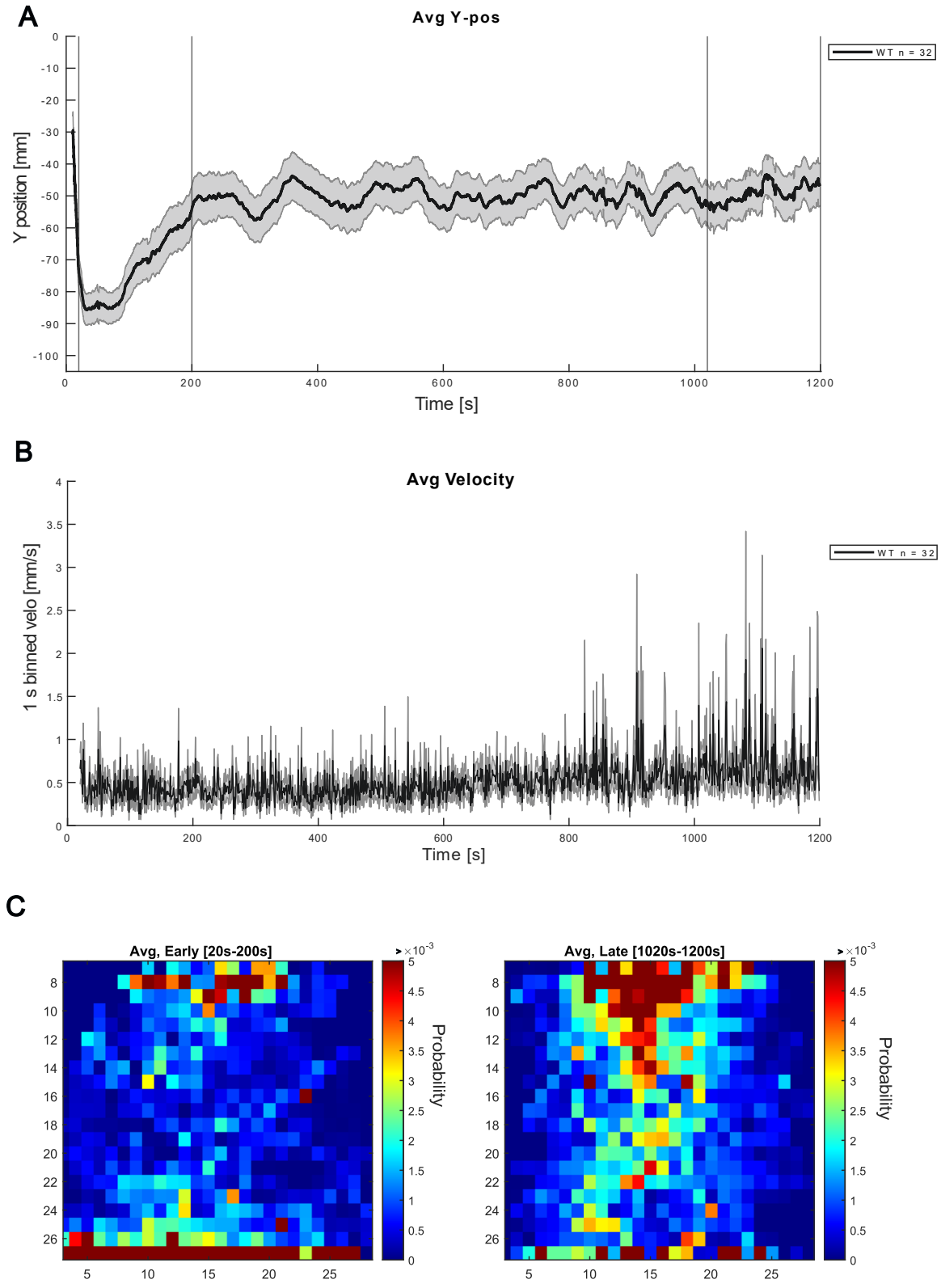

Figure 15: Average Y-position, velocity and tank position for juvenile WT zebrafish (n=32) during the NT-test of the first optimization experiment. *(**A**) Average Y-position for n=32 WT juveniles during the NT-test, which constitutes the first 20 min of the experimental procedure (data for the initial 10 seconds cropped out). X-axis represents time in s, and Y-axis represents vertical distance from the top if the tank in mm. The mean Y-position (black line) and corresponding SEM (shaded error bars) are plotted in mm. Vertical X-lines visualize the time*

*intervals where the "early" and "late" periods of the NT-phase have been sampled from in the corresponding heatmaps below. Total sample time for both intervals is 3 min (180 s) and were 20-200 s for the early phase and 1020–1200 s for the late phase. (***B***) Average velocity of the same animals (n=32) for the NT-period (first 15 s cropped out). X-axis represents time in s, and Y-axis represents speed in mm/s calculated from a 1 s sample interval from the raw data. The mean velocity (black line) and corresponding SEM (shaded error bars) are plotted in mm/s. (***C***) Cumulative heatmaps depicting the tank position probability in the XY-plane of the tank for the "early" (left) and "late" (right) phase of the NT-test (the top pixels from the taped area are cropped out). Figures are adapted to show the tracked areas within the experimental tanks, but with arbitrary axis units not equal to the tank's dimensions in mm. Pixel values are calculated from the average position of all the fish during the respective sample intervals and represented with scaled colors. The plot uses the value range of 0-0.005 to assign the pixel color, and deep-red pixels may therefore have a value of ≥ 0.005.*

The mechano-acoustic VB-test began after the NT-period, when the fish had been habituated to the new tank. Average positional- and velocity results of the entire VB-phase averaged over n=39 WT juvenile animals are shown in Figure 16. These Y-position- and velocity "traces" gave a rough overview of the fluctuations in these parameters over time. In both plots, each vertical X-line (blue) corresponds with a vibration onset for a total of 60 individual stimuli.

Responses in Y-position to the individual stimuli are hard to distinguish in the entire Y-position trace in Figure 16A. Nonetheless, indications of defensive diving responses to individual stimuli could be observed from some of the sharp vertical dips in Y-position below the baseline that coincided in time with the stimulus onset (blue X-lines).

For the velocity responses, there were indications of defensive freezing behavior within whole stimulus trials seen from the average velocity trace in Figure 16B. This can be noticed from the decrease in overall swimming speed during the vibration trials compared to the velocity before and after the trial. The strongest decrease in overall velocity seemed to be in response to deliveries of VIB3 and VIB6 stimuli within their respective trials.

Certain long-term trends in the dataset also became apparent from looking at the results from the entire VB-test duration: there was a prominent decrease in average Y-position after the trial containing VIB3 stimulus repetitions, from which the animals seemingly did not recover from during the remainder of the experiment (Figure 16A). On the other hand, the average swim velocity appeared to increase as the protocol progressed (Figure 16B).

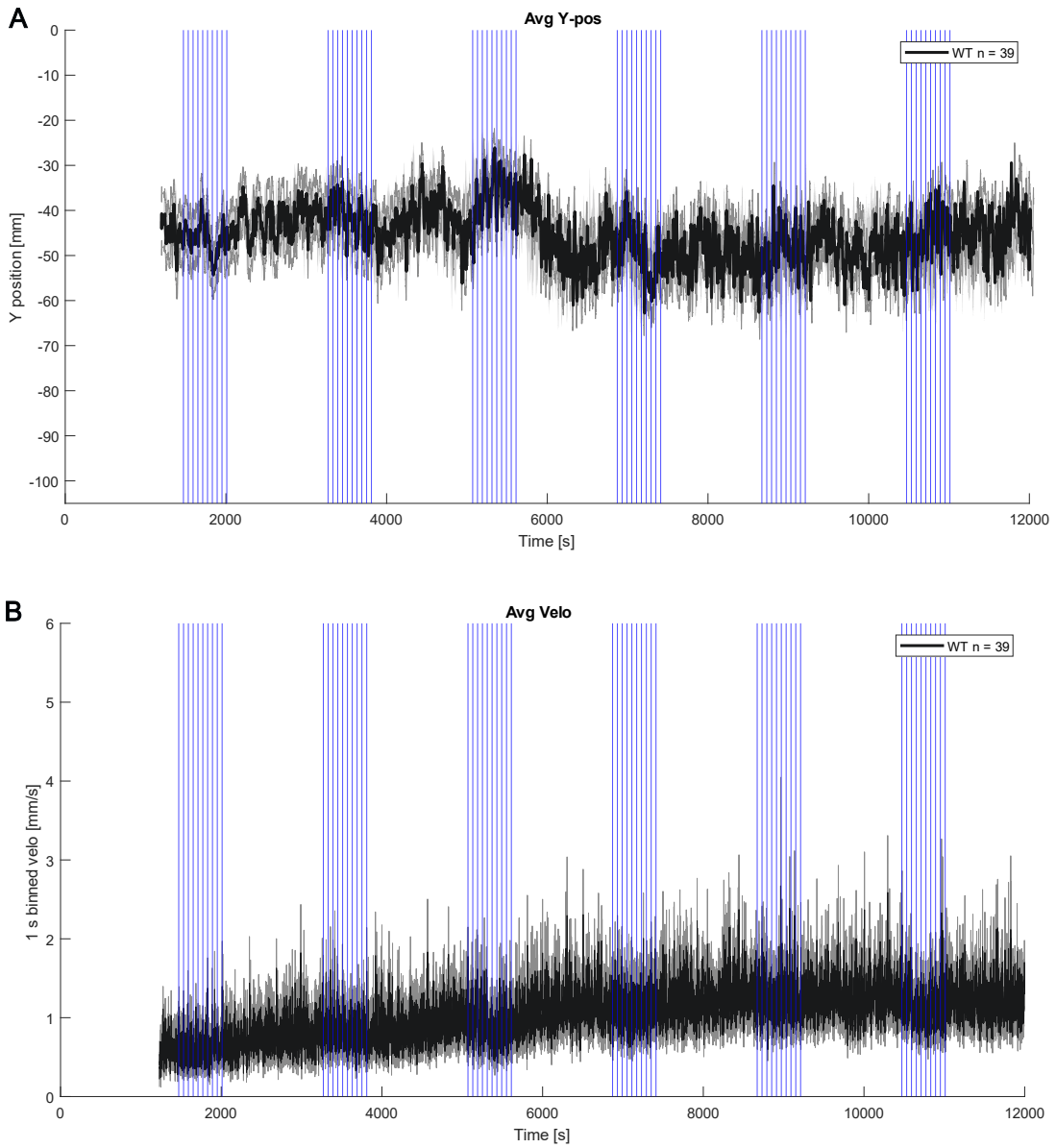

Figure 16: Average Y-position- and velocity trace for juvenile WT zebrafish (n=39) during the VB-test of the first optimization experiment. *(**A**) Average Y-position for (n=39) WT juveniles during the VB-test. The X-axis shows the time in seconds, the Y-axis shows vertical distance from the top if the tank in mm, and blue X-lines denote the time of individual stimulus onsets. The mean Y-position (black line) and corresponding SEM (shaded error bars) are plotted in mm. There are six trial "blocks", each with 10 repetitions of the same stimulus: the first trial block consists of 10 VIB1 type vibration stimuli, the second trial block consists of 10 VIB2 type vibrations stimuli etc., up to VIB6. (**B**) Average velocity of the same animals (n=39) for the VB-period. The X-axis represents time in s and the Y-axis represents speed in mm/s. The mean swim velocity (black line) and corresponding SEM (shaded error bars) are plotted in mm/s calculated from a 1 s sample interval from the raw data. like (**A**), the blue X-lines represent the individual stimuli onsets within the six trials.*

To compare the behavioral effects of vibration stimulus types VIB1-VIB6 in more detail, I next plotted the animals' average responses in swim depth (Y-position) and velocity in response to the each of the stimulus trials by averaging over their 10 respective repetitions (Figure 17 and Figure 18).

Figure 17A shows the average absolute Y-position (mm) for the six stimulus trials. The elevated average Y-position before, during and after VIB1-3 stimulus delivery compared to VIB4-6 type delivery supported the observation from the Y-position trace of the entire VB-test: on average, the fish's overall swim depth decreased after the stimulus trial containing VIB3 vibrations.

Figure 17B represents the change in Y-position (mm), which calculates a baseline in Y-position from a 2 s pre-stimulus sample interval for each of the six plots in Figure 17A, and then aligns this baseline to Y=0 to better compare the responses of the six vibration types. On average, the fish expressed clear diving behavior upon immediate exposure to VIB2-VIB6 stimulus types. This was illustrated by the animals' decrease in Y-position in the first few seconds following the stimulus onset (blue X-line), which is not as prominent from VIB1 stimulations (Figure 17A+B). The magnitude of the initial diving behavior relative to the respective baseline was the greatest for VIB4-VIB6 (Figure 17B). These transient decreases in Y-position in immediate reaction to the vibration stimulus were suggestive of fast-occurring fear-like defensive responses. Furthermore, anxiety-like bottom-dwelling after the initial dive was stronger in response to vibration types VIB3 and VIB4: the average time it took for the incline in Y-position to rise toward pre-stimulus baseline values was longer, indicating slower habituation to these stimulus types (Figure 17A+B).

Figure 18A shows the average absolute swim velocity (mm/s) for the six stimulus trials calculated from a 1 s bin sample size. The swim velocity before, during and after the stimulus deliveries consistently rose across the six trials. This supported the remark from the velocity trace of the entire VB-phase in Figure 16B that the fish's overall velocity increased throughout the whole mechano-acoustic vibration assay.

Figure 18B represents the average change in swim velocity (mm/s) (with a bin size of 1 s). Like Figure 17B, this plot also calculates and aligns the baselines from a 2 s pre-stimulus sample interval for all six trials. Figure 18A+B show that exposure to all six mechano-acoustic vibrations elicited a burst in swim speed, as seen from the very brief, but strong spike in average velocity in immediate response to the stimulus onset (blue X-line). This was indicative of fear-like defensive behaviors. The magnitude of burst speed relative to the respective baseline was the greatest in response to VIB1-3 (Figure 18Figure 17B). After the initial burst swim, the period of decreased locomotion, which is indicative of anxiety-like freezing and risk-assessing defensive behaviors, was most noticeable in response to VIB3, VIB4 and VIB6: the average time it took for the fish to recover their pre-stimulus velocity was longer, indicating slower habituation to these stimulus types (Figure 18A+B).

Taken together, the juvenile WT zebrafish seemed to express particularly strong aversive behavior toward the stimulus types of high frequency (VIB5+6) and/or long duration (VIB3+6). As VIB5 was already utilized in the lab, I therefore chose VIB3 and VIB6 as candidates for my next behavioral experiment.

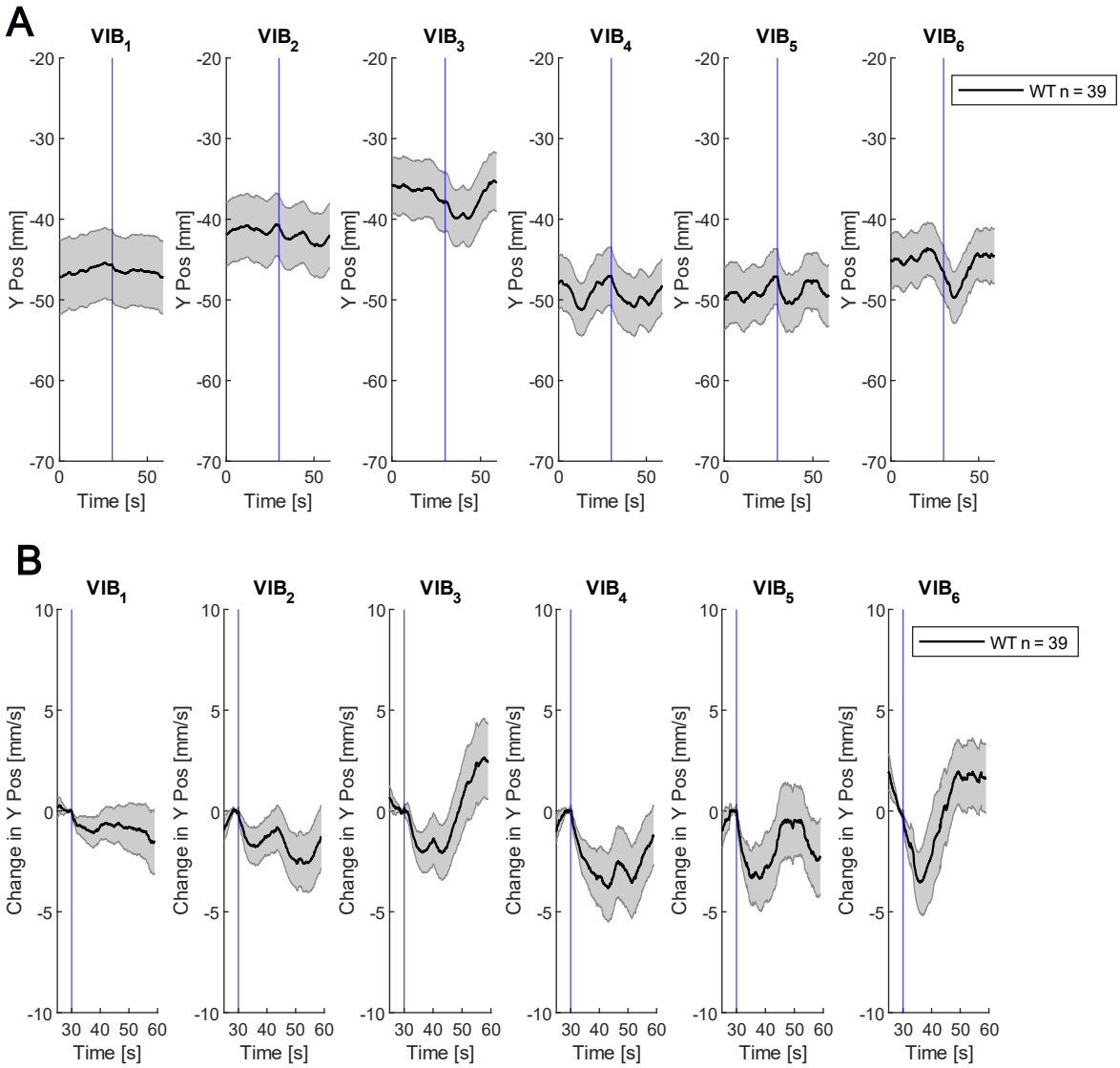

Figure 17: Average absolute Y-position and change in Y-position averaged for the six stimulus trials during the VB-test of the first optimization experiment. *(**A**) Absolute Y-position for (n=39) WT juveniles during the VB-test, averaged over the 10 stimulus repetitions (VIB1-6) within the six trials. Each panel corresponds to a trial. The X-axis shows the time in seconds, the Y-axis shows vertical distance from the top if the tank in mm, and blue X-lines denote the time of individual stimulus onsets. The mean Y-position (black line) and corresponding SEM (shaded error bars) are plotted in mm. (**B**) Change in Y-position for the same animals (n=39) during the VB-test for each of the six trials containing 10 VIB1-VIB6 stimulus repetitions. For each panel, a baseline sampled 2 s before the stimulus onset has been calculated and aligned to Y=0 in each respective plot. Time is shown along the X-axis (s), and Y-position relative to the calculated baseline is shown along the Y-axis (mm). The blue X-lines denote stimulus onset.*

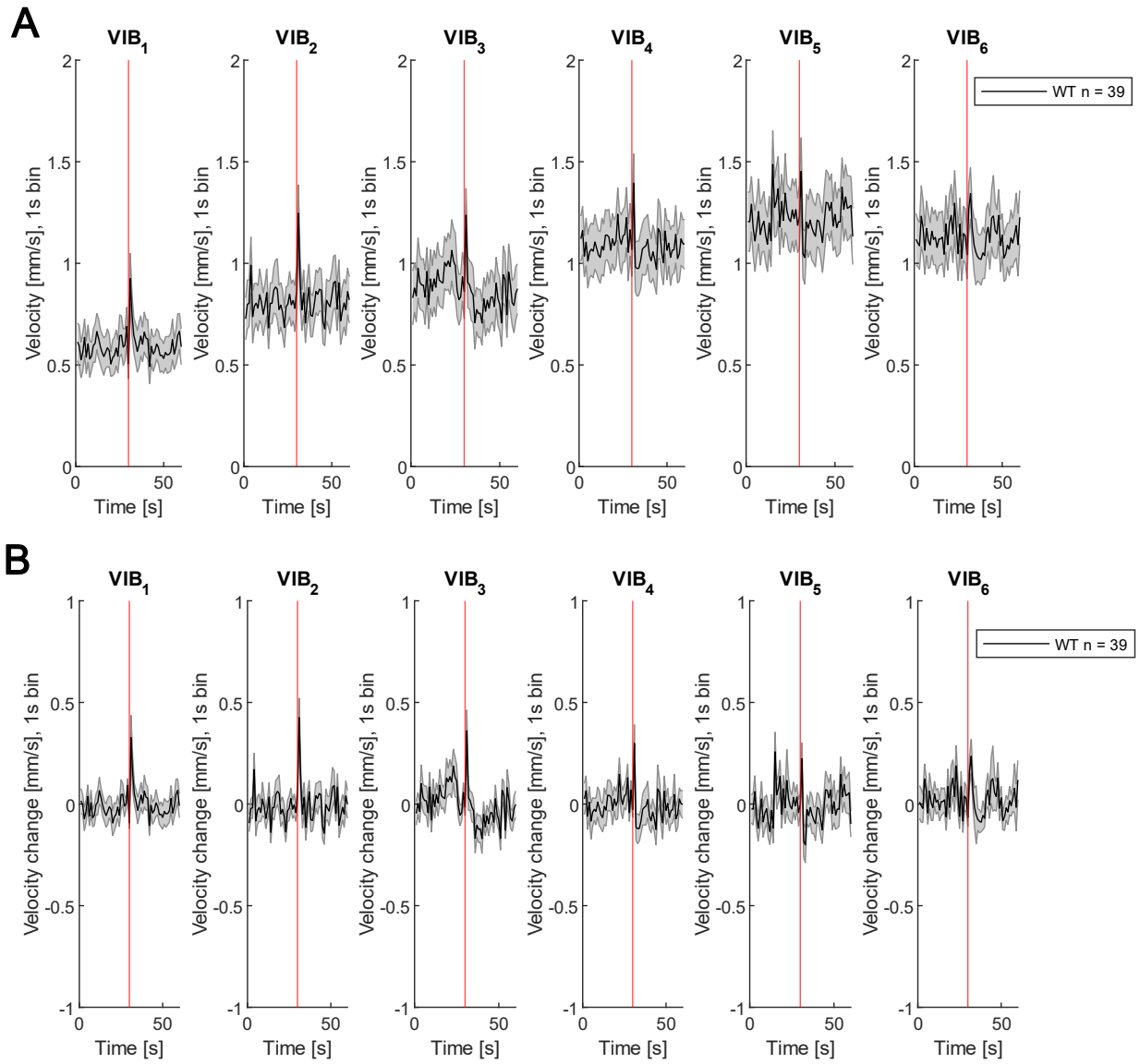

Figure 18: Average absolute velocity and change in velocity for juvenile WT zebrafish (n=39), averaged for the six stimulus trials during the VB-test of the first optimization experiment. *(**A**) Absolute swim velocity for (n=39) WT juveniles during the VB-test, averaged over the 10 stimulus repetitions (VIB1-6) within the six trials. Each panel corresponds to a trial. The X-axis shows the time (s), the Y-axis shows swim speed calculated from a 1 s bin sample size (mm/s), and red X-lines indicate stimulus onset. The mean velocity (black line) and corresponding SEM (shaded error bars) are plotted in mm/s. (**B**) Change in velocity for the same animals (n=39) during the VB-test for each of the six trials containing 10 VIB1-VIB6 stimulus repetitions. For each panel, a baseline sampled 2 s before the stimulus onset has been calculated and aligned to Y=0 in each respective plot. Time is shown along the X-axis (s), and velocity relative to the calculated baseline is shown along the Y-axis (mm/s). The red X-lines denote stimulus onset.*

3.2 Defensive responses to candidate mechano-acoustic vibration stimuli

The second step of the optimization process aimed to further investigate the two candidate stimulus types selected from the previous experimental setup. To study which of the two vibration types elicited the strongest defensive behavior, I performed a set of Zantiks behavioral experiments containing two mechano-acoustic VB-tests exposing a total of n=42 juvenile WT fish to 30 repetitions of the VIB3 (4.2 s, 24 Hz) and VIB6 (4.2 s, 238 Hz) stimulus types respectively (Figure 19). The results from the NT-test were not the focus of this experiment, but are included in Supplementary Figure 2.

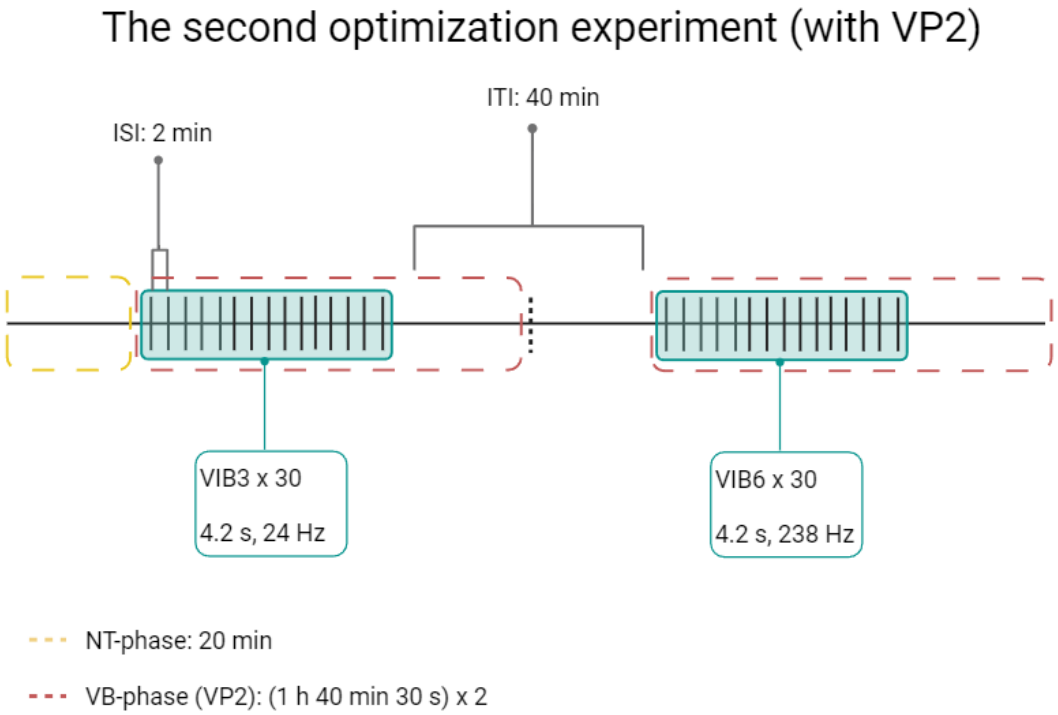

Figure 19: Schematic view of the second optimization experiment using VP2 as presented in the methods section. *The experiment duration is represented by the long horizontal line, which was 3 h 21 min in total. The red dashed rectangles indicate the VB-period for each protocol iteration: 30 VIB3 stimuli for the first, then 30 VIB6 stimuli for the second. Turquoise shaded boxes with vertical lines symbolize the vibration trials, and details about the stimulus delivered are shown in the connected box. The black dashed line in the middle of the figure indicates the divide between the two protocol repetitions. The intertrial interval (ITI) is the total amount of time between the last VIB3-delivery to the first VIB6-delivery: this encompasses the end resting period of the first iteration (20 min), and the habituation period of the second iteration (20 min) plus the auto-reference period from the second iteration (30 s, not shown in the figure). ISI is the same for the whole experiment and was 2 min, contrary to 1 min in VP1 in first optimization experiment's VB-test.*

The fluctuations in average Y-position and velocity responses throughout the entire VB-tests of the second optimization experiment can be seen in Figure 20. The overall Y-position and velocity seemed to be very stable throughout the vibration stimulus assay, contrary to the trends observed in the first optimization experiment using VP1 in the VB-

test (Figure 16A+B). Additionally, the fish seemed to have an equal overall Y-position in response to the two vibration types, but increased overall swim speed in response to VIB6 relative to VIB3.

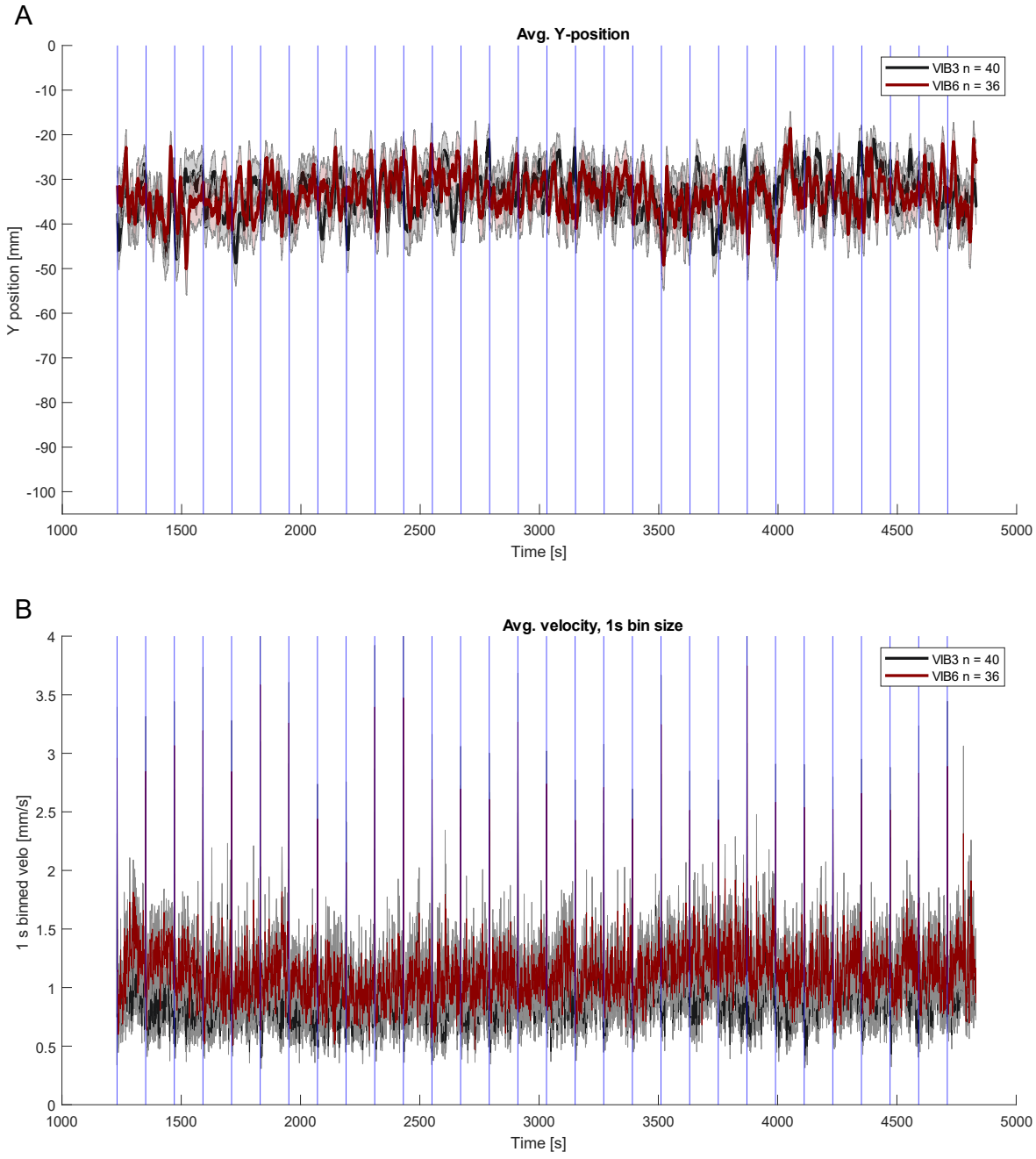

Figure 20: Average Y-position and velocity trace for the juvenile WT fish during the two VB-tests in the second optimization experiment. *(**A**) Average Y-position (mm) when the fish are exposed to the 30 VIB3 stimuli in the first protocol iteration (n=40), and when they were exposed to the 30 VIB6 stimuli in the second iteration (n=36). The X-axis shows the time in seconds from each iteration's starting point. The Y-axis shows vertical distance from the top of the tank in mm. Blue X-lines denote the time of individual stimulus onsets (VIB3 or VIB6 depending on the subprotocol). The mean Y-position for the VIB3 VB-test (black) and corresponding SEM (black shaded error bars), and the mean Y-position for the VIB6 VB-test (red) and corresponding SEM (red shaded error bars) are alle represented in mm. (**B**) Average velocity of the same animals for*

*the VB-period when exposed to VIB3 (n=40) and VIB6 (n=36). The X-axis represents time in s and the Y-axis represents speed in mm/s. The mean swim velocity for the VIB3 VB-test (black) and corresponding SEM (black shaded error bars), and the mean velocity for the VIB6 VB-test (red) and corresponding SEM (red shaded error bars) are plotted in mm/s and calculated from a 1 s sample interval from the raw data. Like (**A**), the blue X-lines represent the individual stimuli onsets (VIB3 or VIB6).*

The response in tank depth and velocity averaged over the 30 respective repetitions in each VB-test can be viewed in Figure 21 and Figure 22, and show that both stimuli generated clear stereotypical fear-like and anxiety-like defensive behaviors in both parameters (tank depth and swim velocity) for the initial- and recovery period, respectively.

Figure 21A shows the average absolute Y-position (mm) in response to VIB3 and VIB6 delivery, and the swim depths between the two stimuli were quite similar before, during and after the stimulus delivery, as noted from the Y-position traces in Figure 20A. Figure 21A+B show that on average, the fish expressed clear diving behavior suggestive of fear-like defensive responses upon immediate exposure to both VIB3 and VIB6 stimuli, seen from the decreased Y-position in the first few seconds following the stimulus onset (blue X-line). On average, the initial diving behavior was the greater in response to VIB3 than VIB6 stimulation, demonstrated by the stronger decrease in Y-position change for VIB3, but the fish responded the fastest to VIB6, which illustrated by the stronger dive slope during VIB6 delivery (Figure 21B). Furthermore, the animals expressed a longer period of recovery bottom-dwelling suggestive of anxiety-like defensive behavior in response to vibration VIB3: the average time it took for the Y-position increase toward pre-stimulus baseline values was longer in response to VIB3, indicating slightly slower habituation to this stimulus type (Figure 21A+B).

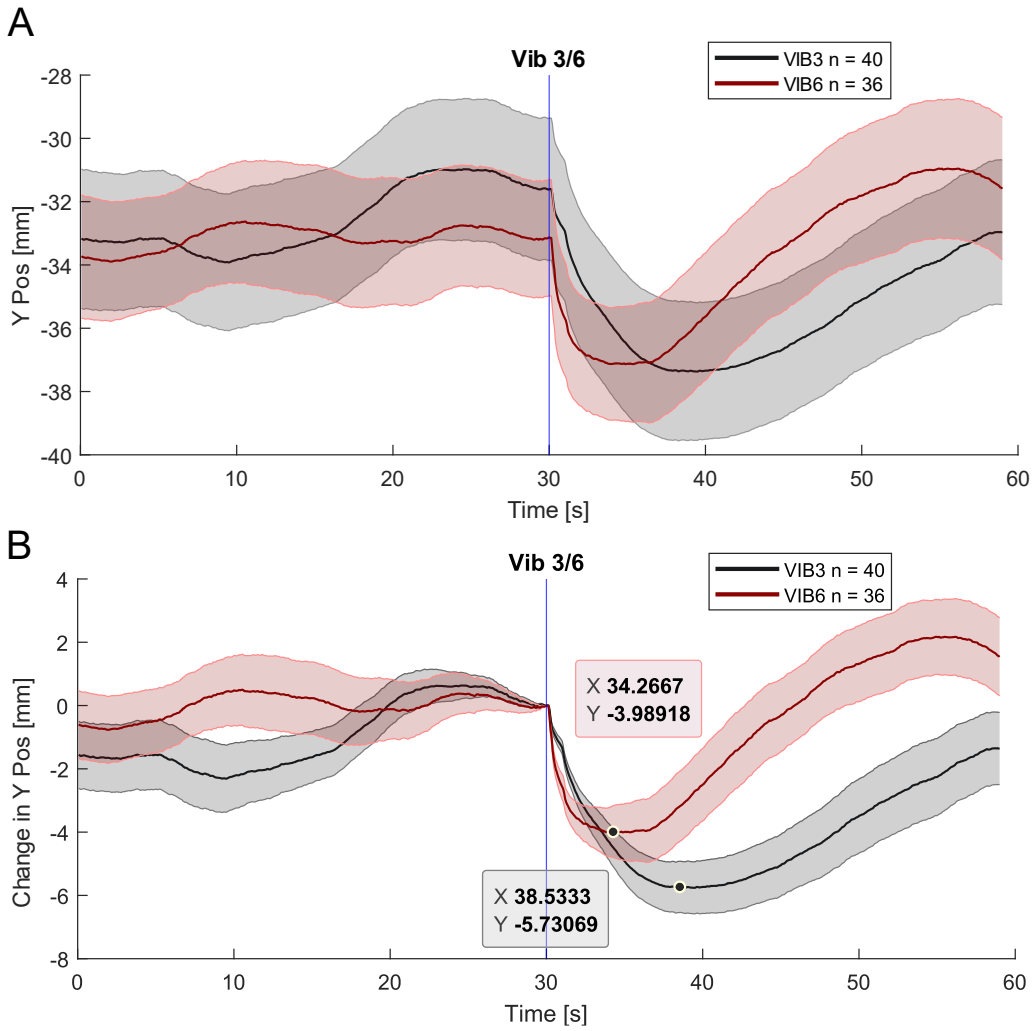

Figure 21: Average absolute Y-position and change in Y-position averaged over the VB-test in each subprotocol of the second optimization experiment. *(**A**) Absolute Y-position (mm) in the VB-phase when the juvenile WT were exposed to VIB3 stimuli and VIB6 stimuli, averaged over the 30 stimulus repetitions of each subprotocol. The X-axis displays time (s), the Y-axis shows vertical distance from the top if the tank (mm), and the blue X-line marks the stimulus onset (VIB3 or VIB6 depending on the subprotocol). The mean Y-position for the VIB3 subprotocol (black, n=40) and corresponding SEM (black shaded error bars), and the mean Y-position for the VIB6 subprotocol (red, n=36) and corresponding SEM (red shaded error bars) are alle represented in mm. (**B**) Mean change in Y-position for the same animals during the VB-test for each subprotocol: VIB3 (black, n=40), and VIB6 (red, n=36). Time is shown along the X-axis (s), and Y-position relative to the baseline (2 s pre-stimulus sample interval) is shown along the Y-axis (mm). The blue X-line denotes stimulus onset.*

Figure 22A shows the average absolute swim velocity (mm/s) calculated from a 1 s bin sample size. This was consistently elevated for the VB-test containing VIB6 repetitions for the pre-stimulus baseline, the immediate stimulus response, and the following recovery period, which supports the findings from the velocity traces in Figure 20B that the fish's overall swim speed was higher in the VIB6-containing VB-test.

On average, the fish increased their swim speed as an immediate reaction to both stimulus types, which was followed by a decrease in velocity, and slow recovery back to baseline values (Figure 22A+B). From Figure 22B, it appeared like the animals expressed a stronger initial fear-like response, in the form of a greater burst swim, when exposed to VIB6 stimulations: the peak in velocity change immediately upon the stimulus onset (blue X-line) was higher in response to VIB6 than VIB3 stimuli on average. Conversely, the period of anxiety-like freezing behavior was slightly lower in response to VIB6, indicating that the fish perhaps habituated somewhat less to this stimulus.

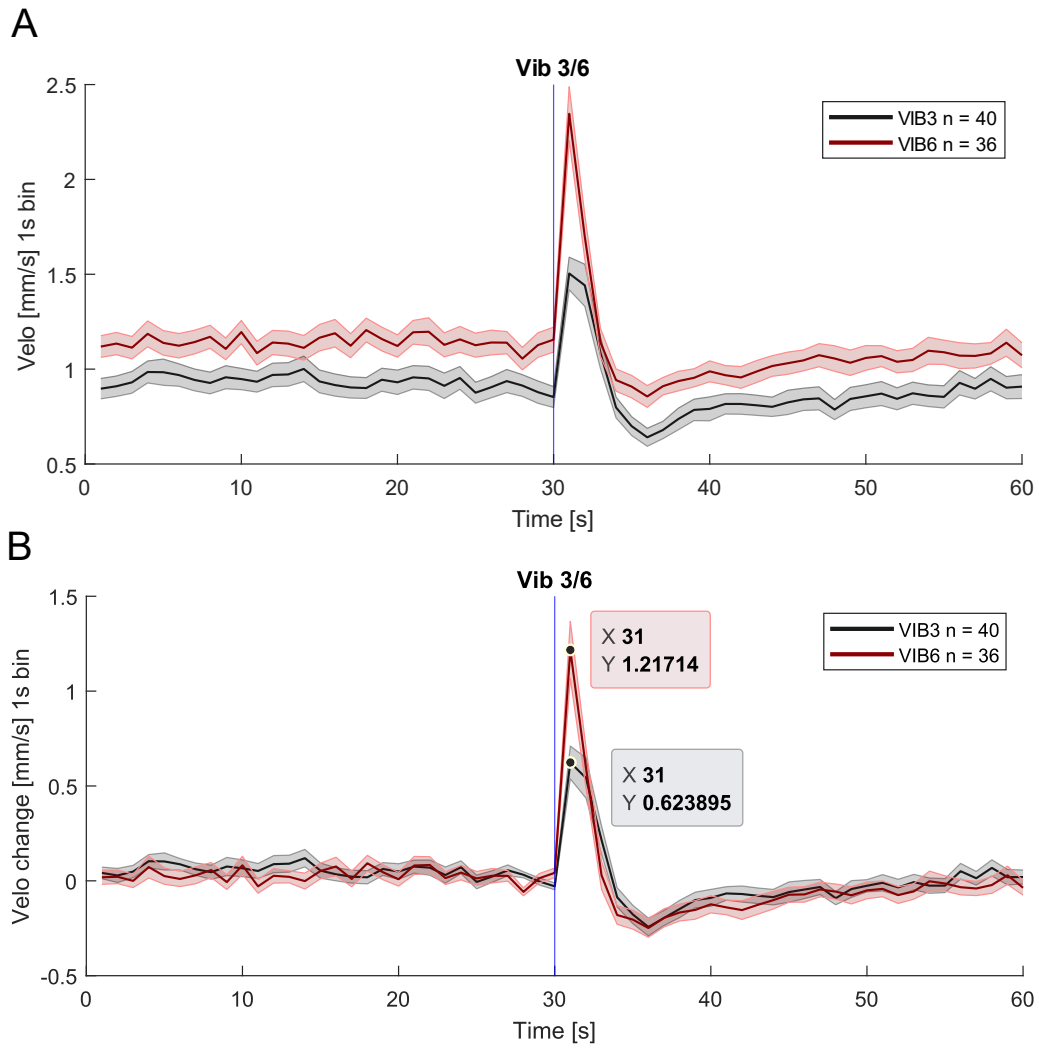

Figure 22: Average absolute velocity and change in velocity averaged over the two VB-tests in the second optimization experiment. *(**A**) Absolute velocity (mm/s) in the VB-phase when the juvenile WT were exposed to VIB3 stimuli and VIB6 stimuli, averaged over the 30 stimulus repetitions of each protocol iteration. The X-axis displays time (s), the Y-axis shows swim speed (mm/s), and the blue X-line indicates stimulus onset (ofVIB3 or VIB6 depending on the VB-test). The mean velocity (mm/s) calculated from a 1 s bin sample size and corresponding SEM (shaded error bar, mm/s) for the VIB3 VB-test (black, n=40) and for the VIB6 VB-test (red, n=36). (**B**) Mean change in velocity (1 s bin sample size, mm/s) and corresponding SEMs (shaded error*

bars, mm/s) for the same animals during the VB-test for each protocol iteration: VIB3 (black, n=40) and VIB6 (red, n=36). Time is shown along the X-axis (s), velocity (mm/s) relative to the calculated baseline (2s pre-stimulus sample interval) is shown along the Y-axis (mm), and the blue X-line denotes stimulus onset.

Since both stimulus types evoked strong defensive behaviors in the WT juvenile fish of the second optimization experiment, I chose to use VIB6 for my mechano-acoustic vibration assay in the upcoming behavioral experiment involving serotonergic manipulation. Additionally, the VIB6 vibration type (4.2 s, 238 Hz) was a prolonged version of VIB5 stimulus (0.84 s, 238 Hz), which was already utilized in the lab as a "strong" stimulus [55]. Choosing the VIB6 stimulus type might therefore have the advantage of being more comparable to previous lab work than choosing VIB3 (4.2 s, 24 Hz), which had an unequal frequency and duration compared to VIB5.

3.3 The effect of serotonergic manipulation on defensive behavior in juvenile zebrafish

I used an experimental protocol combining the NT-test and the VB-test to examine how chemo-genetic ablation of the DR affected the fish's expression of defensive behaviors (Figure 23). The VB-test was adapted to contain VIB6 stimuli, based on the results from the two previous optimization steps, and the protocol used was Vibration Protocol 3 (VP3). The experimental groups were as follows:

1) tph2:Gal4;UAS:ntr-mCherry + MTZ (ablated, total n = 39)
2) tph2:Gal4;UAS:ntr-mCherry + DMSO (sham treated control/placebo, total n = 45)
3) tph2:Gal4;UAS:GCamp6S + MTZ (MTZ treated control, total n = 38)

To approach my aim of studying the DR-ablation effect on defensive behavior, the main focus of the experiment was the comparison between the ablated group (1) and the control group given placebo/sham treatment (2). These animals were siblings from the same generation and fishline. On the other hand, comparing the ablated fish (1) with the MTZ-treated control fish (3) could possibly give some insight about MTZ administration itself as a confounding factor to the behavioral phenotype that could not be credited exclusively to the ablated condition. Nonetheless, this comparison was not the focus nor priority for this thesis and is therefore not discussed in detail in later sections, though the results are included. Additional observations in the screening of the animals during the confocal imaging also contributed to this decision (see methods section 2.4).

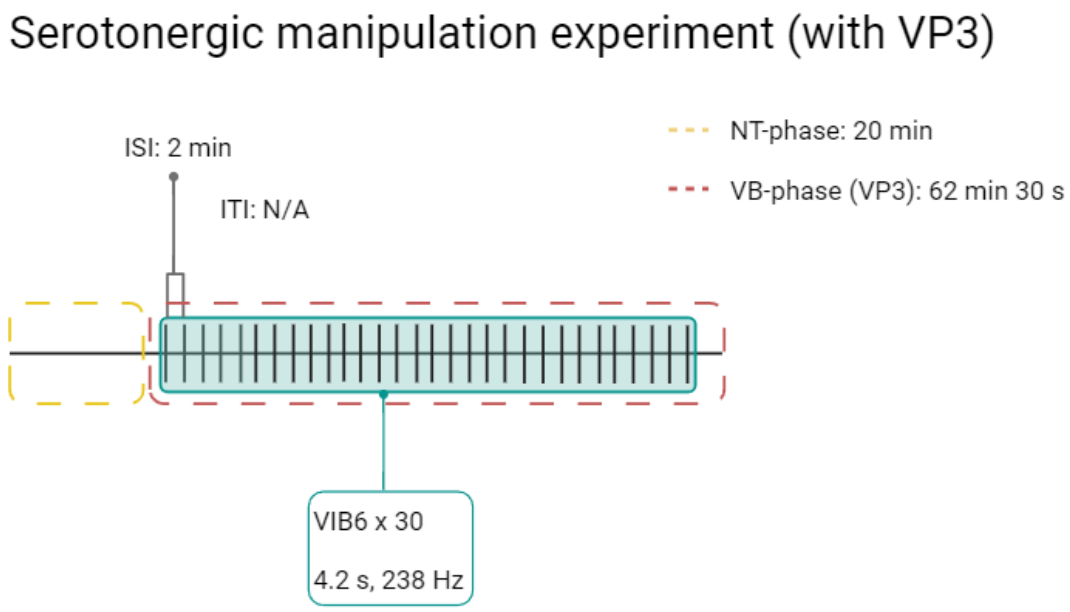

Figure 23: Overview of the serotonergic manipulation experiment using VP3 as presented in the methods section. *Total protocol duration was 1 h and 27 min (5220 s). The initial 20 min made up the NT-test (yellow dashed box). The following baseline period and camera auto reference timeout are not shown in the figure (4.5 min combined). The vibration phase lasted 62.5 min (red dashed box). The stimulus trial (turquoise box with vertical lines) contained 30 VIB6 stimulus repetitions, 2 min apart from each other (ISI).*

For the NT-phase of the experimental protocol, average positional- and velocity results can be seen in Figure 24: these results demonstrated that all three groups expressed typical anxiety-like behaviors associated with novelty exposure, like bottom diving, bottom-dwelling, freezing, cautious exploration and habituation.

The Y-position and tank distribution are shown in Figure 24A, B, and D. Immediate and strong bottom-diving behaviors were prevalent for all three groups, as observed by the sharp decline in average Y-position at the start of the test in Figure 24A. The ablated and placebo groups had similar diving responses (the placebo fish dove marginally deeper than ablated fish), but both dove deeper compared to the MTZ treatment control. Subsequent anxiety-like bottom-dwelling behavior was indicated by the continued low Y-position after the dive. This was least prominent in the ablated group, which began cautious tank exploration much faster than the two control groups: the rise in average Y-position after the bottom dive occurred earlier in the test for the ablated fish. All groups had reached a stable Y-position within approximately 10 minutes into experiment, which remained level for the remainder of the NT-test, indicating that all groups had habituated to the tank. The heatmaps of the tank position distribution probability can be seen in Figure 24B, and strengthens the observation in Figure 24A that the fish preferred the lower part of the tank in the early phase (indicative of bottom-diving and -dwelling), and tended to explore and habituate more during the later stage of the NT-test. In these heatmaps, the warm colored pixels were distributed in a band along the bottom for the early phase plots, and more homogeneously in the tank during the late phase plots.

Supporting evidence that the ablated fish began tank exploration first was also demonstrated from the early phase heatmaps (Figure 24B): ablated animals had an increased vertical spread in warm colored pixels along the tank bottom in this interval compared to the two controls. The scatter plots of the between-group comparison of the

tank position in the early period also supported this, as the mean Y-position for the ablated animals was slightly higher than the two other groups (Figure 24D). Even so, this observation was statistically non-significant from the Wilcoxon rank sum test ($p = 0.052$). The heatmaps and scatter plots for the late period also indicated that the placebo group had a slightly higher Y-position than the ablated group in this interval: this group had several warmer-colored pixels toward the top of the tank (Figure 24B), and a higher Y-position mean value (Figure 24D). There seemed to be a trend where the ablated group on average had a lower tank position than the placebo group for the late phase, but this was still a nonsignificant finding ($p = 0.086$).

Though Figure 24C showing the average velocity for the 20-minute NT-phase is very compact, it seemed that all three groups expressed stereotypical anxiety-like freezing behavior in the form of decreased swim speed after the rapid bottom-dive. This period was most noticeable for approximately the first minute into the experiment, after which the animals' velocity gradually increased and stabilized around 10 min into the experiment. The ablated group appeared to display a stronger freezing response than the placebo fish, as the decrease in velocity was stronger among the ablated animals. On the other hand, the subsequent speed increase seemed to be similar across all three groups, and may suggest that the animals had equal timing and rate of exploration and habituation for the velocity parameter.

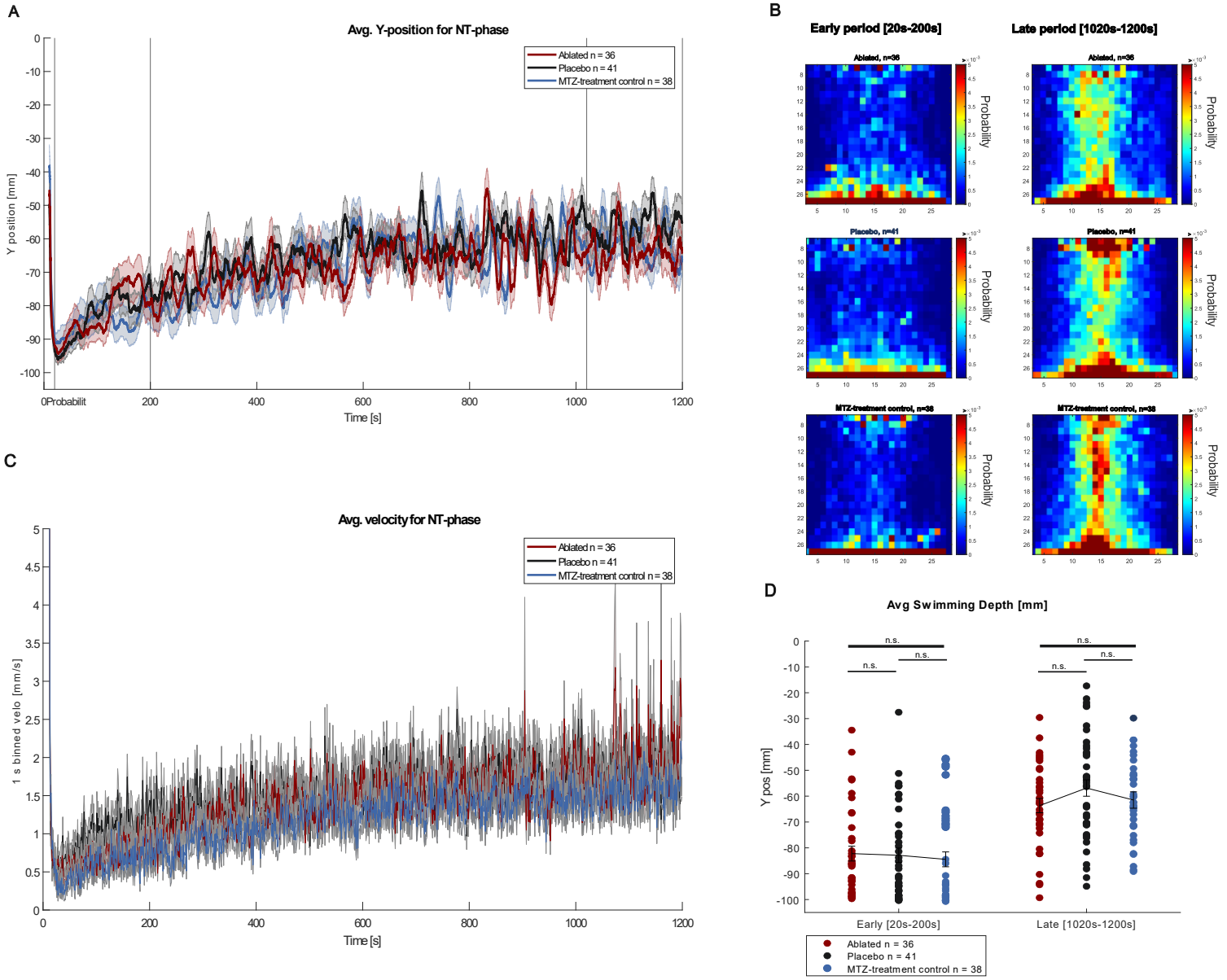

Figure 24: Average positional- and velocity results of the NT-test in the raphe-ablation experiment. *(**A**)* Mean *Y-position (mm) for the ablated group (red, n = 36), placebo group (black, n = 41), and MTZ-treatment control group (blue, n = 38). Corresponding SEM (mm) for each group shown by the shaded error bars in matching colors. X-axis shows time (s), Y-axis show vertical distance from the tank top (mm), and black X-lines visualize the sample intervals for the early and late periods in the heatmaps and the scatterplots. Data from the first 10 s are cropped out. (**B**) Cumulative heatmaps of tank position probability sampled over the early (left panels) and late (right panels) interval of the NT-phase for the same three groups. The pixel color is scaled to the color bar: values of 0 (cold/blue) to above 0.005 (warm/red). (**C**) Mean velocity for the same three groups, as well as their respective SEMs in mm/s. Y-axis shows swim speed (mm/s), and speed values are calculated from a 1 s bin sample size. Data for the first 10 s are cropped out. (**D**) Scatter plots of between-group comparisons of tank position for the early and late intervals of the NT-test for the same three groups (*= p≤0.05, **= p≤0.001 and n.s.= non-significant, two-sided Wilcoxon rank sum test).*

Figure 25A+B show the groups' average Y-position and velocity trace for the entire mechano-acoustic assay of the serotonergic manipulation experiment. Due to the length of the VB-test, and plotting the results from all the groups simultaneously, the graphs are hard to distinguish. Despite this, it seemed that the fluctuations in these two parameters remained stable over time and across groups: the graphs in both plots were relatively flat and in proximity to each other along the Y-axis for the whole assay. Even though the placebo group had a higher average velocity than the MTZ-treated control group before the start of the VB-test, these differences in speed evened out as the stimuli were delivered.

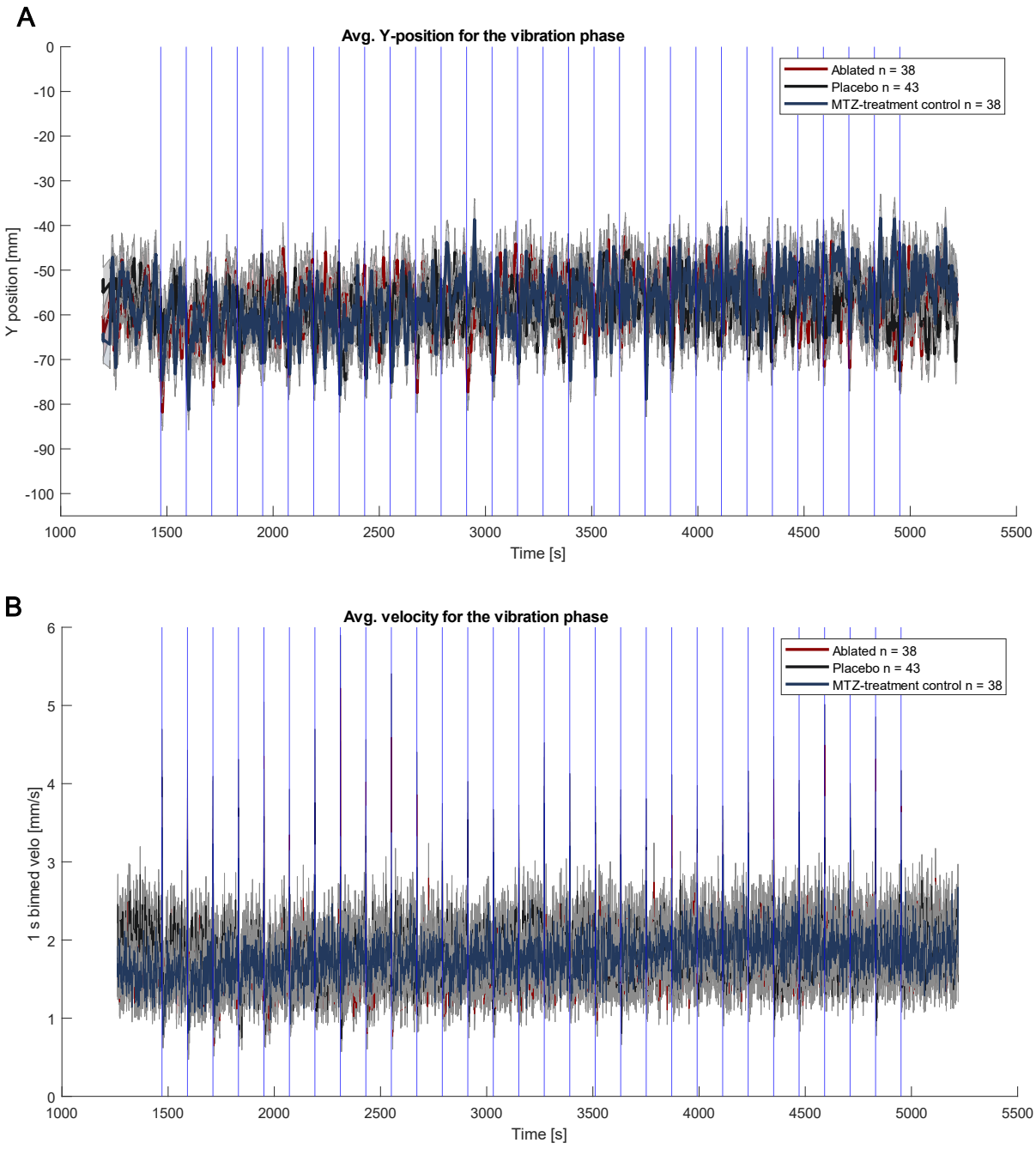

Figure 25: Average Y-position and velocity traces for the entire VB-test of the serotonergic manipulation experiment. *(**A**) Average Y-position (mm) for the ablated group (red, n=38), placebo (black, n=43), and MTZ-treatment control (blue, n=38). Corresponding SEMs*

*are shown as shaded error bars for each graph in matching color (mm). The X-axis shows time (s), the Y-axis shows vertical distance from the tank top (mm), and blue X-lines indicate the onset of individual VIB6 stimulations (30 repetitions in total). (**B**) Average velocity (mm/s) for the same three groups: (red, n=38), placebo (black, n=43), and MTZ-treatment control (blue, n=38). Corresponding SEMs are shown as shaded error bars for each graph in matching color. Speed values are calculated from a bin size of 1 s. The X-axis shows time (s), the Y-axis shows swim speed (mm/s), and blue X-lines indicate the onset of individual stimulations.*

Figure 26 and Figure 27 on the following pages show the average tank depth and swim velocity responses of the three groups for the entire VB-test. These plots are averaged over all the 30 stimulus repetitions in the assay and may not capture interesting trends occurring at a smaller time scale. I later present the three groups' responses averaged over just the first, middle and last 10 stimuli deliveries respectively. Therefore, I chose to perform statistical tests on those three distinct stimulus periods instead of the entire VB-period. This yielded a more in-depth analysis of the animals' behavioral fluctuations in response to continuous stimulation, and not just averaged out across the VB-test.

Figure 26 shows the groups' average response in swim depth as the Y-position and change in Y-position averaged over all 30 VIB6 stimuli of the serotonergic manipulation experiment. These plots demonstrated that all three groups expressed stereotypical fear-like behaviors in the initial period, and anxiety-like behaviors in the recovery period for the parameter. Figure 26B illustrates that the ablated group exhibited a stronger and more pronounced immediate burst dive response compared to the placebo group: on average, the DR-ablated animals dove significantly deeper relative to their baseline, and the sharper decline slope for the ablated group indicated that they reacted faster to the stimulus than the placebo animals. For the phase after the initial tank dive, the ablated group bottom-dwelled for a shorter period than did the placebo group, as seen from the earlier rise in Y-position. The swim depth response for the MTZ-treated control fish was similar to that of the ablated group for the immediate fear-like bottom-dive, but these animals expressed the least period of anxiety-associated bottom-dwelling and remarkably fast exploration after the initial response.

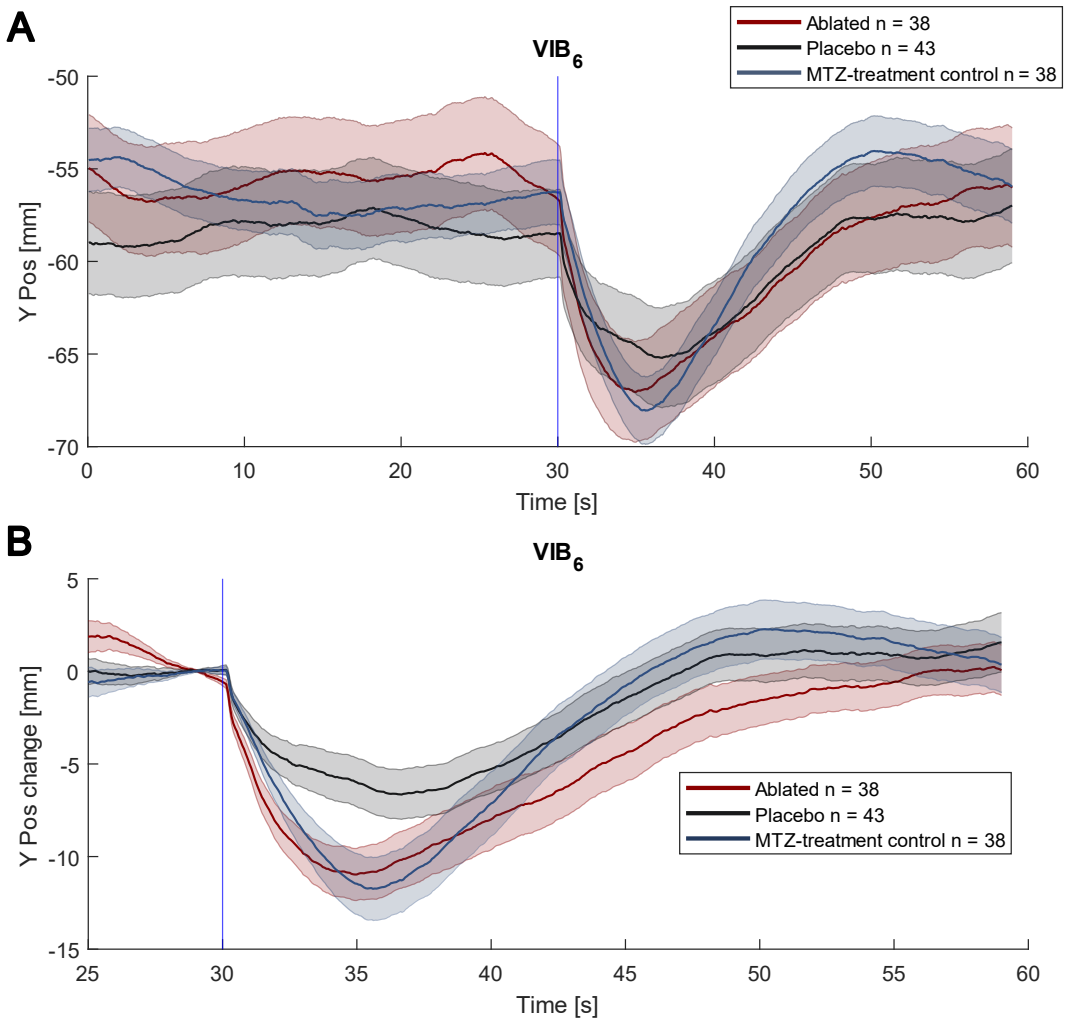

Figure 26: Average Y-position and change in Y-position, averaged over all 30 stimuli in the serotonergic manipulation experiment. *(**A**) Mean absolute Y-position (mm), for the three groups: ablated (red, n=38), placebo (black, n=43), and MTZ-treatment control (blue, n=38). Corresponding SEMs are shown as shaded error bars for each graph in matching color (mm). The X-axis shows time (s), the Y-axis shows vertical distance from the top of the tank (mm), and the blue X-line indicates stimulus onset. (**B**) Mean change in Y-position (mm) and their respective SEMs (mm), for the same three groups: ablated (red, n=38), placebo (black, n=43), and MTZ-treatment control (blue, n=38). The X-axis shows time (s), blue X-line shows stimulus onset, and the Y-axis shows vertical distance (mm) from the baseline sampled from 2 s before stimulus delivery.*

The absolute velocity and change in velocity averaged over all 30 stimuli in the DR-ablation experiment can be viewed in Figure 27. These plots illustrate that animals of each group on average displayed initial fear-like bottom-diving and a period of anxiety-like freezing in response to the VIB6 stimuli.

On average throughout the VB-test, the ablated fish expressed a stronger initial burst swim in reaction to the stimulus onset, represented by their higher peak in velocity relative to their baseline in comparison to the two control groups (Figure 27B). Furthermore, the period after the immediate fear-like response was marked by a decrease in velocity change in all groups, which was suggestive of freezing behavior. The ablated group expressed less of this anxiety-like response than the placebo group, as the magnitude of their speed reduction was smaller compared to the placebo group and their

recovery back toward baseline was faster. The swim speed response for the MTZ-treated control group was similar in magnitude to the placebo group for the immediate fear-like defensive behavior, but this group expressed the least degree of anxiety-like freezing during the recovery period: the MTZ-treated control fish had a minimal decrease in velocity relative to their baseline, and started to recover their speed very early.

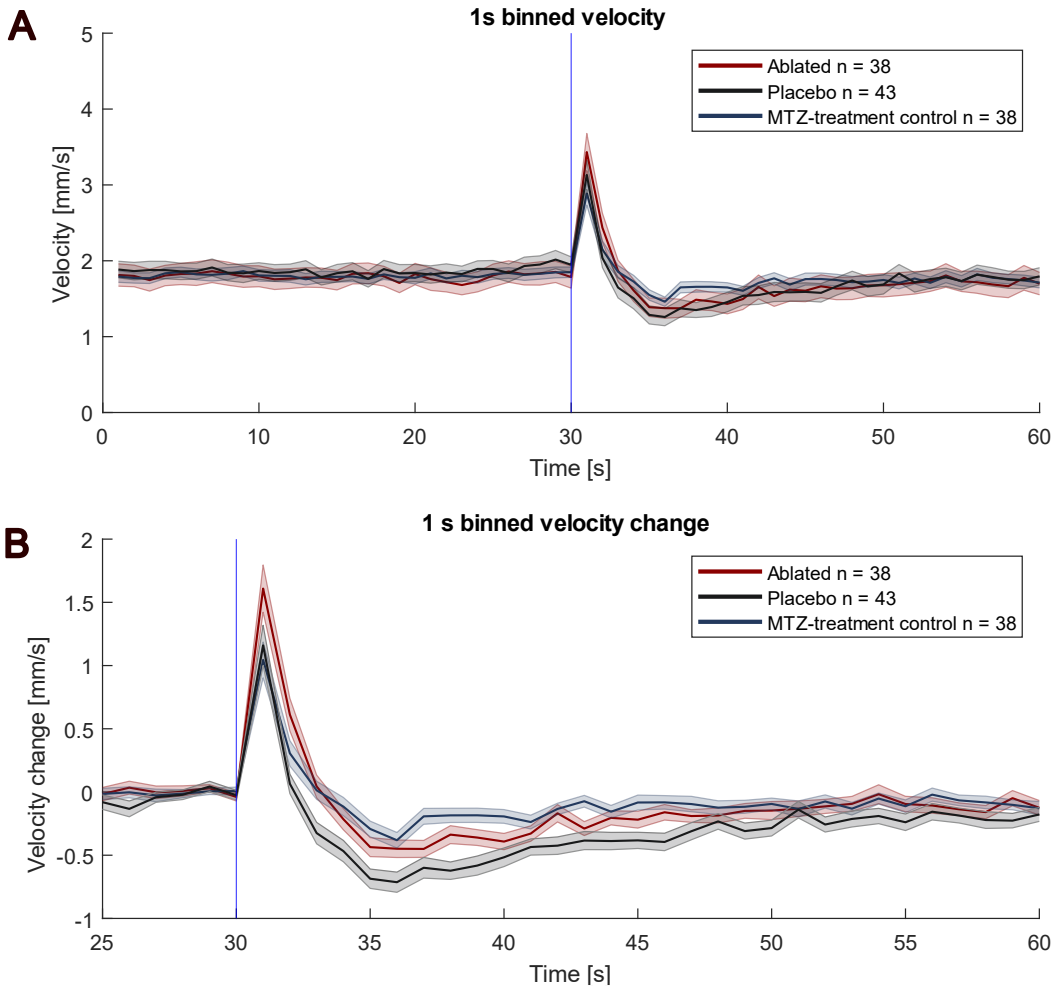

Figure 27: Average velocity and change in velocity, averaged over all 30 VIB6 stimulations. *(**A**) Average absolute velocity in mm/s, calculated with a bin size of 1 s, 30 s before and after the stimulus onset (blue X-line). Graphs show results for ablated group (red, n=38), placebo group (black, n=43), and the MTZ treatment control group (blue, n=38). SEMs are represented with shaded error bars around each corresponding graph. (**B**) Average change in velocity (mm/s) for the same animals, also calculated with a bin size of 1 s. Baselines are sampled 2 s prior to vibration delivery and aligned to 0 mm/s. Graphs show the average velocity relative to the group's baseline 5 s pre-stimulus and 30 s post-stimulus. SEMs are visualized with shaded error bars.*

Lastly, I investigated whether the three groups' defensive responses were consistent for all the delivered vibrations throughout the VB-test. I plotted the groups' absolute and change in Y-position and velocity, averaged over the first/middle/last 10 deliveries of VIB6 stimulations of the VB-test in Figure 28 and Figure 29.

Figure 28A+C depict the three groups' average Y-position and change in Y-position for the three stimulus intervals, respectively: the "Early" plots are averaged over the first ten VIB6 deliveries, the "Middle" plots are averaged over the 11^{th}-20^{th} stimuli, and the "Late" plots are averaged over the 21^{st}-30^{th} stimuli. The data in the corresponding scatter plots are sampled post-stimulus: the "initial" phase is meant to capture the immediate fear-like defensive behaviors (first 5 s post-stimulus), and the "recovery" phase is meant to detect the following anxiety-like defensive behaviors (5-30 s post-stimulus) (Figure 28B+D).

When comparing each groups' consistency in response over the course of the VB-test (early toward late stimulus phase), the initial bottom-diving magnitude was most stable for the ablated and MTZ-treated control group. Conversely, the placebo group's response weakened as the assay progressed (Figure 28C+D). Scatter plots of the within-group comparison of the Y-position change in the early versus late stimulus period for the ablated and placebo groups in Figure 28E further support this observation (two-sided Wilcoxon signed rank test): for the initial phase, the ablated group did not show a significantly difference in their Y-position change between the first and last 10 stimuli of the VB-test. On the other hand, the placebo group exhibited a significantly lower Y-position change in response to the early period than the late period of stimulus delivery ($p = 0.117$). This might be indicative of decreased fear-like bottom-diving and gradual habituation to the repeated stimulus in placebo animals. Interestingly, this was also the case for the recovery period of the stimulus delivery: ablated animals did not significantly alter their tank depth response magnitude from the first to the last 10 vibrations of the VB-test, whereas the placebo group displayed a significantly lower change in Y-position for the early period of the assay ($p < 0.000$). This might indicate that the placebo group expressed decreased anxiety-like bottom-dwelling as the VB-test progressed.

From Figure 28C, it seemed like the ablated animals had a stronger bottom-diving response across the whole VB-test compared to the placebo animals during the initial phase of the stimulus delivery (30s-35s in the plot). The Wilcoxon rank sum test for the initial bottom-dive period revealed no significant differences between the three groups' change in Y-position for the first nor middle 10 VIB6 stimuli (Figure 28D). Yet, during the initial phase of the last ten stimuli, the ablated fish had a significantly lower Y-position relative to their baseline than the placebo animals ($p = 0.0006$), indicating that they expressed a stronger bottom-diving behavior for the late part of the VB-test. MTZ-treated control animals also dove significantly deeper than the placebo animals for the initial phase of the last 10 stimuli ($p = 0.0114$).

For the post-stimulus recovery phase (35-60 s in the plot), the ablated group seemed to bottom-dwell less for the first 10 stimuli compared to the placebo group: their average Y-position reached pre-stimulus values earlier, and the slope of the incline was stronger (Figure 28C). The Wilcoxon rank sum test for this interval was, however, non-significant ($p = 0.0644$). No significant differences in the recovery phase were found for the middle 10 stimuli either. For the recovery phase of the 10 last vibrations, both the ablated and MTZ-treated control fish had a significantly lower Y-position change compared to the placebo fish ($p = 0.0004$, and $p = 0.0189$, respectively). Furthermore, the ablated group seemed recover at a higher rate immediately after the initial period (around 35-40 s in Figure 28C) during the last 10 stimuli, as seen from the sharper in slope incline. An interesting observation was that the MTZ-treated control group appeared to have the highest rate of Y-position recovery for all three periods despite displaying strong bottom-diving in the initial phase for all three stimulus periods.

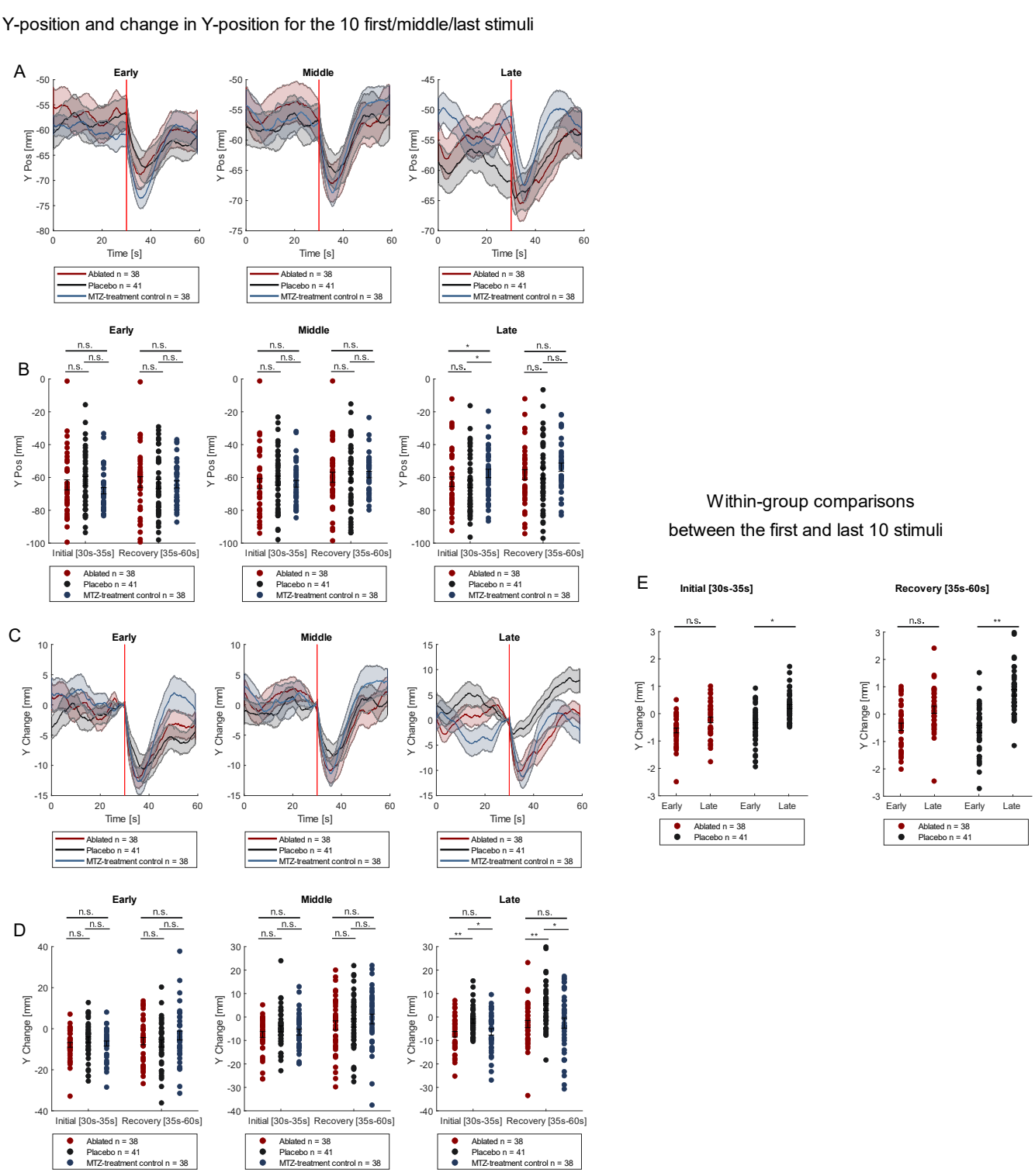

Figure 28: Average absolute Y-position and change in Y-position for the first/middle/last 10 stimuli in the VB-test of the serotonergic manipulation experiment and corresponding scatter plots for the initial and recovery post-stimulus phases. *(**A**) Mean absolute Y-position (mm) for the three groups: ablated (red, n=38), placebo (black, n=41), and MTZ-treatment control (blue, n=38), and corresponding SEMs in matching colors (shaded error bars, mm). The X-axis shows time (s), the Y-axis shows vertical distance from the tank top (mm), and the red X-line indicates stimulus onset. Left plot averages over the first 10 stimuli, the middle plot averages over the middle 10 stimuli, and the right plot averages over last 10 stimuli. (**B**) Scatter plots of the between-group comparisons of the average Y-position for the same three groups over the early/middle/late periods sampled from the "initial" phase (left, 30s-35s) and the "recovery" phase*

*(right, 35s-60s). Two-sided Wilcoxon rank sum tests were performed: *= p≤0.05, **= p≤0.001 and n.s.= non-significant. (**C**) Mean change in Y-position (mm) for the same animals. The Y-axis shows Y-position (mm/s) relative to the calculated baseline (2 s pre-stimulus sample interval). (**D**) Scatter plots of the between-group comparisons of the average change in Y-position for the same three groups over the early/middle/late 10 stimuli for the early (left) and late (right) phase (two-sided Wilcoxon rank sum tests: *= p≤0.05, **= p≤0.001 and n.s.= non-significant). (**E**) Scatter plots for the within-group comparisons of the average change in velocity between the early 10 and late 10 stimuli, for the initial (left panel) and recovery period (right panel), within the ablated and the placebo groups, respectively (two-sided Wilcoxon signed rank tests: *= p≤0.05, **= p≤0.001 and n.s.= non-significant).*

Figure 29A+C show the velocity and change in velocity averaged over the early/middle/late 10 VIB6 stimuli for the experimental groups, respectively. The "initial" phase in the corresponding scatter plots aims to reflect the initial fear-like defensive behaviors (first 3 s post-stimulus), and the "recovery" phase detects the following anxiety-like defensive behaviors (3s-10s post-stimulus).

The burst swim magnitude within each group across the VB-test appeared to be quite consistent within all three groups during initial phase of the three stimulus periods (Figure 29C+D). Figure 29E shows the scatter plots of the within-group comparison of velocity change in the early versus late stimulus period for the ablated and placebo groups (two-sided Wilcoxon signed rank test) for the initial phase. Here, no significant difference in the velocity change was found for the initial phase across the early and late stimulus period for either of the two groups. For the recovery phase, the ablated group had a significantly higher velocity change for the first 10 vibrations compared to the last 10 vibrations during the recovery period of the stimulus delivery, indicative of less freezing during the start of the VB-test. On the other hand, placebo animals did not significantly alter their velocity change from the first to the last 10 vibrations of the VB-test during the recovery period.

Ablated animals appeared to express stronger initial fear-like burst swimming during the whole VB-test compared to two control groups (Figure 29C+D). This is illustrated by this group's stronger peak in velocity change upon stimulus administration. Figure 29E shows the scatter plots of the between-group comparison between the ablated and placebo group (two-sided Wilcoxon rank sum test): for the initial phase (30-33 s in the plot) the DR-ablated animals had a significantly higher velocity change than placebo animals on for all three stimulus periods (early: $p = 0.0180$, middle: $p = 0.0074$, late: $p = 0.0004$). The MTZ-treated control group had a significantly lower burst swim magnitude than the ablated group for the first 10 stimuli ($p = 0.0116$), but significantly higher burst swim magnitude than the placebo group for the last 10 stimuli ($p = 0.0050$).

For the post-stimulus recovery phase (33-40 s in Figure 29C), the ablated group seemed to consistently freeze less than the placebo group during the entire VB-test. This is illustrated by their smaller velocity decrease magnitude and stronger slope in average velocity incline. However, there was no significant difference for the recovery period between the ablated and placebo groups during the first 10 vibrations. On the other hand, the ablated fish had a significantly higher velocity relative to their baseline compared to the placebo fish during the middle ($p = 0.0253$) and late part of the VB-test ($p = 0.0277$). Moreover, the MTZ-treatment control group had a consistently higher velocity change compared to the placebo group throughout the VB-test for the recovery period (early: $p =0.0302$, middle: $p = 0.0001$, late: $p = 0.000$), which was also

significantly higher than the ablated group, but exclusively for the last 10 stimuli (p = 0.0024).

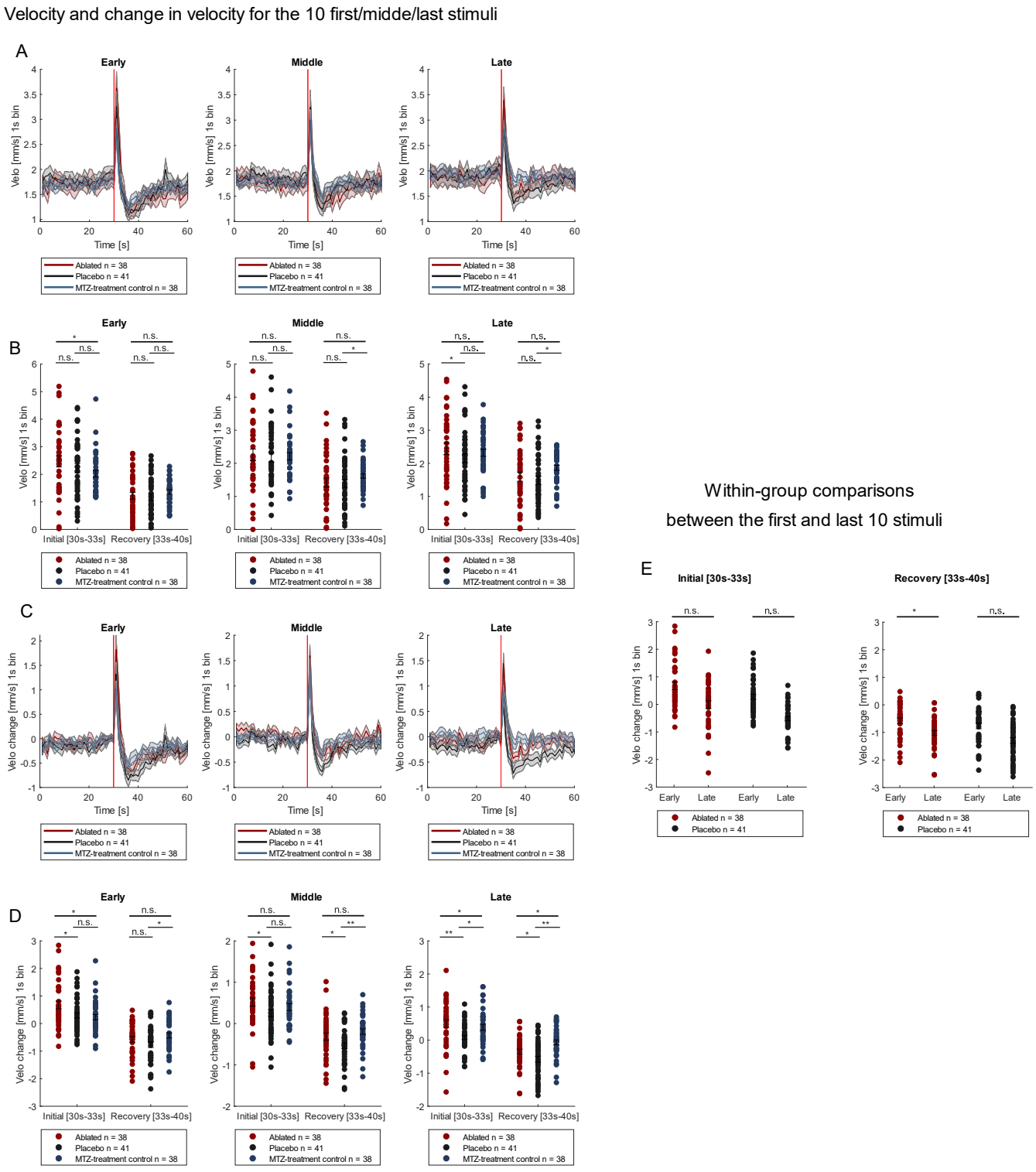

Figure 29: Average absolute velocity and change in velocity for the first/middle/last 10 stimuli in the VB-test of the serotonergic manipulation experiment and corresponding scatter plots for the initial and recovery post-stimulus phases. *(**A**) Mean absolute velocity (mm/s, 1 s bin sample size) for the three groups: ablated (red, n=38), placebo (black, n=43), and*

*MTZ-treatment control (blue, n=38), and corresponding SEMs in matching colors (shaded error bars, mm/s). The X-axis shows time (s), the Y-axis shows swim speed (mm/s), and the red X-line indicates stimulus onset. Left plot averages over the first 10 stimuli. The middle plot averages over stimulus number 11-20. The right plot averages over stimulus number 21-30. (**B**) Scatter plots of the between-group comparisons of the average change in velocity for the same three groups over the early/middle/late 10 stimuli (two-sided Wilcoxon rank sum tests: *= p≤0.05, **= p≤0.001 and n.s.= non-significant). Sampled from the "initial" phase (30s-33s, left) and the "recovery" phase (33s-40s, right). (**C**) Mean change in velocity (mm/s, 1 s bin size, 2 s pre-stimulus baseline interval) and SEMs for the same animals. (**D**) Scatter plots of the between-group comparisons of the average change in velocity for the same three groups over the early/middle/late 10 stimuli, for the initial (left) and recovery (right) phase (two-sided Wilcoxon rank sum tests: *= p≤0.05, **= p≤0.001 and n.s.= non-significant). (**E**) Scatter plots for the within-group comparisons of the average change in velocity in the initial (left) and recovery (right) periods, sampled from the early 10 versus the late 10 stimuli, for the ablated and the placebo groups, respectively (two-sided Wilcoxon signed rank tests: *= p≤0.05, **= p≤0.001 and n.s.= non-significant).*

3.4 The effect of serotonergic manipulation on the neuronal activity in defensive behavior

The final aim of the project was to investigate the neuronal activity in the DR-ablated animals of the previous behavioral experiment. This was done by post-hoc immunostaining of ERK and measuring the ratio of phosphorylated versus total ERK fluorescence signal intensity. The total sample size was 45, with n = 15 animals in each of the previous groups (ablated, placebo, MTZ-treatment control). All the samples were aligned to the Z-projected reference brain (DR-ablated sample) in FIJI (Figure 30, left), and the following data analysis and statistical tests were performed in MATLAB (Figure 30, right).

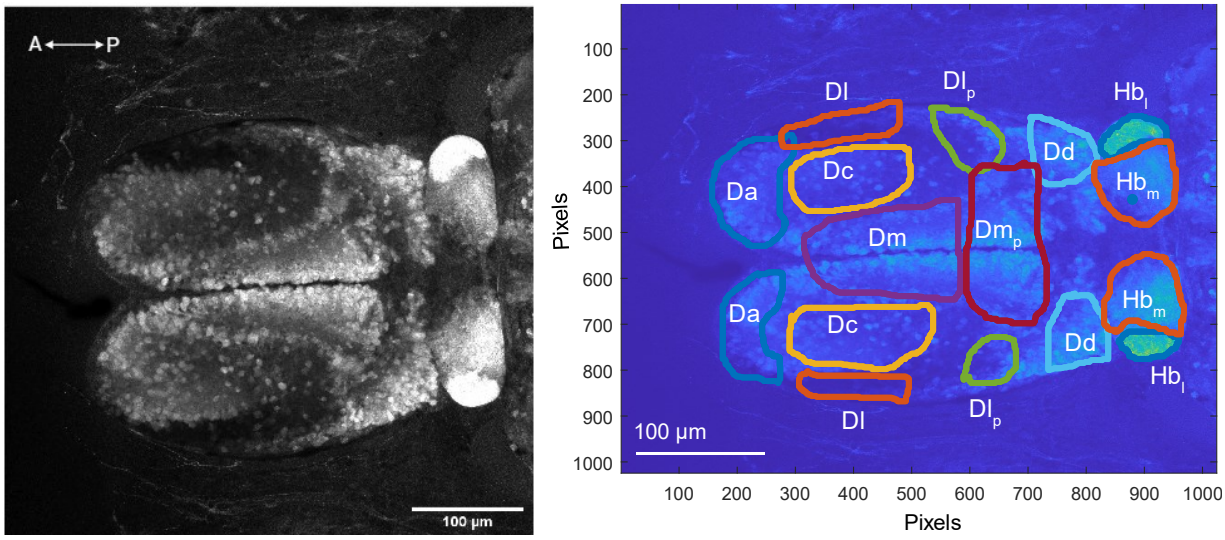

Figure 30: Z-projected reference brain in FIJI, and the delineated forebrain areas in MATLAB used for statistical testing. Left panel: *Z-projected composite image (1024 x 1024-pixels) of the reference brain (horizontal plane) in FIJI (ImageJ). The raw image was taken with a ZEISS LSM confocal microscope with the channel capturing pERK signals. The picture is focused on*

the dorsal parts of the pallium (dorsal telencephalon) and the habenulas in the diencephalon. Right panel: image showing the delineation of the reference brain performed in MATLAB. Pixels within the delineated zones were averaged and p-scored for the segment-based inter-group comparisons in Figure 31C and Figure 32C. Abbreviations of zones in the zebrafish dorsal pallium: anterior (Da), lateral (Dl), lateral posterior (Dl_p) central (Dc), medial (Dm), medial posterior (Dm_p) and dorsal (Dd) regions. Abbreviations of the habenula subregions in the diencephalon: lateral habenula (Hb_l) and medial habenula (Hb_m). As with Figure 5, these Hb subdivisions are relative to the Z-projected image and not the anatomical regions in the mammalian habenulas.

Comparisons between the ablated group and the placebo group (Figure 31), as well as between the ablated and MTZ-treatment control group (Figure 32) were performed. As with the behavioral experiments, the focus of my thesis was the comparison between the ablated and the placebo groups.

Figure 31A-C show the pixel-based neuronal activity measured for the whole dorsal telencephalon (pallium) and the habenulas of the diencephalon in the DR-ablated animals (n = 15) compared to the placebo group (n = 15). This is normalized relative to the max value within each of the samples. Figure 31A-C were made by binning the original 1024x1024 pixel image by 10 along each axis (the mean of 100 pixels in each binned frame) for a plot dimension of 103 x 103 pixels. Figure 31A depicts the delta neuronal activity, which was calculated by subtracting the mean pERK/tERK ratio of the placebo group from the mean pERK/tERK ratio of the ablated group for each binned pixel frame. Red colored areas indicated that the ablated animals on average had a higher neuronal activity, whereas blue color indicated they had a lower activity compared to the placebo group in that region. The ablated animals seemed to have quite a mosaic pattern in the center of the forebrain, with interspersed red and blue areas. Nonetheless, the Dc and the midline of the Dm seemed to exhibit less activity in the ablated animals than the placebo animals, as they had a higher ratio of pixels with blue contra red. Furthermore, ablated fish seemed to harbor increased neuronal activity in the anterior part of the dorsal pallium (Da) as well as several posterior regions of the dorsal pallium: the Dd, the posterior parts of the Dl and Dm (Dl_p and Dm_p respectively), and the lateral and medial regions of the Hb (Hb_l and Hb_m, respectively).

Figure 31B+C depict which binned pixel frames that demonstrated significantly higher (B) or lower (C) neuronal activity in the ablated group versus the placebo group, which have been applied as a mask over the delta activity in each respective plot. p-scoring was performed by Wilcoxon rank sum testing of the pERK/tERK ratio between the ablated and placebo groups for each of the binned pixel frames (right-tailed for Figure 31B and left-tailed for Figure 31C). Figure 31B confirmed that the DR-ablated animals on average had a significantly higher pERK/tERK ratio in their anterior and posterior dorsal pallial regions compared to the placebo animals. Likewise, Figure 31C demonstrated that the ablated animals had significantly lower pERK/tERK ratio in the Hb area of the diencephalon as well as regions centrally in the telencephalon compared to the placebo animals.

The scatter plots in Figure 31D show the absolute comparison of neuronal activity (pERK/tERK ratio) specific and relative to the delineated regions between the ablated and placebo groups (Figure 30B). This was calculated by averaging (mean) all the binned pixel frames within the area for all the samples, and p-scoring with Wilcoxon rank sum testing. Contrary to the pixel-based plot depicting areas of higher activity in ablated animals contra the placebo animals (Figure 31B), no significant findings were found for the delineated areas in the posterior telencephalon. Despite this, a higher mean could be observed in the DR-ablated group for both the Dm_p and Dd in the scatter plots (Figure

31D). However, the ablated group had a significantly higher neuronal activity in the anterior dorsal telencephalon (Da) than placebo animals ($p = 0.0381$). Lastly, the observed lower neuronal activity in the dorsal pallium's lateral regions (Dl and Dl_p), central and medial regions (Dc and Dm) for the ablated animals compared to the placebo animals (Figure 31C), was also non-significant for the delineation-based analysis. This was also the case for the Hb_l and Hb_m portions of the habenulas.

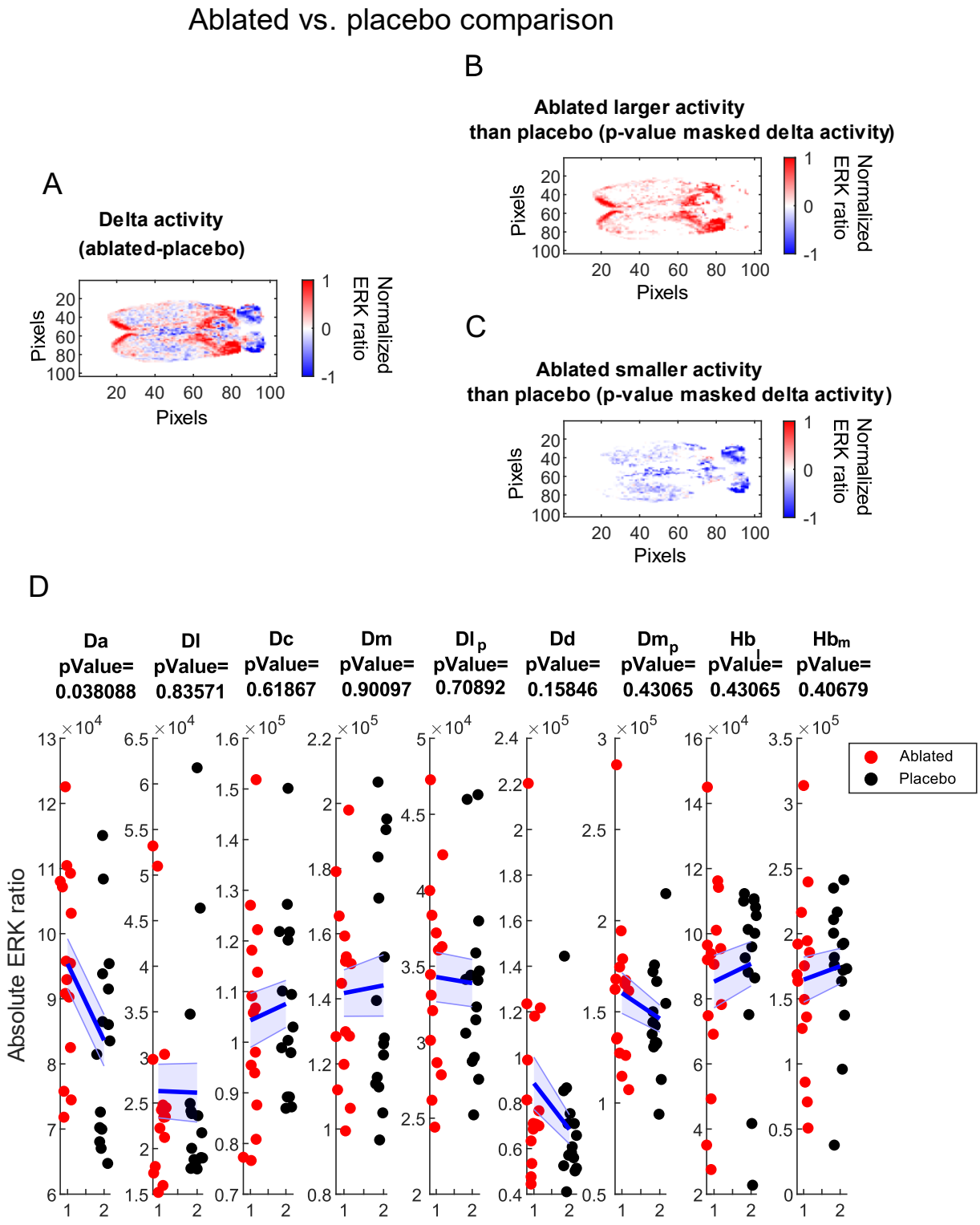

Figure 31: pERK/tERK ratio comparison between the ablated group and the placebo group, for the whole telencephalon, and for each brain region. *(**A**) Delta activity of the normalized mean pERK/tERK ratios, where the placebo group (n=15) is subtracted from the ablated group (n=15) for each binned pixel frame (10-pixel bin size). The axes show the binned image dimensions (103 X 103 pixels). Red color indicates a higher ERK ratio, whereas blue color indicates lower ERK ratio on average for the DR-ablated animals compared to the placebo animals. (**B**) The binned pixel frames with significantly higher activity in DR-ablated animals compared to placebo animals. This was visualized by performing a right-tailed Wilcoxon rank sum test, where significant pixel bins (p-values ≤ 0.05) were projected as a mask over the delta activity. (**C**) The*

*binned pixel frames with significantly lower activity in DR-ablated animals compared to placebo animals. This was visualized by performing a left-tailed Wilcoxon rank sum test, where significant pixel bins (p-values ≤ 0.05) were projected as a mask over the delta activity. (**D**) Scatter plots for the comparison of the absolute pERK/tERK ratio between the ablated (red, n=15) and placebo (black, n=15) groups, for each of the delineated regions. The brain region and the corresponding p-value are noted at the top of each plot. The Y-axis shows the absolute pERK/tERK ratio. Each data point indicates a sample's mean pERK/tERK ratio averaged over the binned pixels within the delineated area. The mean value for each group and corresponding SEMs are visualized from the interconnected blue lines and shaded error bars between the two groups.*

The comparison of the pERK/tERK data between the ablated group and the MTZ-treated control group is shown in Figure 32. Trends for this comparison seemed to be largely consistent with the ablated versus placebo comparison: pixel-based significance testing indicated that ablated animals had a higher average activity for the anterior and posterior regions of the dorsal pallium (Figure 32B), and lower activity in telencephalic central and lateral regions as well as the diencephalon compared to the MTZ-treatment control group (Figure 32C). One difference between the two comparisons was that the ablated group displayed a higher pERK/tERK ratio for the entire medial region of the dorsal pallium compared to the MTZ-treated control, which was not observed for the first comparison (Figure 31A-C). These observations were also found to be statistically significant for the delineated regions of Da, Dm, Dd and Dm_p as demonstrated by Figure 32D.

The scatter plots of the delineated brain regions in Figure 32D confirmed a significantly higher pERK/tERK ratio for the ablated animals compared to the MTZ-treated control animals for the anterior dorsal pallium (Da), and the Dd in the posterior parts of the forebrain. These animals also seemed to have increased activity in their Dm (and Dm_p): these observations were close to statistically significant but still too ambiguous to form a conclusion. The ablated group appeared to have less neuronal activity in the lateral (Dl and Dl_p) and central (Dc) telencephalon as well as the habenulas (Hb_l and Hb_m). The DR-ablated fish seemed to harbor a smaller neuronal activity for the centrally located forebrain regions of Dc, Dl, Dl_p and Hb, but the delineation-based findings were non-significant. Taken together, the ablated/MTZ-treatment control comparison yielded similar results as the ablated/placebo comparison, but the differences observed seemed to be stronger and thus yield more statistically significant findings.

Taken together, the ablated group seemed to have a stronger difference in neuronal activity compared to the MTZ-treatment control group, than compared to the placebo group. This was not expected since the ablated and MTZ-treatment control groups displayed strikingly similar behavioral results in both of the behavioral assays. Furthermore, the MTZ-treatment control group behaved very differently from the placebo control group, which also was surprising due to their shared control condition. Due to these discrepancies between expressed behavior and the pERK results, I chose to not interpret the effect of ablation based on the MTZ-treatment control, but instead discuss the behavioral effect of DR-ablation solely in context of the placebo treatment further in my thesis. The uncertainty regarding the MTZ-treatment control group as a valid control is addressed further in the limitations section.

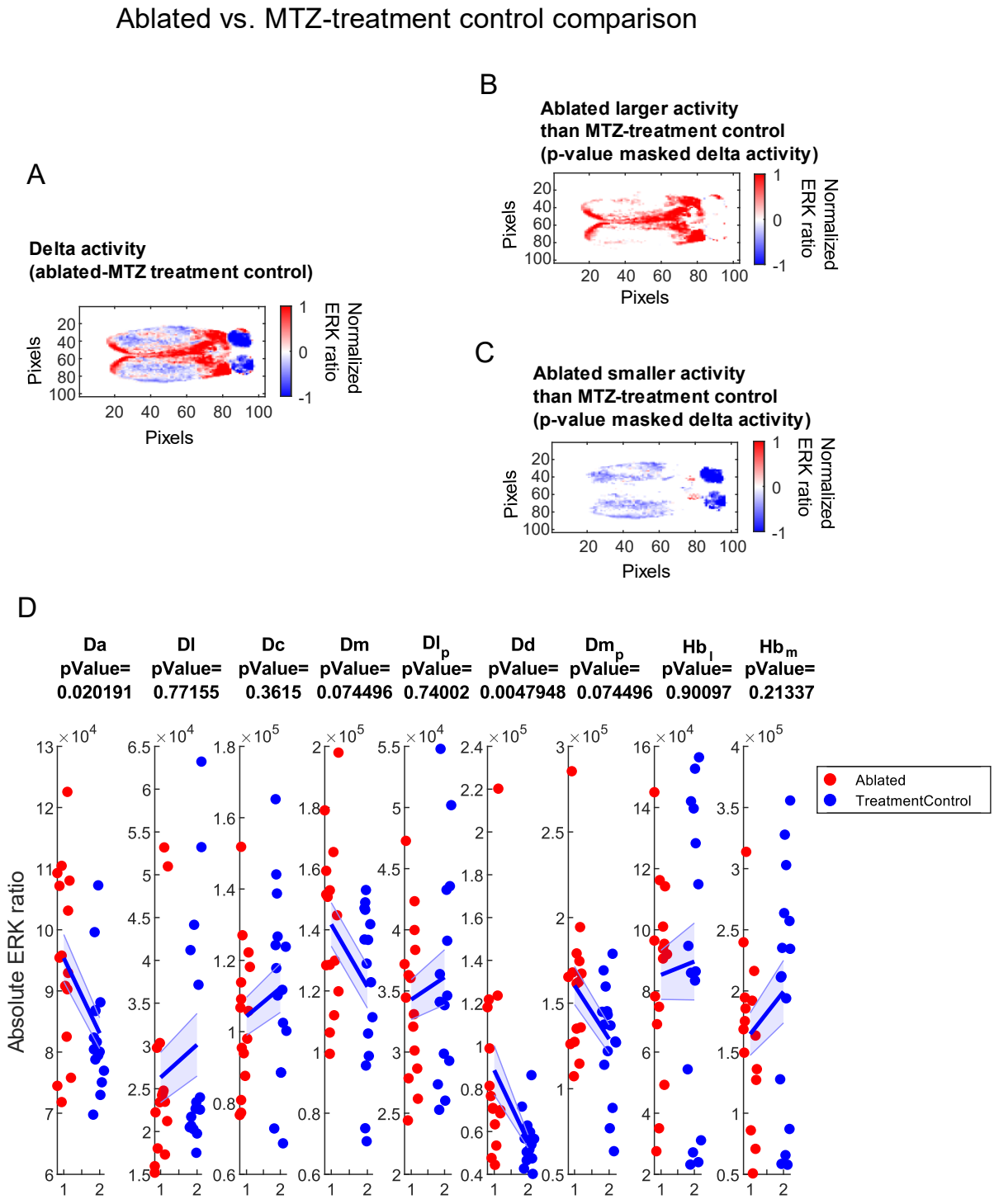

Figure 32: pERK/tERK ratio comparison between the ablated group and the MTZ-treatment group, for the whole telencephalon, and for each brain region. *(**A**) Delta activity of the normalized mean pERK/tERK ratios, where the placebo group (n=15) is subtracted from the MTZ-treatment group (n=15) for each binned pixel frame (10-pixel bin size). The axes show the binned image dimensions (103 X 103 pixels). Red color indicates a higher ERK ratio, whereas blue color indicates lower ERK ratio on average for the DR-ablated animals compared to the MTZ-treatment animals. (**B**) The binned pixel frames with significantly higher activity in DR-ablated animals compared to placebo MTZ-treatment animals. This was visualized by performing a right-tailed Wilcoxon rank sum test, where significant pixel bins (p-values ≤ 0.05) were projected as a mask over the delta activity. (**C**) The binned pixel frames with significantly lower activity in DR-ablated animals compared MTZ-treatment animals. This was visualized by performing a left-tailed*

*Wilcoxon rank sum test, where significant pixel bins (p-values ≤ 0.05) were projected as a mask over the delta activity. (**D**) Scatter plots for the comparison of the absolute pERK/tERK ratio between the ablated (red, n=15) and MTZ-treatment (blue, n=15) groups, for each of the delineated regions. The brain region and the corresponding p-value are noted at the top of each plot. The Y-axis shows the absolute pERK/tERK ratio. Each data point indicates a sample's mean pERK/tERK ratio averaged over the binned pixels within the delineated area. The mean value for each group and corresponding SEMs are visualized from the interconnected blue lines and shaded error bars between the two groups.*

4 Discussion

4.1 Vibration types with long duration and high frequency evoke the strongest defensive behaviors in the VB-test

In my thesis, I used an experimental paradigm that exposed freely behaving juvenile zebrafish to novelty and subsequently, aversive mechano-acoustic stimulations in the Zantiks behavioral setup. The novel tank test (NT-test) measures reactions to unfamiliar surroundings, and typical responses are bottom-diving, bottom-dwelling, and freezing, which are behaviors associated with anxiety [78-81]. These decrease by time as the trial progresses, and the fish typically habituate 5-10 minutes into the test [82]. Findings corroborating these behavioral tendencies have been observed in the lab with both the older setup and the current Zantiks system [55, 85, 86]. My first experiment using juvenile wildtype (WT) zebrafish successfully demonstrated behavioral responses that are stereotypical for novelty exposure, and thus supported the validity of the NT-test (Figure 15).

Furthermore, the vibration test (VB-test) is designed to deliver aversive stimulations that are startling for the juvenile zebrafish. Initial behaviors associated with fear and panic upon immediate stimulus exposure are bottom-diving and burst swimming [81, 83, 84]. After the threat is over, the animals express recovery behaviors reminiscent of anxiety and risk-assessment such as bottom-dwelling and freezing [60]. Previous work in the lab with the vibration stimulus assay has shown to evoke varying degrees of these defensive responses, which is why I aimed to optimize this behavioral assay [55, 85, 86]. My hypothesis was that the stimulus properties influence the expressed behavioral phenotype strength, and more specifically that stimuli of longer duration and higher frequency would elicit stronger defensive responses.

The VB-test of my first optimization step delivered ten repetitions of six unique vibration stimulus types to WT juvenile zebrafish and measured their tank depth as well as swim velocity (1 min between repetitions of the same type (ISI), 20 min between each of the six trials (ITI)). Here, I validated that the vibration test with the Zantiks setup successfully promotes fear-like behaviors, which was demonstrated by robust burst swimming and bottom-diving for several of the stimulus types (Figure 17 and Figure 18). Moreover, I found that these unique vibration types did not elicit uniform strength of defensive responses, which aligned with my hypothesis. Specifically, stimuli with longer duration (VIB3 and VIB6), or with higher frequency (VIB4, VIB5, VIB6) seemed to alter the animals' Y-position the most from baseline, indicating robust bottom-diving responses (Figure 17B). On the other hand, all the six stimulus types successfully generated a transient velocity increase indicative of burst swimming, but those of lower frequency seemed to generate the largest magnitude on average (Figure 18B). However, it is important to note that the low baseline velocity during these stimuli trials might be misleading. The average baseline speeds during the delivery of VIB4-VIB6 were comparable to or even exceeding the burst swim responses to VIB1 and VIB2 (Figure 18A + Figure 16B). Therefore, the absence of a pronounced fear-like response in swim speed may be attributed to the fact that the fish were already swimming at their

maximum speed. This baseline alteration was also apparent for the Y-position data, which is why I doubled the inter-stimulus and inter-trial interval (ISI = 2 min and ITI = 40 min, respectively) for the next optimization step. Finally, the longest stimuli also seemed to elicit the more freezing in the recovery period, illustrated by the prolonged interval of decreased speed relative to the baseline after the initial response.

Taken together, a prominent swim depth response seemed to be dependent on stimuli with either a long duration (VIB3), a high frequency (VIB4, VIB5), or both (VIB6). On the other hand, a robust burst response in velocity did not seem to require a specific stimulus property, whereas freezing appeared to be most robust for long duration stimulations (VIB3 and VIB6). My investigation thus far suggested that there are vibration types better suited for eliciting defensive behaviors than the type that is currently used in the lab (VIB5). Based on this, the mechano-acoustic vibrations I selected as candidate stimuli for further optimization testing were VIB3 and VIB6.

4.2 High-frequency vibrations elicit stronger velocity responses, while low-frequency vibrations evoke more distinct tank depth responses

Although the mechano-acoustic assay was of more interest for the second optimization experiment, the WT juvenile fish did express characteristic NT-test behaviors on average (Supplementary Figure 2). For the VB-test, I compared the behavioral phenotype in response to repetitions of VIB3 and VIB6, which both had a duration of 4.2 s, but had different frequencies (24 Hz and 238 Hz, respectively). My original hypothesis was that the highest frequency vibration stimulus would promote the strongest defensive behaviors for both the tank depth and the swim velocity. However, based on the results in the first experiment, I expected VIB3 to generate stronger tank depth responses.

The result for the 30 repetitions in each stimulus trial indicated that juvenile WT fish on average had a stronger diving and bottom-dwelling tendency in response to the stimulus with low frequency (VIB3), which supported my adjusted hypothesis (Figure 21). On the other hand, the animals' immediate burst swim response was greater when exposed to the high frequency stimulus (VIB6), which supported my original hypothesis (Figure 22). Interestingly, my findings may therefore suggest that various features of the stimulus might influence different aspects of the responses. Thus, contrary to my original hypothesis, there might not exist one optimal stimulus type that promotes the strongest responses for all parameters. Indeed, my data indicated that both VIB3 and VIB6 could promote stereotypical fear-like responses, but their distinctive frequencies might be suitable to elicit different defensive responses.

Taken together, the second optimization experiment further underlined the observations from the first experiment that unique vibration stimuli affect the overall defensive behavior strength. Additionally, my results suggested that the expression of behavioral phenotypes is more nuanced than anticipated, namely that a long stimulus duration in combination with either a low or high frequency affects different aspects of the defensive response. Overall, both stimuli were capable of promoting strong defensive behaviors for both parameters. Therefore, I opted to use VIB6 in my serotonergic manipulation experiments, which had the added benefit of being the most similar to the VIB5 stimulus

already used in the lab. This concluded the optimization process of the aversive stimulus in the mechano-acoustic vibration assay.

4.3 DR-ablated animals exhibit stronger defensive burst swimming, as well as disturbed habituation to repeated mechano-acoustic stimulation

The dorsal raphe (DR) has been found to influence the defensive behavior with opposing effects through different serotonergic circuitries; in mammals, serotonergic modulation decreases fear-like defensive behaviors in the periaqueductal gray (PAG), but increases anxiety-like defensive responses in the amygdala [26, 29, 31, 36-38]. Additionally, an extended role of DR serotonin release in zebrafish has been proposed to function as a neurobehavioral switch that transitions the fish from an acute panicked state to a more passive state of risk-assessment after the danger has passed [60]. My hypothesis was that DR-ablated animals would express habituate quicker to their unfamiliar surroundings in the NT-test compared to the controls, but show stronger defensive responses to the aversive stimulations, yet habituate faster within each individual stimulus. I also expected the control animals to attenuate their initial fear-response over the course of the VB-test.

For the NT-assay of the experimental protocol, the DR-ablated animals seemed to display an equally strong diving response as the placebo animals, and less bottom-dwelling than both control groups (Figure 24A). These results were statistically non-significant, but the suggested trend in swim depth aligned with my hypothesis that ablated fish would start to habituate earlier than the control groups (Figure 24D). The DR-ablated animals seemed to dwell higher in the tank on average than the control groups, seen from the probability of tank position distribution for the first 3 min of the NT-test (Figure 24B). The ablated group's Y-position recovery slope was also steeper than the controls for the first minute after the dive, which evened out to match the other two groups' incline for the rest of the test. These results may suggest that the ablated fish indeed exhibited less anxiety-like behaviors for the first 3 min of the assay and thus started exploration earlier than the control groups, but that they did not habituate at a faster rate. These results were more ambiguous compared to expectation that the ablated fish would habituate earlier and at a faster rate than the controls. A result that was not in line with my hypothesis was that the DR-ablated animals seemed to display more freezing behavior compared to the placebo animals throughout the NT-test, illustrated by their lower average swim speed, which was most evident for the first 5 minutes (Figure 24C, no significance test was performed for the velocity data in the NT-test). The slope of speed recovery was also very similar for the three groups, indicating a similar rate of habituation, which was also contrary to the hypothesis.

These observations may be interpreted in context of the postulated dual role of serotonin in the aversive brain system [60]. Animals with disrupted serotonin release from the DR may have an impaired regulation of anxiogenic behaviors in the zebrafish amygdala-homolog Dm, which normally is responsible of promoting anxiety-like responses [29]. This may explain why the ablated fish seemed to express less bottom-dwelling and initiate exploratory behaviors earlier than the control fish. Similarly for the

neurobehavioral switch hypothesis, the lack of serotonin to instigate the behavioral transition into passive risk-assessment (switch-ON) might also be a contributing factor to the earlier habituation in the ablated fish [60]. On the other hand, a stronger freezing response and lower tank depth baseline may be attributed to a disinhibited fear-modulation in the zebrafish PAG-homolog griseum centrale (GC) [29]. The NT-test mainly measures anxiety-like behaviors, but the action of being dropped into the experimental tanks might be an additional aversive experience for the fish besides the unfamiliar tank. The fish might therefore express fear-like reactions along with anxiety-like response. The lack of serotonergic inhibition of fear by the GC in ablated animals may therefore explain why they showed a stronger freeze response than the placebo animals as well as a lower tank depth baseline after habituation.

For the vibration stimulus assay, the results for the average responses to all 30 stimuli supported my hypothesis that the ablated animals would show a stronger defensive response. This was illustrated by a larger magnitude of bottom-diving as well as burst swimming compared to the placebo group for the first seconds following a vibration delivery, and was indicative of stronger fear-like behaviors (Figure 26+Figure 27). However, the averaged responses of all 30 stimuli may not be representative of my results. In fact, the ablated group's initial dive response was not significantly stronger than the placebo animals until the last 10 repetition of the stimulus (Figure 28C+D). Moreover, their diving magnitude stayed the same (non-significant difference) across the test, whereas the placebo animals significantly decreased their bottom-dive magnitude as the test progressed (Figure 28E). On the other hand, the initial burst velocity was significantly stronger on average for the ablated fish compared to the control groups throughout the entire assay, which supported my hypothesis that DR-ablation would increase the defensive behaviors (Figure 29C+D). As with the diving response, this was most apparent for the last 10 delivered stimulations.

My results indicated that the ablated fish had a stronger defensive phenotype for stimulus exposure. Furthermore, the differences in the initial defensive behaviors were stronger toward the late period of the VB-test, and perhaps in addition to having a stronger initial defensive response (i.e., burst swimming), the ablated fish also had a disturbance in their inter-stimulus habituation. Meanwhile, placebo animals decreased their acute fear-like behaviors through the experiment, which aligned with past findings that continuous stimulus application can reduce the adaptive fear response [83, 96]. This supported the hypothesis that the ablated fish would fail to attenuate their initial panic-like defensive behavior across stimuli, possibly due to the impaired serotonergic modulation of the GC [29]. This could imply a role of serotonergic modulation from the raphe in adaptive fear learning. The serotonergic switch model might also explain why the ablated fish had a stronger initial fear-like response, since their lack of the serotonergic modulation rendered the DR-ablated animals unable to change defensive strategy from panic to risk-assessment [60].

Ablated animals had a higher velocity during the initial and the recovery phase after stimulus exposure for the entire mechano-acoustic tap assay (Figure 29). This was indicative of stronger fear-like burst swimming and anxiety-like less freezing responses, which further supported my hypothesis and corroborated the aversive brain hypotheses of Deakin and Greaff as well as Lima Maximino and colleagues: the increased fear-like reaction might be attributed to the absence of GC-mediated fear inhibition, as well as the lack of state transition into passive coping mechanism, which inhibits fear while enhancing anxiety [29, 60].

For the recovery phase of the stimulus delivery, the ablated animals had a lower tank depth than the placebo animals on average (Figure 28C+D). However, due to their significantly stronger bottom-diving in the initial phase, this result might be misleading. A better indication of anxiety-like bottom-dwelling could therefore be the slope of Y-position recovery, for which the ablated animals seemed to have a sharper incline during the first 5 s of the recovery phase (Figure 28A+C). My results could therefore suggest that the ablated fish started exploratory behaviors earlier than the placebo group, and as a result displayed faster intra-trial habituation. This was also the case for the swim speed in the recovery phase: on average the DR-ablated fish had a significantly higher velocity than the ablated fish, which was indicative of less anxiety-like freezing behavior (Figure 29C+D). These observations for the recovery phase of the stimulus exposure supported my hypothesis that fish lacking serotonergic modulation of the aversive brain system would exhibit quicker intra-stimulus habituation. A possible explanation for this phenomenon could be the lack of serotonin mediated neurobehavioral switch-ON transition into anxiety-like risk-assessment after the threat exposure in DR-ablated animals [60].

Taken together, the serotonergic manipulation experiment demonstrated more similarities than differences between the three experimental groups in the NT-test. However, the DR-ablated animals appeared to bottom-dwell slightly less than control groups and start exploration earlier, which indicated less anxiety-like behaviors, and aligned with my hypothesis. On the other hand, ablated animals also exhibited more freezing behavior and did not seem to habituate at a faster rate than the two control groups. For the VB-test, however, DR-ablated animals displayed significantly stronger fear-like initial defensive behavior than the placebo group, and significantly less anxiety-like recovery behaviors. These results were in line with my expectation and supported my hypothesis for the VB-test. My results also demonstrated the ability of placebo animals to gradually attenuate their initial fear response across the vibration deliveries, as observed in previous literature [83, 96]. Meanwhile, the ablated animals displayed an impaired inter-trial habituation, which may underline the role of serotonin in adaptive fear learning.

4.4 DR-ablated animals display decreased neuronal activity in the central telencephalon and habenulas, but increased activity in the anterior and posterior telencephalon

Previous lab work with pERK analysis and 2-photon calcium imaging have generally found the neuronal activity to be lower in the DR-ablated animals in most forebrain regions in response to aversive mechano-acoustic stimulation compared to controls. Work from Kadir Aytac Mutlu measuring neuronal activity with 2-photon calcium imaging while delivering a series of mechano-acoustic taps demonstrated a lower neuronal activity for the whole dorsal telencephalon (pallium) as well as the habenula (Hb) of the diencephalon in ablated animals versus control animals (Mutlu et al., in preparation [97]). And for the pERK immunostaining of DR-ablated fish that had been exposed to a 15 min tapping essay, results in the lab from Oda Bjørnevik Håheim and Ricarda Bardenhewer also suggested a trend of decreased neuronal activity in the forebrain compared to the control group [85, 86]. This was found to be most prominent in the

central (Dc) and lateral (Dl) zones of the dorsal pallium as well as the Hb, but one exception was the posterior part of the medial dorsal pallium (Dm_p), in which the ablated fish seemed to have more activity than the control group (*tph2:Gal4;UAS:GCamp6s* animals given MTZ) [85]. Based on these previous lab findings, my hypothesis was that the ablated fish on average would display a lower neuronal activity (pERK/tERK ratio) in the forebrain.

My pERK immunostaining analysis corroborated the results from the lab on some points, but differed in other regards. The results must, however, be interpreted with care due to a relatively low sample size (n=15 per group). The post-hoc analysis of the pERK/tERK ratio from the behavioral experiment indicated that certain regions in the ablated animals' telencephalon (Dc, Dm, Dl, Dl_p) and diencephalon (Hb), exhibited areas with lower neuronal activity compared to the placebo animals (Figure 31A+C). Here, the most noticeable differences were observed in the Dc and Hb as well as the midline of the Dm. However, these prosencephalon zones also displayed areas with higher activity levels, which balanced out the overall differences when averaged across each delineated region. Thus, the neuronal activity in these regions was not significantly lower in the ablated group compared to the placebo group when calculated for the delineated areas (Figure 31D). Despite this, my results indicated a trend of decreased forebrain activity for centrally located zones in the forebrain and the habenulas, which aligned with my hypothesis. Furthermore, the anterior and posterior areas in the ablated animals' dorsal pallium (Da, Dm_p and Dd) seemed to harbor a higher pERK/tERK ratio on average, indicating more neuronal activity in these regions compared to the placebo animals, though this difference was only significant for the delineated Da region (Figure 31D). A higher neuronal activity in the Dm_p was in line with prior pERK immunostaining, but a similar trend especially for the Da was unexpected [85]. 2-photon calcium imaging within the lab had no data on this brain region as the imaging plane did not include this particular zone (Mutlu et al., in preparation [97]).

Before interpretating the results further, it is important to note that these brain regions receive modulations other than serotonergic, and the resulting brain activity as well as the displayed behaviors stem from these diverse inputs. The observations in my data is likely credited to the interplay between several circuits. Moreover, the nature of the serotonergic receptors in the target forebrain regions may also contribute to the neuronal activity pattern in the ablated animals. Activation of different serotonin receptors are linked to either activation (5-HT_4, 5-HT_6, 5-HT_7, and 5-HT_3) or inhibition (5-HT_1 and 5-HT_5) of the postsynaptic cell based on their serotonin receptor type [22, 23]. Consequently, regions in the DR-ablated animals that are typically excited by serotonin may display less neuronal activation due to the lack of serotonergic modulation, whereas regions with inhibitory receptors may be disinhibited, and therefore express stronger neuronal activation. One example is the Da, the anterior extension of the Dl, which is postulated to be functionally homologous to the mammalian hippocampus and has serotonergic projections, possibly from the DR [42, 47, 106, 107]. Given the observation that DR-ablated animals fail to habituate across continuous stimulations, it may be possible that the Da, which had significantly altered activity between the ablated and placebo groups, is involved in adaptive fear learning and thus fear attenuation [83, 96]. If the serotonergic input in healthy animals leads to activation of inhibitory 5-HT_1 and or 5-HT_5 receptors, it could explain the increased activity in fish with absent serotonergic modulation.

The Dm is involved in promotion of anxiety-like defensive behaviors, and my results indicated that this area had subregions of increased (Dm_p) and decreased activity (along the midline). For the DR-ablated group, a higher activity in their Dm's posterior zone may explain why they on average displayed stronger anxiety-like bottom-dwelling during the recovery phase of the stimulus than the placebo group. This also corroborates the findings of Hale and colleagues that projections to the rat amygdala display higher neuronal activity (by c-Fos expression) when the animals were exposed to an aversive experience [37].

The decreased activity in the rest of the Dm (excluding the posterior zone) support the neurobehavioral switch hypothesis of Lima Maximino and colleagues that serotonin released from the DR is important for risk-assessment in the recovery-period after stimulus exposure [60]. This is also reflected in my behavioral data, demonstrated by the seemingly stronger incline of Y-position and significantly higher velocity for the ablated group compared to the placebo animals in the stimulus recovery phase (Figure 28 and Figure 29). These observations may be indicative of less anxiety, faster intra-stimulus tank depth habituation and less freezing behavior (respectively), and could be a consequence of an impaired ability to initiate the switch-ON mechanism that inhibits acute fear, but upregulates anxiety-like risk-assessment [60]. Decreased Hb activity also aligns with the less observed freezing in ablated versus placebo animals, since the Hb is involved in freezing behavior through the interpeduncular nucleus (IPN) [63].

Furthermore, the behavioral results hinted that intra-stimulus habituation to the continuous vibration delivery occurs for the placebo animals, but not the ablated animals (Figure 28E). This may be attributed to the desensitization of 5-HT_{1A} receptors in the GC, which are important for serotonergic inhibition of fear responses, thus attenuating of the startle response [35, 83, 96, 108]. Since 5-HT_{1A} receptors also are found in serotonergic presynaptic cells as inhibitory autoreceptors (in the placebo animals), a desensitization of feedback inhibition mediated by these receptors could potentially lead to increased serotonin release to other DR target regions, such as the Dm. If this was the case, it could further explain the lower neuronal activity observed in the Dm for the ablated group compared to the placebo group. Previous findings have also demonstrated that inescapable aversive stimulation of rats gives rise to increased serotonin release from the DR and increased defensive behaviors [7]. The vibration stimuli applied in my setup can be considered inescapable because the stimulus source is hard to discern. This may contribute to an elevated defensive response in the placebo animals and also explain the indication of lower activity in the Dm, whose serotonergic input is anxiogenic, for ablated animals compared to the placebo animals [29].

Overall, my results indicated less neuronal activity in centrally located forebrain regions (Dc, Dl, and Dm midline) as well as the habenulas, and more activity in the posterior region of the Dm (Dm_p) in ablated animals compared to placebo animals. These results were either in line with my hypothesis, or expected from previous pERK immunostaining results in the lab [85]. Contrary to my hypothesis, the trend for the ablated DR-ablated animals' Dd, located posterior in the telencephalon, seemed to have more neuronal activity than in the placebo, which was contrary to my hypothesis. This was, however, a nonsignificant finding. Another surprising result was that ablated fish had significantly more activity in the anterior part of the telencephalon (Da) compared to placebo animals, which was not previously observed in the lab.

4.5 Limitations and future directives

4.5.1 Other factors contributing to the behavioral phenotype

The optimization process of the behavioral setup (mainly the mechano-acoustic vibration assay) focused on the properties of the delivered vibration stimulus. However, it is important to acknowledge that other influences besides just the vibration duration and frequency most likely contribute to the displayed behavior in all my juvenile experiments. Possible examples are the length of the protocol, the number of stimulus repetitions, the intervals between the stimuli (ISI) and between the vibration trials (ITI), the water temperature, and the handling of the fish prior to experiment start. These factors may affect the fish in unaccounted for ways, which could impact the overall behavioral phenotype, and were not analyzed in my thesis.

For instance, the first optimization step revealed conspicuous trends over time in the WT animals' spontaneous baseline swimming during the VB-test (Figure 16). On average, the tank depth baseline substantially decreased after the stimulus trial containing VIB3 vibration types, whereas the swim velocity progressively increased throughout the whole test. This did not only make it challenging to compare the potency of each of the six vibration types, but it may also be an indication that the fish were increasingly stressed through the experiment, as demonstrated by increased bottom-dwelling and panic-like erratic swimming. Based on this observation, I therefore doubled the ISI and ITI in the second optimization experiment (into 2 min and 40 min, respectively). The spontaneous baseline swimming for these WT fish were much more stable across the two stimulus trials without any of the trends observed in the first WT experiment, which made the comparison between the candidate stimuli more reliable. This was also seen for the three groups in the serotonergic manipulation experiment, which also had an ISI of 2 min. This could indicate that the timing of the stimulus deliveries also is a parameter for defensive behavior besides just the stimulus properties itself.

A second example of factors that can affect the animals' behaviors is the water temperature. In my experiments, I used room-temperature artificial fish water (AFW) instead of incubator AFW holding the same 28 °C as the fish are kept at prior to experiments. This was because the behavioral setup cannot keep a stable temperature within the system. Zebrafish are more active at higher water temperatures, and additionally, a sudden change in water temperature can induce stress in the fish [109, 110]. Therefore, transferring the animals into the experimental system may have altered their behavior, and lasted through both behavioral assays.

Another source of influence on the defensive behavior is the handling of the zebrafish before the experiment starts. An interesting observation in the NT-test of the serotonergic manipulation experiment was that the placebo and MTZ-control groups did not display pronounced bottom-dwelling at the start of the test (Figure 24). Given their control conditions, I expected them to have a stronger anxiety-like response, similar to the WT fish from my first optimization experiment (Figure 15). I would not necessarily conclude that the NT-test was unsuccessful at eliciting anxiety-like behaviors in the serotonergic manipulation experiment, as many factors could contribute to the observed differences, for example inherent differences between transgenic and WT fishlines. Additionally, it would be reasonable to expect improvement of the animal handling with more experience. Since the serotonergic manipulation experiments were performed last

in my project, the animals might have been treated more gently than the fish in my first experiment. A less traumatic handling at the start of the serotonergic manipulation experiment might therefore explain why these two control groups (placebo and MTZ-treatment control) did not express quite as strong defensive behavior as the WT fish in the first optimization experiment. This could possibly highlight a key role of pre-experiment stress as a factor for the behavioral phenotype. Future behavioral studies with the NT-test may therefore standardize the way to initiate assay, which might generate more comparable results across experiment sets.

From all the examples listed, it is clear that the displayed behavior is a complex phenomenon and a result of many influences, not just the factor that I have optimized, namely the vibration stimulus. For future behavioral experiments, refinement measures of some of these other variables could possibly standardize or even negate some of these behavioral effects and improve the data quality of both the NT-test and the VB-test.

4.5.2 Uncertainty regarding the validity of tph2:Gal4;UAS:GCamp6s animals as a MTZ-treatment control

My animals were screened at 3 dpf, but not after the drug/sham treatment at 21-28 dpf, before the behavioral experiment. However, I screened them in the confocal microscope after fixation and staining. I observed an absence of the expected fluorescent signal in the raphe region of all 15 MTZ-treatment control fish during confocal imaging, although the Tg(*tph2:Gal4;UAS:GCamp6s*) fishline's green marker should be present here (Figure 13). Since these animals were confirmed to express fluorescence when they were screened pre-ablation at 3 dpf, this was surprising.

One explanation is that the staining protocol caused degradation of the fishline's inherent GCamp6s fluorescence, and that the raphe is, indeed, intact. On the contrary, another possible explanation is that the *tph2*-expressing cells, and thus the serotonergic DR neurons, were ablated in this group. The Tg(*tph2:Gal4;UAS:GCamp6s*) fishline was derived from the Tg(*tph2:Gal4;UAS:ntr-mCherry*) line in the lab, from which both the ablated and the placebo group came from. It is possible that some faint transgenic traces of ntr-mCherry still is present in the GCamp6s fishline. If so, these animals would express nitroreductase in their DR, which would cause cell death when exposed to the MTZ prodrug, similar to the DR-ablated group. The behavioral similarities between these animals (GCamp6s + MTZ) compared to the original DR-ablated group (mCherry + MTZ) through both the NT-test and the VB-test aligns with this hypothesis. And the fact that the MTZ-treatment control also behaved very differently from the placebo control further highlights its ambiguity as a control group against DR-ablated fish. If the raphe was indeed intact in Tg(*tph2:Gal4;UAS:GCamp6s*) animals, the striking difference between the two controls might indicate that these two fishlines are inherently very different. This would mean that the MTZ-treatment control group in my experiment is not optimal to compare my ablated animals to.

To confirm whether the Tg(*tph2:Gal4;UAS:GCamp6s*) line is a suitable control with MTZ administration, I crossed a new generation of this line to investigate if the animals had expression of both GCamp6s and mCherry marker genes, which would indicate transgenic contamination of the fishline. I screened them at 3, 4 and 5 dpf due to a slow grow rate. Neither green nor red fluorescence was seen at 3 dpf. Green fluorescence was

observed in the raphe and the spinal cord at 4 dpf, but red was not seen. Red fluorescence is hard to detect, and I suspected its expression would be weak due to competition of Gal4 binding, which prefers the strongest UAS region. Due to selective crossing and raising upon establishment of the line, this would be the UAS:GCamp6s rather than UAS:ntr-mCherry gene sequence. Some traces of red fluorescence and thus nitroreductase might therefore be present, but too weak to detect.

Future behavioral studies with Tg(*tph2:Gal4;UAS:GCamp6s*) treated with MTZ as a control against an MTZ-ablated animals should further validate that the prodrug treatment is harmless in the control. One could breed and raise these animals until 3-4 weeks old. The generation might then be split into two, and half the animals could be administered with MTZ, whereas the other should remain non-treated or sham treated. Screening would be conducted before and after the protocol to confirm if these animals retained their serotonergic cells or not. This investigation is currently in process.

4.5.3 Limitations of pERK post-hoc immunostainig as a measure of neuronal activity and suggestions for future analysis

In my project, I used the ratio between phosphorylated and total ERK as an indicator of neuronal activity during the mechano-acoustic behavioral assay, which was obtained in post-hoc. A drawback of this approach is its low temporal sensitivity. pERK is an indirect way to measure neuronal activity: ERK phosphorylation requires activation of upstream elements in the intra-cellular signal transduction cascade, and there is therefore a delay between the neuronal event and the point of detection. Furthermore, the time window pERK remains in the brain is also debated on, and considered to persist for maximum 10-15 min [56, 92]. The animals must also be sacrificed and fixated for the analysis, so only the end of the behavioral experiment, specifically the last part of the VB-test is reflected in the pERK results. For this reason, the behavioral protocol in the serotonergic manipulation experiment was designed to capture the neuronal activity during the last few vibration deliveries. But with an uncertain peak pERK phosphorylation interval as well as different fixation times of all the animals, it made it challenging to analyze the neuronal activity at a consistent timepoint in addition to determine when in the 10 min interval the data reflected.

Another limitation is that the pERK immunostaining method yields results for a single point in time. It is therefore vulnerable to influences from spontaneous fluctuation in neuronal activity that could otherwise be filtered out as artifacts. These noise signals could lead to misinterpretations, suggesting correlations and causations with the experimental manipulation. pERK immunostaining is also unable to give insight into the dynamics of which precise neuron populations are involved because all activity involving this signaling pathway is captured with this method.

My analysis of the neuronal activity across brain regions was accomplished by averaging over the ERK images based on manually delineated areas. These images were composed by Z-projection and aligned to a reference brain. Individual differences in brain morphology across samples affected both the Z-projection sample interval as well as the degree of image distortion during alignment, and these variations made it challenging to obtain comparable data. Despite attempting to be consistent for all the samples, possible limitations of the data processing are perhaps that different planes of the brain were

sampled and therefore not containing all of the same regions, and that the aligning procedure shifted neuron populations out of their position within the processed image. Furthermore, my pixel-based activity analyses revealed that several brain regions had subpopulations of neurons with increased activity and others with decreased activity (ablated group compared to either the placebo group in Figure 31A-C) or to the MTZ-treatment control group in Figure 32A-C). The segment-based analysis, then proceeds to calculate the average of the pixels within each delineated brain region. Drawbacks with this representation of the data are the dependency on the delineation itself, and that these nuanced differences within regions are averaged out.

Another comment regarding the pERK analysis is that four channels were used for the confocal imaging to capture signals from mCherry, GCamp6s, GAR 647+ (pERK) and GAM 405+ (tERK). It is possible that some signals with similar wavelengths interfered with each other despite adjusting the settings to accommodate their peak emission wavelength. Overlapping signals could influence the resulting pERK/tERK ratio and the neuronal activity analysis. Future pERK analyses might consider employing only three channels for confocal imaging to minimize the overlap of signals. This could be done by only having two experimental groups, or include fishlines with the same fluorescent background.

My pERK immunostaining results revealed that the anterior part of the dorsal pallium (Da) had significantly higher neuronal activity in DR-ablated animals compared to placebo animals. This finding was contrary to previous pERK data in the lab [85, 86]. Additionally, the prior 2-photon calcium imaging results in the lab did not include this brain area in the imaging plane. An interesting experiment could be to perform neuronal activity mapping with calcium imaging at an imaging plane that includes the Da for live DR-ablated juvenile fish while administering the same mechano-acoustic stimulus used in my freely behaving VB-test. This could demonstrate if the differences observed in the Da for my pERK analysis is reflected in an approach with much higher temporal specificity, and possibly elucidate when the observed difference occurs. Calcium imaging could also reveal information about activation dynamics of possible neuron subpopulations, which is something the confocal images cannot contribute to.

5 Conclusion

The first aim of my thesis was to optimize the mechano-acoustic vibration delivered in the aversive stimulation behavioral assay for freely behaving juvenile zebrafish. The second objective in my project was to investigate the role of serotonin from the dorsal raphe (DR) in the defensive behavior of juvenile zebrafish utilizing the optimized stimulus in the aversive vibration test (VB-test).

I have tested a range of different stimuli, and my results demonstrated that vibration types of long duration elicited a stronger defensive response, which supported my hypothesis. Furthermore, a long-duration vibration in combination with a high frequency elicited a somewhat stronger fear-like burst swimming response than combined with a low frequency, which in turn evoked slightly stronger fear-like bottom-diving and anxiety-like bottom-dwelling behaviors. I was therefore able to devise an optimized experimental protocol ("Vibration Protocol 3") utilizing the aversive mechano-acoustic stimulus with a long duration and a high frequency (VIB6) to investigate the serotonergic system's effect on defensive behaviors.

For this purpose, I exposed DR-ablated juvenile fish to two behavioral assays designed to evoke fear- and anxiety-like responses, a novel tank test (NT-test) and a VB-test. Afterwards, I performed a post-hoc analysis of their neuronal activity measured by phosphorylation of ERK (pERK). My results suggested that serotonergic modulation from the DR plays a key role in the display of defensive behaviors. This could possibly be in a dynamic manner that facilitates escape in response to acute threat. Fear-like responses are then followed by anxiety-like risk-assessment when the danger is over, and cautious investigation if normal behavior can be resumed. My neuronal activity analysis was largely in line with previous pERK immunostaining of DR-ablated animals as well as 2-photon calcium imaging within the lab: ablated animals displayed a lower activity than the controls in parts of the forebrain, and higher activity in the posterior parts of the telencephalon. A new finding in the lab was that the anterior part of the ablated animals' forebrain had higher activity than the placebo (Da).

Behavioral and neural activity studies on defensive behaviors help uncover how fear and anxiety is represented in and affects the brain. Furthermore, it could broaden our understanding of the computational mechanisms in which they are involved, and how they malfunction in clinical and psychiatric disorders. This project validates the use of zebrafish in the study of defensive behaviors as well as the experimental and analytical methodology applied to study them.

References

1. Branco, T. and P. Redgrave, *The Neural Basis of Escape Behavior in Vertebrates.* Annu Rev Neurosci, 2020. **43**: p. 417-439.
2. Davis, M. and C. Shi, *The extended amygdala: are the central nucleus of the amygdala and the bed nucleus of the stria terminalis differentially involved in fear versus anxiety?* Ann N Y Acad Sci, 1999. **877**: p. 281-91.
3. McNaughton, N. and P.J. Corr, *A two-dimensional neuropsychology of defense: fear/anxiety and defensive distance.* Neurosci Biobehav Rev, 2004. **28**(3): p. 285-305.
4. Blanchard, D.C., et al., *Risk assessment as an evolved threat detection and analysis process.* Neurosci Biobehav Rev, 2011. **35**(4): p. 991-8.
5. McNaughton, N., K.S. Panickar, and B. Logan, *The pituitary-adrenal axis and the different behavioral effects of buspirone and chlordiazepoxide.* Pharmacol Biochem Behav, 1996. **54**(1): p. 51-6.
6. Maier, S.F. and L.R. Watkins, *Stressor controllability and learned helplessness: The roles of the dorsal raphe nucleus, serotonin, and corticotropin-releasing factor.* Neuroscience & Biobehavioral Reviews, 2005. **29**(4): p. 829-841.
7. Amat, J., et al., *Escapable and inescapable stress differentially alter extracellular levels of 5-HT in the basolateral amygdala of the rat.* Brain Res, 1998. **812**(1-2): p. 113-20.
8. Maximino, C., *Serotonin in the Nervous System of Vertebrates*. 2012, Springer New York. p. 15-36.
9. Mohammad-Zadeh, L.F., L. Moses, and S.M. Gwaltney-Brant, *Serotonin: a review.* Journal of Veterinary Pharmacology and Therapeutics, 2008. **31**(3): p. 187-199.
10. Lucki, I., *The spectrum of behaviors influenced by serotonin.* Biological Psychiatry, 1998. **44**(3): p. 151-162.
11. Fanet, H., et al., *Tetrahydrobioterin (BH4) Pathway: From Metabolism to Neuropsychiatry.* Curr Neuropharmacol, 2021. **19**(5): p. 591-609.
12. Wyler, S.C., et al., *Pet-1 Controls Tetrahydrobiopterin Pathway and Slc22a3 Transporter Genes in Serotonin Neurons.* ACS Chem Neurosci, 2015. **6**(7): p. 1198-205.
13. Hasegawa, H. and K. Nakamura, *CHAPTER 2.3 - Tryptophan Hydroxylase and Serotonin Synthesis Regulation*, in *Handbook of Behavioral Neuroscience*, C.P. Müller and B.L. Jacobs, Editors. 2010, Elsevier. p. 183-202.
14. McDevitt, R.A. and J.F. Neumaier, *Regulation of dorsal raphe nucleus function by serotonin autoreceptors: a behavioral perspective.* J Chem Neuroanat, 2011. **41**(4): p. 234-46.
15. Descarries, L., M. Riad, and M. Parent, *CHAPTER 1.4 - Ultrastructure of the Serotonin Innervation in the Mammalian Central Nervous System*, in *Handbook of Behavioral Neuroscience*, C.P. Müller and B.L. Jacobs, Editors. 2010, Elsevier. p. 65-101.
16. Dafny, N. and G.C. Rosenfeld, *Chapter 33 - Neurobiology of Drugs of Abuse*, in *Conn's Translational Neuroscience*, P.M. Conn, Editor. 2017, Academic Press: San Diego. p. 715-722.
17. Walker, E.P. and P. Tadi. *Neuroanatomy, Nucleus Raphe*. [Book] 2023 01.05.2023 [cited 2023 14.08.]; Available from: https://www.ncbi.nlm.nih.gov/books/NBK544359/.
18. Hornung, J.-P., *The human raphe nuclei and the serotonergic system.* Journal of Chemical Neuroanatomy, 2003. **26**(4): p. 331-343.

19. Hornung, J.-P., *CHAPTER 1.3 - The Neuronatomy of the Serotonergic System*, in *Handbook of Behavioral Neuroscience*, C.P. Müller and B.L. Jacobs, Editors. 2010, Elsevier. p. 51-64.
20. Abrams, J.K., et al., *Anatomic and Functional Topography of the Dorsal Raphe Nucleus.* Annals of the New York Academy of Sciences, 2004. **1018**(1): p. 46-57.
21. Blumenfeld, H., *Neuroanatomy through clinical cases.* 2002.
22. Hoyer, D., et al., *International Union of Pharmacology classification of receptors for 5-hydroxytryptamine (Serotonin).* Pharmacol Rev, 1994. **46**(2): p. 157-203.
23. Derkach, V., A. Surprenant, and R.A. North, *5-HT3 receptors are membrane ion channels.* Nature, 1989. **339**(6227): p. 706-709.
24. Jenck, F., C.L.E. Broekkamp, and A.M.L. Van Delft, *5-HT1C receptors in the serotonergic control of periaqueductal gray induced aversion in rats.* Psychopharmacology, 1990. **100**(3): p. 372-376.
25. Blanchard, R.J. and D.C. Blanchard, *Defensive reactions in the albino rat.* Learning and Motivation, 1971. **2**(4): p. 351-362.
26. Sanford Kiser, R., et al., *Dorsal raphe nucleus stimulation reduces centrally-elicited fearlike behavior.* Brain Research, 1980. **191**(1): p. 265-272.
27. Wise, C.D., B.D. Berger, and L. Stein, *Benzodiazepines: anxiety-reducing activity by reduction of serotonin turnover in the brain.* Science, 1972. **177**(4044): p. 180-3.
28. Hodges, H., S. Green, and B. Glenn, *Evidence that the amygdala is involved in benzodiazepine and serotonergic effects on punished responding but not on discrimination.* Psychopharmacology (Berl), 1987. **92**(4): p. 491-504.
29. Deakin, J.F. and F.G. Graeff, *5-HT and mechanisms of defence.* J Psychopharmacol, 1991. **5**(4): p. 305-15.
30. Graeff, F.G., M.B. Viana, and P.O. Mora, *Dual role of 5-HT in defense and anxiety.* Neurosci Biobehav Rev, 1997. **21**(6): p. 791-9.
31. Paul, E.D., et al., *The Deakin/Graeff hypothesis: Focus on serotonergic inhibition of panic.* Neuroscience & Biobehavioral Reviews, 2014. **46**: p. 379-396.
32. Cervo, L., et al., *Roles of 5-HT1A receptors in the dorsal raphe and dorsal hippocampus in anxiety assessed by the behavioral effects of 8-OH-DPAT and S 15535 in a modified Geller–Seifter conflict model.* Neuropharmacology, 2000. **39**(6): p. 1037-1043.
33. Paul, E.D. and C.A. Lowry, *Functional topography of serotonergic systems supports the Deakin/Graeff hypothesis of anxiety and affective disorders.* Journal of Psychopharmacology, 2013. **27**(12): p. 1090-1106.
34. Viana, M.B., F.G. Graeff, and P.-A. Löschmann, *Kainate Microinjection into the Dorsal Raphe Nucleus Induces 5-HT Release in the Amygdala and Periaqueductal Gray.* Pharmacology Biochemistry and Behavior, 1997. **58**(1): p. 167-172.
35. Pobbe, R.L.H. and H. Zangrossi, *5-HT1A and 5-HT2A receptors in the rat dorsal periaqueductal gray mediate the antipanic-like effect induced by the stimulation of serotonergic neurons in the dorsal raphe nucleus.* Psychopharmacology, 2005. **183**(3): p. 314-321.
36. Pobbe, R.L.H., et al., *Involvement of dorsal raphe nucleus and dorsal periaqueductal gray 5-HT receptors in the modulation of mouse defensive behaviors.* European Neuropsychopharmacology, 2011. **21**(4): p. 306-315.
37. Hale, M.W., et al., *Exposure to an open-field arena increases c-Fos expression in a subpopulation of neurons in the dorsal raphe nucleus, including neurons projecting to the basolateral amygdaloid complex.* Neuroscience, 2008. **157**(4): p. 733-748.
38. Abrams, J.K., et al., *Serotonergic systems associated with arousal and vigilance behaviors following administration of anxiogenic drugs.* Neuroscience, 2005. **133**(4): p. 983-997.
39. Hale, M.W., et al., *Multiple anxiogenic drugs recruit a parvalbumin-containing subpopulation of GABAergic interneurons in the basolateral amygdala.* Progress in Neuro-Psychopharmacology and Biological Psychiatry, 2010. **34**(7): p. 1285-1293.

40. Grahn, R.E., et al., *Activation of serotonin-immunoreactive cells in the dorsal raphe nucleus in rats exposed to an uncontrollable stressor.* Brain Res, 1999. **826**(1): p. 35-43.
41. Rozeske, R.R., et al., *Uncontrollable, But Not Controllable, Stress Desensitizes 5-HT_{1A} Receptors in the Dorsal Raphe Nucleus.* The Journal of Neuroscience, 2011. **31**(40): p. 14107-14115.
42. Ganz, J., et al., *Subdivisions of the adult zebrafish pallium based on molecular marker analysis.* F1000Res, 2014. **3**: p. 308.
43. Mueller, T., et al., *The dorsal pallium in zebrafish, Danio rerio (Cyprinidae, Teleostei).* Brain Res, 2011. **1381**: p. 95-105.
44. Ganz, J., et al., *Subdivisions of the adult zebrafish subpallium by molecular marker analysis.* J Comp Neurol, 2012. **520**(3): p. 633-55.
45. Yáñez, J., et al., *The organization of the zebrafish pallium from a hodological perspective.* Journal of Comparative Neurology, 2022. **530**(8): p. 1164-1194.
46. Braford, M.R., Jr., *Comparative aspects of forebrain organization in the ray-finned fishes: touchstones or not?* Brain Behav Evol, 1995. **46**(4-5): p. 259-74.
47. Northcutt, R.G., *Connections of the lateral and medial divisions of the goldfish telencephalic pallium.* J Comp Neurol, 2006. **494**(6): p. 903-43.
48. Portavella, M., et al., *The effects of telencephalic pallial lesions on spatial, temporal, and emotional learning in goldfish.* Brain Res Bull, 2002. **57**(3-4): p. 397-9.
49. Castro, A., et al., *Calretinin immunoreactivity in the brain of the zebrafish, Danio rerio: Distribution and comparison with some neuropeptides and neurotransmitter-synthesizing enzymes. I. Olfactory organ and forebrain.* Journal of Comparative Neurology, 2006. **494**(3): p. 435-459.
50. Lal, P., et al., *Identification of a neuronal population in the telencephalon essential for fear conditioning in zebrafish.* BMC Biology, 2018. **16**(1): p. 45.
51. Portavella, M., B. Torres, and C. Salas, *Avoidance Response in Goldfish: Emotional and Temporal Involvement of Medial and Lateral Telencephalic Pallium.* The Journal of Neuroscience, 2004. **24**(9): p. 2335-2342.
52. Lau, B.Y., et al., *Identification of a brain center whose activity discriminates a choice behavior in zebrafish.* Proc Natl Acad Sci U S A, 2011. **108**(6): p. 2581-6.
53. Ruhl, T., et al., *The endocannabinoid system and associative learning and memory in zebrafish.* Behav Brain Res, 2015. **290**: p. 61-9.
54. Rupprecht, P. and R.W. Friedrich, *Precise Synaptic Balance in the Zebrafish Homolog of Olfactory Cortex.* Neuron, 2018. **100**(3): p. 669-683.e5.
55. Serneels, B., *Yaksi Lab research including behavioral experiments, confocal imaging and data analysis*. Norwegian University of Science and Technology.
56. Randlett, O., et al., *Whole-brain activity mapping onto a zebrafish brain atlas.* Nat Methods, 2015. **12**(11): p. 1039-46.
57. Lillesaar, C., *The serotonergic system in fish.* Journal of Chemical Neuroanatomy, 2011. **41**(4): p. 294-308.
58. Oikonomou, G., et al., *The Serotonergic Raphe Promote Sleep in Zebrafish and Mice.* Neuron, 2019. **103**(4): p. 686-701.e8.
59. do Carmo Silva, R.X., M.G. Lima-Maximino, and C. Maximino, *The aversive brain system of teleosts: Implications for neuroscience and biological psychiatry.* Neurosci Biobehav Rev, 2018. **95**: p. 123-135.
60. Lima-Maximino, M., et al., *Phasic and tonic serotonin modulate alarm reactions and post-exposure behavior in zebrafish.* Journal of Neurochemistry, 2020. **153**(4): p. 495-509.
61. Olson, I., et al., *Griseum centrale, a homologue of the periaqueductal gray in the lamprey.* IBRO Reports, 2017. **2**: p. 24-30.
62. Wullimann, M.F., B. Rupp, and H. Reichert, *Functional anatomy of the zebrafish brain: a comparative evaluation*, in *Neuroanatomy of the Zebrafish Brain: A Topological Atlas*, M.F. Wullimann, B. Rupp, and H. Reichert, Editors. 1996, Birkhäuser Basel: Basel. p. 89-101.

63. Agetsuma, M., et al., *The habenula is crucial for experience-dependent modification of fear responses in zebrafish.* Nature Neuroscience, 2010. **13**(11): p. 1354-1356.
64. Kalueff, A.V., A.M. Stewart, and R. Gerlai, *Zebrafish as an emerging model for studying complex brain disorders.* Trends in Pharmacological Sciences, 2014. **35**(2): p. 63-75.
65. Liu, Y., *Zebrafish as a Model Organism for Studying Pathologic Mechanisms of Neurodegenerative Diseases and other Neural Disorders.* Cellular and Molecular Neurobiology, 2023. **43**(6): p. 2603-2620.
66. Son, M., D.Y. Kim, and C.-H. Kim, *Disease Modeling of Rare Neurological Disorders in Zebrafish.* International Journal of Molecular Sciences, 2022. **23**(7): p. 3946.
67. Eisen, J.S., *Chapter 1 - History of Zebrafish Research*, in *The Zebrafish in Biomedical Research*, S.C. Cartner, et al., Editors. 2020, Academic Press. p. 3-14.
68. Tonelli, F., et al., *Zebrafish: A Resourceful Vertebrate Model to Investigate Skeletal Disorders.* Frontiers in Endocrinology, 2020. **11**.
69. Detrich, H.W., M. Westerfield, and L.I. Zon, *Chapter 1 Overview of the Zebrafish System*, in *Methods in Cell Biology*, H.W. Detrich, M. Westerfield, and L.I. Zon, Editors. 1998, Academic Press. p. 3-10.
70. Parichy, D.M., et al., *Normal table of postembryonic zebrafish development: Staging by externally visible anatomy of the living fish.* Developmental Dynamics, 2009. **238**(12): p. 2975-3015.
71. Bussmann, J. and S. Schulte-Merker, *Rapid BAC selection for tol2-mediated transgenesis in zebrafish.* Development, 2011. **138**(19): p. 4327-4332.
72. Asakawa, K. and K. Kawakami, *Targeted gene expression by the Gal4-UAS system in zebrafish.* Dev Growth Differ, 2008. **50**(6): p. 391-9.
73. Howe, K., et al., *The zebrafish reference genome sequence and its relationship to the human genome.* Nature, 2013. **496**(7446): p. 498-503.
74. Lam, P.-Y. and R.T. Peterson, *Developing zebrafish disease models for in vivo small molecule screens.* Current Opinion in Chemical Biology, 2019. **50**: p. 37-44.
75. Belzung, C. and G. Griebel, *Measuring normal and pathological anxiety-like behaviour in mice: a review.* Behavioural Brain Research, 2001. **125**(1): p. 141-149.
76. Seibenhener, M.L. and M.C. Wooten, *Use of the Open Field Maze to measure locomotor and anxiety-like behavior in mice.* J Vis Exp, 2015(96): p. e52434.
77. Makino, J., K. Kato, and F.W. Maes, *Temporal structure of open field behavior in inbred strains of mice.* Japanese Psychological Research, 1991. **33**(4): p. 145-152.
78. Blaser, R.E., L. Chadwick, and G.C. McGinnis, *Behavioral measures of anxiety in zebrafish (Danio rerio).* Behav Brain Res, 2010. **208**(1): p. 56-62.
79. Egan, R.J., et al., *Understanding behavioral and physiological phenotypes of stress and anxiety in zebrafish.* Behav Brain Res, 2009. **205**(1): p. 38-44.
80. Levin, E.D., Z. Bencan, and D.T. Cerutti, *Anxiolytic effects of nicotine in zebrafish.* Physiol Behav, 2007. **90**(1): p. 54-8.
81. Maximino, C., et al., *Measuring anxiety in zebrafish: a critical review.* Behav Brain Res, 2010. **214**(2): p. 157-71.
82. Wong, K., et al., *Analyzing habituation responses to novelty in zebrafish (Danio rerio).* Behavioural Brain Research, 2010. **208**(2): p. 450-457.
83. Pittman, J.T. and C.S. Lott, *Startle response memory and hippocampal changes in adult zebrafish pharmacologically-induced to exhibit anxiety/depression-like behaviors.* Physiology & Behavior, 2014. **123**: p. 174-179.
84. Eilam, D., *Die hard: A blend of freezing and fleeing as a dynamic defense—implications for the control of defensive behavior.* Neuroscience & Biobehavioral Reviews, 2005. **29**(8): p. 1181-1191.
85. Håheim, O.B., *Defensive Behaviors - Manipulations of the Habenula-Raphe System in Freely Behaving Juvenile Zebrafish*, in *Kavli Institute of Systems*

Neuroscience. 2020, Norwegian University for Science and Technology: NTNU Open.
86. Bardenhewer, R., *The role of habenula/dorsalraphe circuity in sensory responses and internal states*, in *Institute of Biology*. 2020, RWTH Aachen.
87. Corradi, L., et al., *Using pERK immunostaining to quantify neuronal activity induced by stress in zebrafish larvae.* STAR Protocols, 2022. **3**(4): p. 101731.
88. Pearson, G., et al., *Mitogen-activated protein (MAP) kinase pathways: regulation and physiological functions.* Endocr Rev, 2001. **22**(2): p. 153-83.
89. Rosen, L.B., et al., *Membrane depolarization and calcium influx stimulate MEK and MAP kinase via activation of Ras.* Neuron, 1994. **12**(6): p. 1207-1221.
90. Monje, P., et al., *Regulation of the transcriptional activity of c-Fos by ERK. A novel role for the prolyl isomerase PIN1.* J Biol Chem, 2005. **280**(42): p. 35081-4.
91. Gao, Y.J. and R.R. Ji, *c-Fos and pERK, which is a better marker for neuronal activation and central sensitization after noxious stimulation and tissue injury?* Open Pain J, 2009. **2**: p. 11-17.
92. Ji, R.-R., et al., *Nociceptive-specific activation of ERK in spinal neurons contributes to pain hypersensitivity.* Nature Neuroscience, 1999. **2**(12): p. 1114-1119.
93. Draisci, G. and M.J. Iadarola, *Temporal analysis of increases in c-fos, preprodynorphin and preproenkephalin mRNAs in rat spinal cord.* Molecular Brain Research, 1989. **6**(1): p. 31-37.
94. Hunt, S.P., A. Pini, and G. Evan, *Induction of c-fos-like protein in spinal cord neurons following sensory stimulation.* Nature, 1987. **328**(6131): p. 632-634.
95. Yaksi, E. and R.W. Friedrich, *Reconstruction of firing rate changes across neuronal populations by temporally deconvolved Ca2+ imaging.* Nature Methods, 2006. **3**(5): p. 377-383.
96. Faria, M., et al., *Development of a vibrational startle response assay for screening environmental pollutants and drugs impairing predator avoidance.* Sci Total Environ, 2019. **650**(Pt 1): p. 87-96.
97. Mutlu, A.K., et al., *Dorsal raphe modulates the ongoing activity, functional, and sensory responses of zebrafish forebrain circuits*. Norwegian University of Science and Technology.
98. Avdesh, A., et al., *Regular care and maintenance of a zebrafish (Danio rerio) laboratory: an introduction.* J Vis Exp, 2012(69): p. e4196.
99. Gill, G. and M. Ptashne, *Negative effect of the transcriptional activator GAL4.* Nature, 1988. **334**(6184): p. 721-724.
100. Yokogawa, T., M.C. Hannan, and H.A. Burgess, *The Dorsal Raphe Modulates Sensory Responsiveness during Arousal in Zebrafish.* The Journal of Neuroscience, 2012. **32**(43): p. 15205-15215.
101. Kim, S., *Drosophila GAL4/UAS System*, in *BioRender*, D.G.U. System, Editor. 2022, BioRender: BioRender.
102. Zhang, J., V. Kale, and M. Chen, *Gene-directed enzyme prodrug therapy.* Aaps j, 2015. **17**(1): p. 102-10.
103. Curado, S., D.Y. Stainier, and R.M. Anderson, *Nitroreductase-mediated cell/tissue ablation in zebrafish: a spatially and temporally controlled ablation method with applications in developmental and regeneration studies.* Nat Protoc, 2008. **3**(6): p. 948-54.
104. Mathias, J.R., et al., *Enhanced cell-specific ablation in zebrafish using a triple mutant of Escherichia coli nitroreductase.* Zebrafish, 2014. **11**(2): p. 85-97.
105. Palumbo, F., et al., *The Zebrafish Dorsolateral Habenula Is Required for Updating Learned Behaviors.* Cell Rep, 2020. **32**(8): p. 108054.
106. Vargas, R., H. Þorsteinsson, and K.Æ. Karlsson, *Spontaneous neural activity of the anterodorsal lobe and entopeduncular nucleus in adult zebrafish: A putative homologue of hippocampal sharp waves.* Behavioural Brain Research, 2012. **229**(1): p. 10-20.
107. Cheng, R.K., S.J. Jesuthasan, and T.B. Penney, *Zebrafish forebrain and temporal conditioning.* Philos Trans R Soc Lond B Biol Sci, 2014. **369**(1637): p. 20120462.

108. Barton, B.A., *Stress in fishes: a diversity of responses with particular reference to changes in circulating corticosteroids.* Integr Comp Biol, 2002. **42**(3): p. 517-25.
109. Gordon, C.J., *Temperature and toxicology: an integrative, comparative, and environmental approach*. 2005: CRC press.
110. McClelland, G.B., et al., *Temperature- and exercise-induced gene expression and metabolic enzyme changes in skeletal muscle of adult zebrafish (Danio rerio).* The Journal of Physiology, 2006. **577**(2): p. 739-751.

Appendices

Appendix 1: Supplementary figures

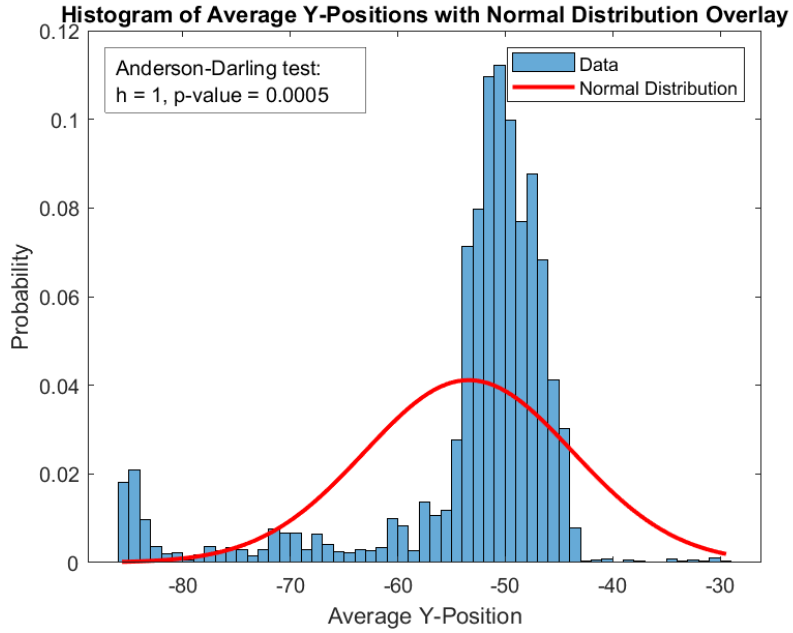

Supplementary Figure 1: Normality test for the average Y-position during the NT-test (20 min) of the juvenile WT fish (n=42) in the first optimization experiment. *The Anderson-Darling normality test was used to test for normal distribution of the datapoints for the early phase of the NT-test in the first optimization step. This is a variation of the Kolmogorov-Smirnov test that is very sensitive to deviations from normality in the tails. The dataset (blue histogram) clearly deviated from a normal distribution curve (red), supporting the use of non-parametric statistical techniques in the data analysis. Normality tests were not performed for the rest of the data analysis in the other experiments.*

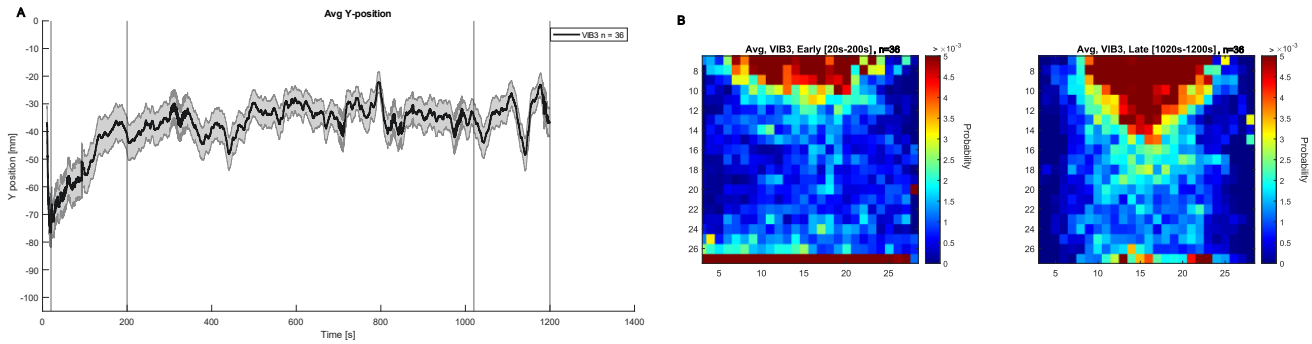

Supplementary Figure 2: Average Y-position and tank distribution for the second optimization experiment. *(**A**) Mean Y-position and SEM (mm) for the WT juvenile fish (black,*

*n=36). X-axis shows time (s), Y-axis shows vertical distance from the top of the tank (mm). Vertical lines indicate sample intervals for early and late NT-phase. (**B**) Heatmap of tank position probability distribution for the early (left) and late (right) 3 min of NT-phase in the second optimization experiment. The entire tracked area of the tank is represented in the figure, but axis units are arbitrary and based on the pixel bin size. Average tank position for the WT juvenile fish (n=36) for the first 3 min (sampling starts 20 sec into the experiment to exclude mis-tracking), and last 3 min of the NT-phase in the second optimization experiment. Bottom-dwelling indicated by the band of warm-colored pixels for the early phase of the NT-test.*

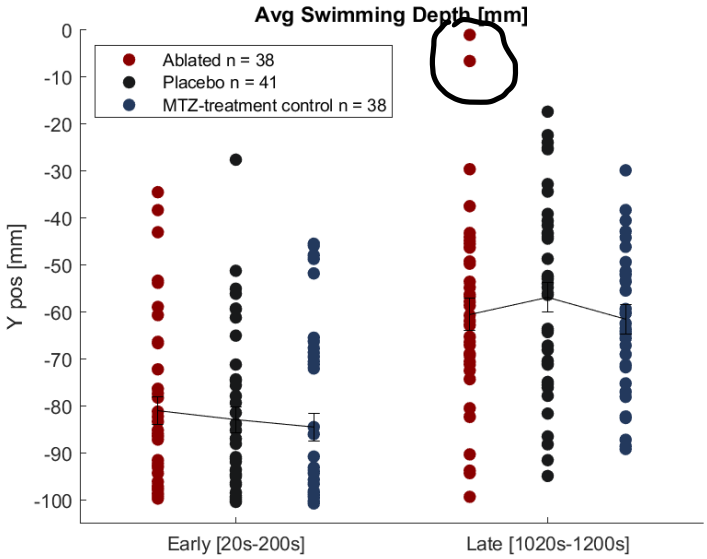

Supplementary Figure 3: Visualization of outliers in raphe-ablated animals' Y-position during the late phase in the NT-test of the serotonergic manipulation experiment. *Reviewing the raw data recording of the NT-test revealed that two of the ablated fish were not tracked properly, thus causing mist-tracking of their actual movement. The figure shows the scatter plot of the tank depth data without removal of these two outliers in the ablated group (red) during the late period of NT-phase (right side of the plot).*

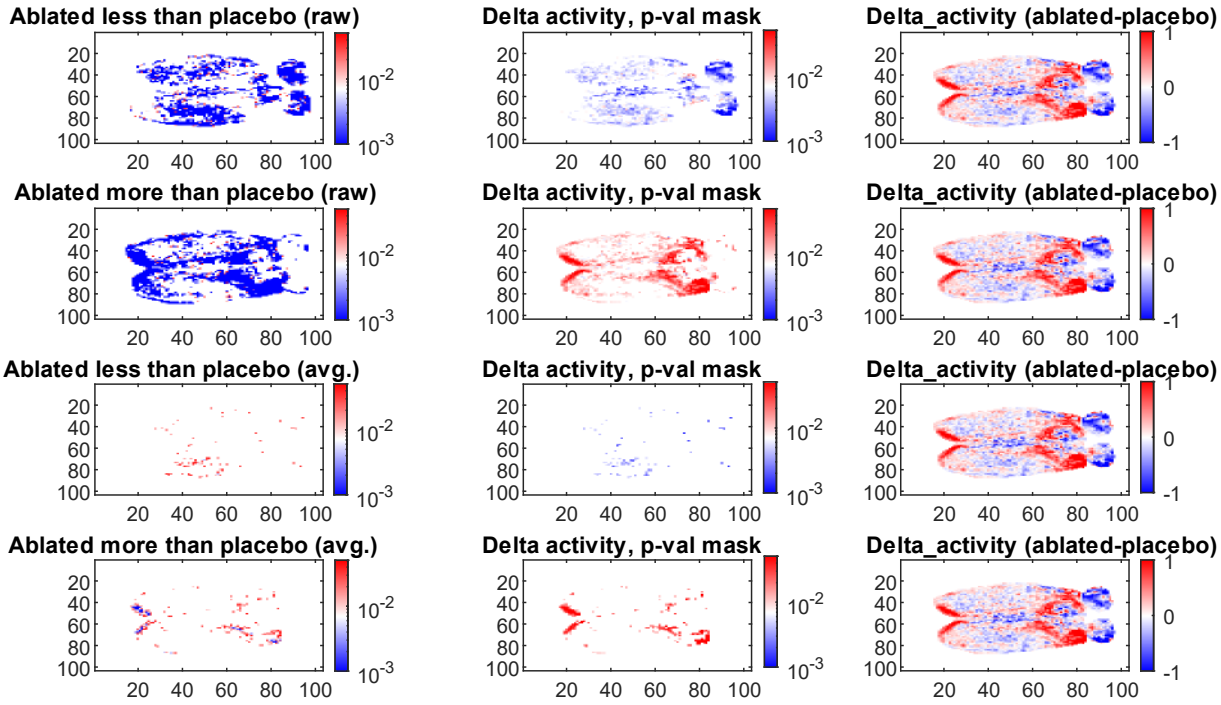

Supplementary Figure 4: All the plots generated from the whole-telencephalon comparison of pERK/tERK ratio between the ablated and the placebo groups. *Plots that were excluded from the results section were the three duplicates of the delta-activity plot in the right column. Panels in the left column showing the significant pixels from the Wilcoxon rank sum test were also, as this was an alternative way to represent the data and redundant. The bottom two panels in the middle column were also excluded, as they show the same data filtered through a very stringent significance threshold.*

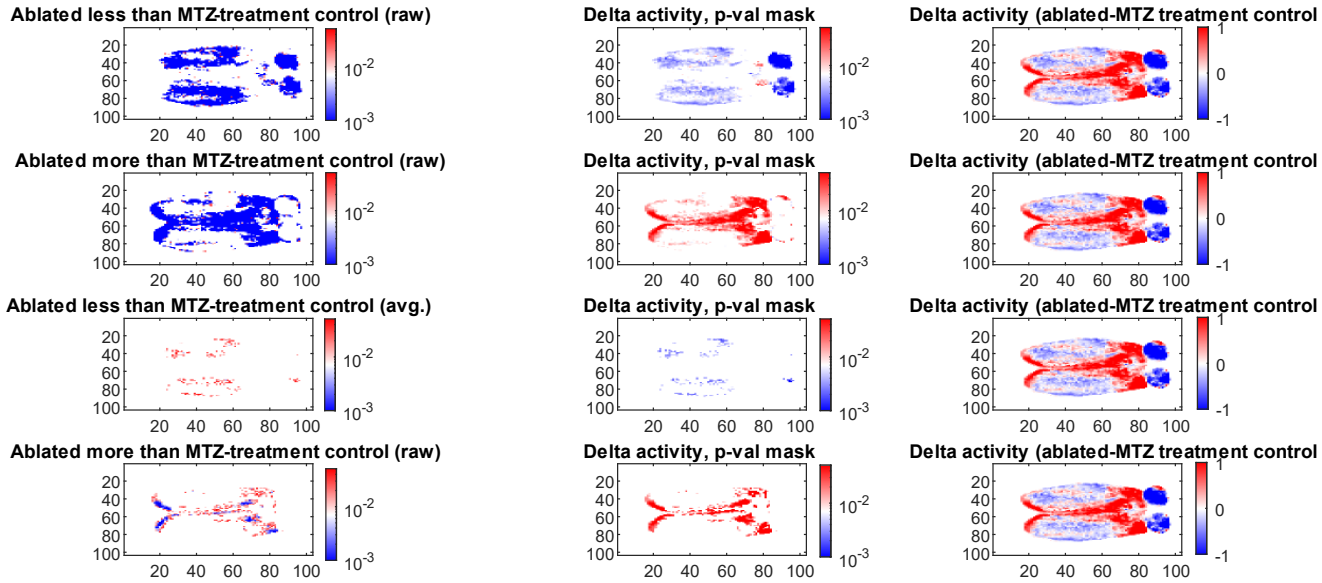

Supplementary Figure 5: All plots generated from the whole-telencephalon comparison of pERK/tERK ratio between the ablated and the MTZ-treatment control groups. *The plots excluded from the results section follow the same reasoning as in Supplementary Figure 4.*

Appendix 2: ERK staining protocol, adapted from Bram Serneels [55]

ERK staining protocol (pERK/tERK/DAPI)

Staining for neuronal activity and synaptic plasticity. Phosphorylated ERK (pERK) appears to remain for max. 10-15min. Best to detect activity is to fix within 5min after ending of the experimental procedure (e.g. behavior). Dissection prior to fixation might have an impact on the neuronal activity, advised to perform dissection after fixation.

Steps in blue can be performed in advance.

Day 1

Collecting and fixation

- Collect the fish from the previous experimental procedure and put in cooled artificial fish water (AFW).
- Remove the artificial fish water and add 500 µL cooled 4% PFA[1] in PBTx (0.25% Triton-X100)[2] overnight (O/N) at 4°C (cooler room).
    - Do not store the samples longer than a few days in PFA.

Day 2

Wash and dissection

- Wash at least 3 to 6x 5min in PBTx (0.25% Triton-X100) at RT to remove all PFA.
    - The samples can be stored up to a month in PBTx until further use.
    - Working in PBS in these steps could make dissection easier.

Storage point.

- Dissect and save the brain in PBTx (0.25%) for later use that day until all are collected in a 96-well plate.
    - Adult fish: complete dissection of the brain.
    - Larvae/Juvenile fish: remove lower jaws, skin on top of the brain and the tail.

Storage point.

Permeabilization

- Incubate the larvae in 250µL/well of 0.05% Trypsin-EDTA [3]on ice for approximately 40min.
    - Time and concentration can be dependent on the thickness of sample.
    - If you have added 225µL PBTx before at washing, add 25µL Trp
- Wash 2x quickly and 1x 10min in PBTx (0.25%).
    - All trypsin must be removed.

Blocking

- Incubate ≥ 1hour in 200µL/well of blocking solution[4] at RT on a shaker.

Incubation with 1st Abs

- Prepare primary ERK antibodies[5] (Abs) 1:500.
- Incubate the larvae in 150µL/well of primary Abs O/N at 4°C on a shaker.

Bram Serneels – ERK staining protocol (pERK/tERK/DAPI)

Day 3

Incubation with 2nd Abs

- Wash 3x 15min in PBTx (0.25%) at RT.
- Wash 1x quickly with 1X PBS.
- Incubate with 150 µL of Neurotrace Nissl solution (dilution 1:100) for 45-60min.
- Wash 1x 10min with 0.25% PBTx and 2x 5min with 1X PBS.
- Prepare secondary antibodies[6] (1:1000 for + antibodies, 1:200 for **non-+** antibodies).

There is a possibility to include the DAPI staining in this step (1:1000) instead of at day 4.

- Incubate in 150µL/well of secondary Abs O/N at 4°C on a shaker.

Day 4

***DAPI staining** (can also be included with the secondary antibodies at day 3)*

- Wash 1x quickly with PBTx (0.25%).
- Incubate >2.5h (preferably more) with DAPI staining solution [7](1:1000).

Washing

- Wash 3x 15min in PBTx (0.25%) at RT.
- Treat the samples in a series of increasing glycerol concentration (25-50-75%) until they sink to the bottom.

Mounting and confocal imaging

- Mount the brains in 75% Glycerol[8] (medium differs from person to person) and use for confocal microscopy.
- The brains then can be saved (cooled) for later use (keep away from light).

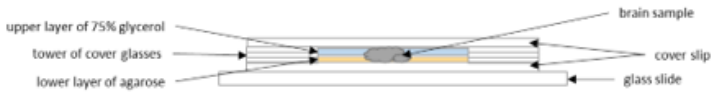

[1] For 1mL of 4% PFA in PBTx (0.25) per larvae: use 110µL of 36-38% PFA and 890µL of 1X PBTx.

[2] For 50mL of 1% PBTx (PBS + Triton-X100) use 500µL of 100% Triton-X100 and 49.50mL of 1X PBS. For 40mL of 0.25% PBTx use 10mL of 0.50% PBTx and 30mL 1X PBS (the rest of the 1% PBT can be saved for later).

[3] Prepare a 0.50% Trypsin-EDTA solution: for 1mL use 200µL of 2.5% Trypsin, 13.3µL 15% (0.5M) of EDTA and 786.7µL of PBTx (0.25%). This 0.50% solution can be prepared in higher quantity and saved in the freezer. Dilute 100µL of 0.50% Trypsin-EDTA with 900µL of PBTx (0.25%) for 1mL of 0.05% Trypsin-EDTA to use in the permeabilization.

[4] Blocking solution (2% Normal Goat Serum, 1% BSA, 1% DMSO in PBTx): for 1mL of blocking solution use 20µL of 100% NGS, 10mg of 100% BSA, 10µL of 100% DMSO and 970µL of PBTx (0.25%).

[5] Primary Abs (1:500): for 2mL use 20mg of 100% BSA, 20µL of 100% DMSO, 4µL of each antibody and 1972µL of PBTx (0.25%). tERK (total): mouse and pERK (phosphorylated): rabbit.

[6] Secondary Abs (1:1000): for 2mL use 20mg of 100% BSA, 20µL of 100% DMSO, 2µL of each antibody and 1976µL of PBTx (0.25%). GAM (mouse) and GAR (rabbit) for 555nm or 488nm.

[7] DAPI staining solution (1:1000): For 1mL of solution: 1µL DAPI, 10µL of 100% DMSO and 989µL PBTx 0.25%.
[8] Dilute 30mL of 100% Glycerol with 10mL of 1X PBS.

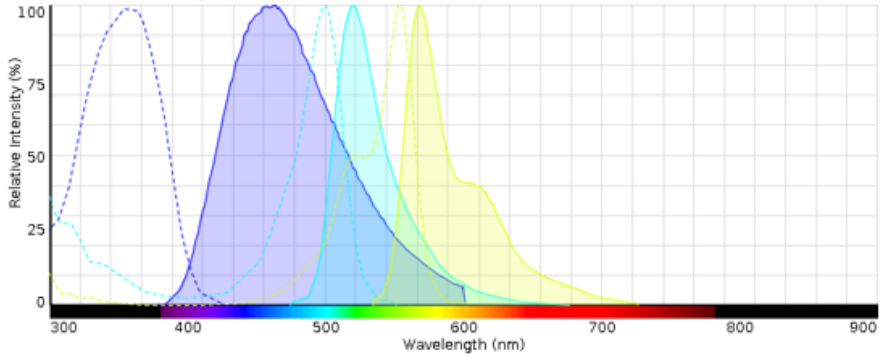

Nacre:
Blue: DAPI
Light Blue: Alexa fluor 488+
Yellow: Alexa fluor 555+

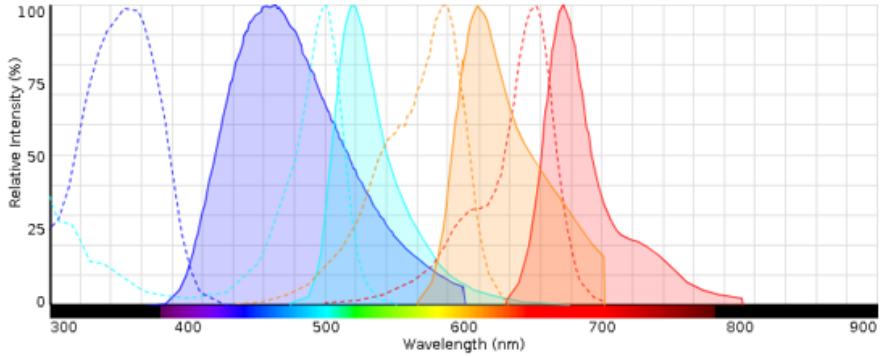

Transgenic line with mCherry:
Blue: DAPI
Light Blue: Alexa fluor 488+
Orange: mCherry
Red: Alexa fluor 647+

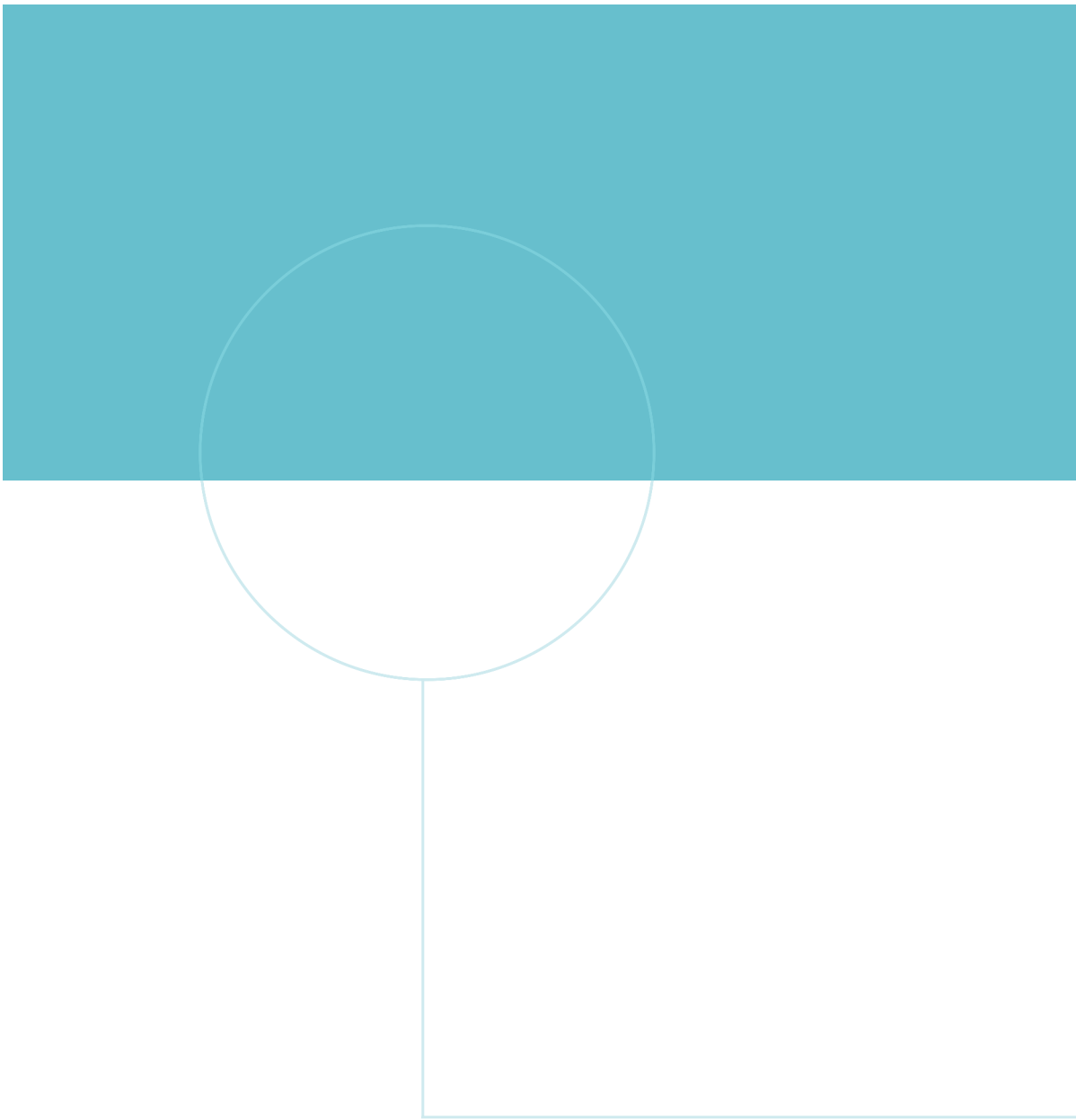

NTNU

Norwegian University of
Science and Technology